

# Hybrid Si/III-V Lasers for Next-generation Coherent Optical Communication

Thesis by  
Zhewei Zhang

In Partial Fulfillment of the Requirements for  
the degree of  
Doctor of Philosophy

The logo for the California Institute of Technology (Caltech), featuring the word "Caltech" in a bold, orange, sans-serif font.

CALIFORNIA INSTITUTE OF TECHNOLOGY  
Pasadena, California

2021  
(Defended February 19, 2021)

© 2021

Zhewei Zhang

ORCID: 0000-0002-1211-7957

## ACKNOWLEDGEMENTS

First and foremost, I would like to thank my advisor, Prof. Amnon Yariv, for giving me opportunities to participate in several great research projects to develop cutting-edge photonic technologies. Prof. Yariv's attitudes towards science, work and life have always inspired me. It is truly my honor and fortune to study in his group.

I would also like to thank Prof. Vahala, Prof. Faraon and Prof. Marandi, three experts on photonics, for serving on my defense committee.

I am very grateful to all the group members, especially Dr. Mark Harfouche, Dr. Dongwan Kim and Dr. Huolei Wang, who taught me how to conduct experiments and guided me to become an independent researcher. I also want to thank Dr. Hetuo Chen, who visited us for two years, for his collaboration on research and warm friendship.

I would like to express my sincere gratitude to Dr. Naresh Satyan, Dr. George Rakuljic, Dr. Reginald Lee, Dr. Bruno Crosignani and Dr. Christos Santis for their discussions and comments in the group meetings. In addition, I would like to thank all the staff at Kavli Nanoscience Institute and Alireza Ghaffari for their help and training in nanofabrication.

I appreciate all the help from my collaborators, Dr. Peicheng Liao and Kaiheng Zou, from University of Southern California (USC). I really enjoy working with them and have learned a lot from them in the collaboration.

Last but not least, I would like to thank my family for their support and love.

## ABSTRACT

The most important application of semiconductor lasers is, without doubt, optical communication, the backbone of the information age. In the past few decades, incoherent optical communication with conventional semiconductor lasers, the III-V distributed feedback (DFB) lasers, has successfully fulfilled the global demand for the data rate. However, in order to support the rapidly growing Internet traffic of the 21<sup>st</sup> century, the transition from incoherent to coherent optical communication is inevitable, requiring new types of lasers, as the conventional III-V DFB lasers lack the phase coherence needed to serve as the light sources in coherent optical communication. The existent alternatives with high phase coherence are external cavity lasers (ECLs) and fiber lasers, whose high price and bulky size effectively thwart the upgrade of the current communication networks. This is the main motivation for us to develop high-coherence semiconductor lasers.

To achieve the goal, we shall rethink and redesign semiconductor lasers. Advanced modern fabrication technology helps us to turn bold ideas into reality. Not only do we build semiconductor lasers on hybrid platforms, but also engineer elaborately the optical mode to enhance the lasers' phase coherence. The newly developed semiconductor lasers, hybrid Si/III-V lasers, are the core of the entire thesis. Their design principles, fabrication process, properties and performance in the coherent optical communication system will be presented and discussed. The experimental results show the Si/III-V lasers' superiority to their conventional counterparts.

Aside from possessing high phase coherence, the Si/III-V lasers have great potential to be the light sources on the integrated photonic platforms. The fundamental obstacle thwarting photonic integration is optical feedback, to which the conventional semiconductor lasers are very sensitive. Without the protection provided by optical isolators, which unfortunately cannot be fabricated on chip, the performance of the conventional III-V DFB lasers could get significantly degraded by optical feedback. The Si/III-V lasers, with their built-in high-Q resonators, are very robust against optical feedback and can function properly in the isolator-free coherent optical communication systems. Thus, the cost of future optical

networks can be further reduced by monolithically integrating passive photonic devices such as modulators and demodulators with the Si/III-V lasers.

Finally, all the studies centered on laser coherence trigger us to think deeply about the underlying relation between different means of characterizing laser coherence. A rigorous mathematical relation, the Central Relation, has been derived here, which not only unveils the fundamental relation between laser lineshape and frequency noise power spectral density (PSD) but also provides new methods of frequency noise controlling like optical filtering.

## PUBLISHED CONTENT AND CONTRIBUTIONS

- [1] M. Harfouche, D. Kim, H. Wang, C. T. Santis, Z. Zhang, H. Chen, et al., "Kicking the habit/semiconductor lasers without isolators," *Optics Express*, vol. 28, pp. 36466-36475, 2020.  
<https://doi.org/10.1364/OE.411816>  
Z.Z. aided in conducting the experiments and writing the manuscript.
- [2] Z. Zhang, K. Zou, H. Wang, P. Liao, N. Satyan, G. Rakuljic, et al., "High-speed Coherent Optical Communication with Isolator-free Heterogeneous Si/III-V Lasers," *Journal of Lightwave Technology*, pp. 1-1, 2020.  
<https://doi.org/10.1109/JLT.2020.3015738>  
Z.Z. participated in designing the experiments, conducting the experiments, analyzing the data and writing the manuscript.
- [3] K. Zou, Z. Zhang, P. Liao, H. Wang, Y. Cao, A. Almaiman, et al., "Higher-order QAM data transmission using a high-coherence hybrid Si/III-V semiconductor laser," *Optics Letters*, vol. 45, pp. 1499-1502, 2020/03/15 2020.  
<https://doi.org/10.1364/OL.383137>  
Z.Z. participated in designing the experiments, conducting the experiments, analyzing the data and writing the manuscript.
- [4] Z. Zhang and A. Yariv, "A General Relation Between Frequency Noise and Lineshape of Laser Light," *IEEE Journal of Quantum Electronics*, vol. 56, pp. 1-5, 2020.  
<https://doi.org/10.1109/JQE.2020.2980011>  
Z.Z. participated in designing the experiments, conducting the experiments, analyzing the data and writing the manuscript.
- [5] Q.-F. Yang, B. Shen, H. Wang, M. Tran, Z. Zhang, K. Y. Yang, et al., "Microresonator Spectrometer Using Counter-propagating Solitons," in *Conference on Lasers and Electro-Optics*, San Jose, California, 2019, p. AF2K.1.  
[https://doi.org/10.1364/CLEO\\_AT.2019.AF2K.1](https://doi.org/10.1364/CLEO_AT.2019.AF2K.1)  
Z.Z. aided in conducting the experiments and writing the manuscript.
- [6] Z. Zhang, H. Wang, N. Satyan, G. Rakuljic, C. T. Santis, and A. Yariv, "Coherent and Incoherent Optical Feedback Sensitivity of High-coherence Si/III-V Hybrid Lasers," in *Optical Fiber Communication Conference (OFC) 2019*, San Diego, California, 2019, p. W4E.3.  
<https://doi.org/10.1364/OFC.2019.W4E.3>  
Z.Z. participated in designing the experiments, conducting the experiments, analyzing the data and writing the manuscript.
- [7] K. Zou, Z. Zhang, P. Liao, H. Wang, Y. Cao, A. Almaiman, et al., "Using a Hybrid Si/III-V Semiconductor Laser to Carry 16- and 64-QAM Data Signals over an 80-km

Distance," in 2019 Optical Fiber Communications Conference and Exhibition (OFC), 2019, pp. 1-3.

<https://doi.org/10.1364/OFC.2019.M3A.2>

Z.Z. participated in designing the experiments, conducting the experiments, analyzing the data and writing the manuscript.

- [8] Q.-F. Yang, B. Shen, H. Wang, M. Tran, Z. Zhang, K. Y. Yang, et al., "Vernier spectrometer using counterpropagating soliton microcombs," *Science*, vol. 363, p. 965, 2019.

<https://doi.org/10.1126/science.aaw2317>

Z.Z. aided in conducting the experiments and writing the manuscript.

## TABLE OF CONTENTS

Acknowledgements.....	iii
Abstract .....	iv
Published Content and Contributions.....	vi
Table of Contents.....	viii
List of Illustrations and/or Tables.....	x
Chapter 1: Introduction.....	1
1.1 Deployment of coherent optical communication systems .....	1
1.2 Desire of the right light sources .....	2
1.3 Content of this thesis .....	3
Chapter 2: Theory of laser coherence and high-coherence Si/III-V lasers .....	5
2.1 Coherence of semiconductor lasers .....	5
2.1.1 Spontaneous emission and quantum noise .....	5
2.1.2 Coupling between intensity noise and frequency noise .....	8
2.1.3 Direct current modulation of semiconductor lasers .....	9
2.1.4 Laser frequency noise PSD .....	11
2.2 High-coherence Si/III-V lasers .....	13
2.2.1 Reduce quantum noise with mode engineering.....	13
2.2.2 Hybrid Si/III-V lasers.....	14
2.2.3 Laser characterization: power and spectrum .....	19
2.2.4 Laser characterization: relaxation resonance frequency and alpha parameter .....	20
2.2.5 Laser characterization: frequency noise PSD .....	22
2.3 Conclusions .....	25
Chapter 3: Coherent optical communication .....	26
3.1 Fundamental of coherent optical communications.....	26
3.1.1 Quadrature amplitude modulation .....	27
3.1.2 Demodulation and detection .....	31
3.1.3 Digital signal processing (DSP).....	33
3.1.4 System performance.....	35
3.2 Si/III-V lasers as the light sources .....	36
3.2.1 Back-to-Back coherent communications.....	36
3.2.2 Si/III-V laser vs III-V DFB laser vs external cavity laser.....	37
3.2.3 ZR coherent communications .....	42
3.3 Conclusions .....	46
Chapter 4: Impacts of optical feedback on laser coherence .....	47
4.1 Coherent optical feedback and incoherent optical feedback.....	48
4.2 Coherent optical feedback effects on laser coherence.....	49
4.3 Incoherent optical feedback effects on laser coherence .....	52
4.4 Lasers' sensitivity to optical feedback.....	54
4.5 Sensitivity to coherent optical feedback .....	55

4.6 Sensitivity to incoherent optical feedback .....	59
4.7 System performance under coherent optical feedback .....	66
4.8 System performance under incoherent optical feedback.....	68
4.9 OSNR penalty due to optical feedback.....	71
4.10 Conclusions.....	72
<b>Chapter 5: A general relation between laser frequency noise and lineshape...</b>	<b>74</b>
5.1 Derivation of the general relation.....	74
5.2 Validation of the Central Relation .....	78
5.3 Insights into the Central Relation.....	80
5.3.1 Optical filtering of laser frequency noise PSD .....	81
5.3.2 Is laser linewidth a good measure for laser coherence .....	85
5.4 Conclusions.....	88
<b>Bibliography .....</b>	<b>89</b>

## LIST OF ILLUSTRATIONS AND/OR TABLES

Figure 2.1 Phasor model of spontaneous emission.....	7
Figure 2.2 Coupling between laser intensity noise and frequency noise .....	8
Figure 2.3 Normalized direct current modulation response of semiconductor lasers.....	11
Figure 2.4 Frequency noise PSD of semiconductor lasers when (a) photon lifetime $\ll$ electron lifetime and (b) photon lifetime $\sim$ electron lifetime .....	13
Figure 2.5 Structure and mode profile of Si/III-V lasers. The red dash line indicates that the lasing mode is evanescently coupled to the quantum wells.....	16
Figure 2.6 (a) Flow chart of laser fabrication, (b) SEM image of the silicon resonators, (c) Optical image of the laser chip after wafer-bonding and (d) Optical image of the final laser chip.....	18
Figure 2.7 (a) LIV curves under various temperature and (b) optical spectra of Si/III-V lasers.....	20
Figure 2.8 Measurement setups for laser modulation response .....	21
Figure 2.9 Modulation responses and alpha parameters of Si/III-V lasers .....	22
Figure 2.10 Measure setup for laser frequency noise PSD. RFSA: radio frequency spectrum analyzer.....	23
Figure 2.11 Frequency noise PSD of the Si/III-V laser.....	24
Figure 2.12 Frequency noise PSD of a commercial III-V DFB laser .....	24
Figure 3.1 A coherent optical communication link .....	27
Figure 3.2 (a) An optical waveform of QAM, (b) Structure of an IQ modulator and (c) Constellation diagrams of QAM.....	30
Figure 3.3 (a) Structure of coherent receivers (b) Demodulation .....	32
Figure 3.4 Digital signal processing module .....	34
Figure 3.5 BER as a function of OSNR and phase noise. Black arrows indicate	

the direction in which the phase noise increases .....	36
Figure 3.6 Measurement setup for coherent optical communications .....	37
Figure 3.7 Frequency noise PSD of lasers used in the experiments .....	38
Figure 3.8 20 GBaud 16-QAM (a) system performance and (b) Constellation diagrams .....	40
Figure 3.9 20 GBaud 64-QAM system performance .....	42
Figure 3.10 ZR communication system performance (a) 16-QAM (b) power optimization for 16-QAM (c) 64-QAM (d) power optimization for 64-QAM.....	44
Figure 4.1 Optical feedback .....	48
Figure 4.2 Schematic diagram of coherent optical feedback .....	50
Figure 4.3 Noise coupling (a) w/o coherent optical feedback and (b) w/ coherent optical feedback.....	51
Figure 4.4 Schematic diagram of incoherent optical feedback .....	53
Figure 4.5 Noise coupling (a) w/o incoherent optical feedback and (b) w/ incoherent optical feedback.....	54
Figure 4.6 Measurement setup for laser frequency noise PSD under coherent optical feedback.....	56
Figure 4.7 Frequency noise PSD of (a) the III-V laser and (b) the Si/III-V laser under various levels of coherent optical feedback .....	57
Figure 4.8 Coupling between intensity noise and phase noise.....	59
Figure 4.9 Measurement setup for laser frequency noise PSD under incoherent optical feedback .....	60
Figure 4.10 (a) ASE noise spectrum and optical spectra of (b) the hybrid Si/III-V laser and (c) the III-V laser with ASE noise injected .....	61
Figure 4.11 Frequency noise PSD of (a) the III-V laser and (b) Si/III-V laser w/ and w/o the existence of incoherent optical feedback and (c) the corresponding linewidth as a function of ASE power.....	63
Figure 4.12 (a) Intensity noise PSD of the III-V DFB laser at various injected ASE power and (b) the increment of laser intensity noise and laser	

frequency noise, respectively .....	65
Figure 4.13 Measurement setup for coherent optical feedback.....	66
Figure 4.14 System measurement of (a) the Si/III-V laser and (b) the III-V DFB laser under coherent optical feedback .....	67
Figure 4.15 Constellation diagrams of the III-V DFB laser (a) w/o optical feedback and (b) with the feedback level beyond -41 dB .....	68
Figure 4.16 Measurement setup for incoherent optical feedback .....	69
Figure 4.17 System measurement of (a) the Si/III-V laser and (b) the III-V DFB laser under incoherent optical feedback.....	70
Figure 4.18 Constellation diagrams of the III-V DFB laser (a) w/o optical feedback and (b) with the ASE power of 0.7 mW.....	71
Figure 4.19 Power penalty due to (a) coherent and (b) incoherent optical feedback .....	72
Figure 5.1 Measurement setups for (a) frequency noise power spectral density and (b) lineshape. PC: polarization controller; RFSA: radio frequency spectrum analyzer. A narrow-linewidth fiber laser is used as the reference laser.....	79
Figure 5.2 (a) Frequency noise PSD of the laser (b) Corresponding phase noise PSD and lineshape of the laser .....	80
Figure 5.3 Measurement setup for the frequency noise PSD of laser output modified by the MZI with the free spectral range of 203 MHz .....	82
Figure 5.4 Schematic plot of the laser lineshape and transmission spectrum of the MZI; the laser frequency aligned to maximum transmission frequency of the MZI.....	83
Figure 5.5 (a) Frequency noise PSD of the laser and laser passing through the MZI (b) Ratio between the two frequency noise PSDs.....	84
Figure 5.6 Frequency noise PSD of the Si/III-V laser.....	86
Figure 5.7 Frequency noise PSD of the III-V DFB laser w/o and w/ small coherent optical feedback.....	86
Figure 5.8 Optical lineshape of the three lasers.....	87

Figure 5.9 System performance of the three lasers..... 88

*Chapter 1*

## INTRODUCTION

The invention of semiconductor lasers has revolutionized the information technology industry. It enables high-speed optical communications, leading to the birth of the modern Internet, which is one of the main engines of the world's advancement over the past several decades [1-6]. However, human society has developed to the point when traditional optical communication technology can no longer satisfy the fast-increasing needs on the data rate. Hence, it is indispensable to employ new optical communication systems, i.e. coherent optical communication systems, which require lasers with much higher phase coherence than the conventional III-V DFB lasers as the light sources. Certainly, the 21<sup>st</sup> century communication infrastructure will be powered by new-generation semiconductor lasers.

**1.1 Deployment of coherent optical communication systems**

We are living in the information age, when a huge amount of data is collected, stored, analyzed and transmitted on the daily basis. In the upcoming future, more and more users around the world will have access to the Internet; more electronic devices such as smart phones, tablets, and computers will be connected to the Internet; new companies based on big data, cloud computing and artificial intelligence, along with new business models, are going to emerge; people demand faster and faster Internet speed for both work and personal enjoyment. The annual global data traffic growth rate is predicted to be 26% by Cisco, which is a huge burden for the current optical communication systems. At this moment, upgrading current optical communication networks to meet the ever-increasing demands on the data rate has become the primary task in the field [7-9].

Conventional optical communications employ 2-level pulse amplitude modulation (PAM2), where information is encoded in the intensity of semiconductor lasers, with high and low laser intensity representing 1 and 0, respectively. The simplicity of such a modulation scheme makes possible the construction of the optical communication systems with inexpensive

optical components such as directly modulated lasers (DMLs) and electro-absorption modulated lasers (EMLs) [10-12]. Thus, traditional optical networks are exclusively powered by conventional III-V DFB lasers. However, the spectral efficiency, defined as the ratio between the data rate and the modulation frequency, of PAM2 is quite low, rendering it unable to support the ultra-high data rate which the world is demanding.

Coherent optical communications employ more complex modulation schemes such as quadrature amplitude modulation (QAM), where information is encoded in both the intensity and the phase of lasers, and therefore have higher spectral efficiency, boosting the capacity of communication links to meet the increasing demands on the data rate [13, 14]. Currently, major players in this area are racing towards developing coherent transceivers supporting the data rate of 400 Gbits/s or even higher. Coherent optical communication networks are likely to be widely deployed in the next decade or so and we are now witnessing the beginning of such a transition.

## **1.2 Desire of the right light sources**

Despite the advantages, the construction cost of coherent optical communication systems is much higher because of the increased complexity of the optoelectronic components, inevitably slowing down the transition towards coherent optical networks. The key to reducing the cost is integration, where electronic and photonic devices can be miniaturized and fabricated massively on a chip. While integrated electronics has moved progressively towards sub-10nm technology, the development of photonic integration has been far slower. The major challenge lies at integrating semiconductor lasers with passive photonic devices. Conventional III-V DFB lasers, the main light sources in the present optical networks, can be easily fabricated on chip but lack the phase coherence and the feedback insensitivity to serve as the integrated light sources in coherent optical communications. Instead, what has been practically used now in commercial coherent transceivers is the Micro Integrable Tunable Laser Assembly (u-ITLA), an ECL with high phase coherence [15, 16]. Its fabrication requires extra elaborate assembling, rendering the ECL expensive and unsuitable for photonic integration. Thus, new types of semiconductor lasers are necessary.

Here, we are going to present heterogeneous semiconductor lasers on silicon, a widely used platform for integrated photonics [17-21]. Such a new type of semiconductor lasers, i.e. the hybrid Si/III-V lasers, whose high coherence and feedback insensitivity will be demonstrated later in the thesis, is exactly the light source needed for the upcoming coherent optical communication networks.

### **1.3 Content of this thesis**

The core devices discussed in this thesis are, of course, the Si/III-V lasers. Different experiments have been carried out to characterize various properties of the Si/III-V lasers and to illustrate their superiority to the commercial counterparts. The whole thesis is organized as follows.

Chapter 2 starts with the conventional theory of laser coherence, explaining the origin of quantum noise in semiconductor lasers. The theoretical linewidth and frequency noise PSD, which are two common measures for laser coherence, of semiconductor lasers will be introduced. Next, we are going to discuss how to design high-coherence Si/III-V lasers with mode engineering, focusing on how to reduce quantum noise based on the physics. After that, the lasers' fabrication process will be mentioned. Lastly, the properties of the Si/III-V lasers such as power, threshold and frequency noise PSD will be measured.

Chapter 3 focuses on coherent optical communications. In the first half of this chapter, we are going to show how a coherent optical communication link is constructed. First, we are going to explain how the modulation and demodulation processes are done physically. The two key photonic components, namely the inphase-quadrature (IQ) modulator and demodulator, will be discussed. Next, we will talk about digital signal processing (DSP), which is used to recover the information from the distorted signals obtained after demodulation. We will pay special attention to how the phase information is recovered by DSP, as it is directly related to the phase coherence of the light sources. In the second half of this chapter, the system performances of the Si/III-V laser, a conventional III-V DFB laser and an ECL will be measured, analyzed and compared.

Chapter 4 is about semiconductor lasers' feedback sensitivity. This old but important subject regains our attention as large-scale photonic integration faces optical feedback as the main obstacle. Because optical isolators cannot be integrated on chip, any unwanted optical feedback can potentially degrade semiconductor lasers, rendering the communication systems dysfunctional. In this chapter, we will first establish the theories on how optical feedback affects laser coherence and then measure the feedback sensitivity of the hybrid Si/III-V lasers in comparison to the conventional III-V DFB laser. Finally, we are going to show that the Si/III-V lasers can function properly in an isolator-free coherent optical communication system.

In Chapter 5, we will discuss the relation between different means of characterizing laser coherence. A general relation between laser frequency noise PSD and lineshape, named as the Central Relation, will be derived. The Central Relation brings us new insights such as new methods of tailoring laser frequency noise PSD with optical filtering.

## THEORY OF LASER COHERENCE AND HIGH-COHERENCE SI/III-V LASERS

In this chapter, we are going to introduce the quantum mechanical theory of laser coherence, discuss how to apply the theory to designing high-coherence Si/III-V lasers and characterize the properties of the Si/III-V lasers such as power, threshold and frequency noise PSD.

### 2.1 Coherence of semiconductor lasers

Coherence, a critical concept in laser physics, describes how far the laser field deviates from being monochromatic. Mathematically, the laser field can be expressed as

$$E(t) = \{E_0 + \delta(t)\}e^{i\{\omega_0 t + \varphi(t)\}}, \quad (2.1)$$

where  $E_0$  and  $\omega_0$  represent the amplitude and the angular frequency of the laser field, respectively.  $\delta(t)$  and  $\varphi(t)$  are laser amplitude and phase noise. Because of gain saturation in semiconductor lasers, the amplitude noise in general is largely suppressed so that the monochromaticity is mainly determined by the phase noise. Later, we will explain where the laser phase noise arises from with quantum mechanics. In addition, two major means of quantifying laser coherence, namely laser linewidth and frequency noise PSD, will be introduced.

#### 2.1.1 Spontaneous emission and quantum noise

The core of semiconductor laser physics lies at the interaction between the laser field and the semiconductor quantum wells. The interaction Hamiltonian can be written as

$$H_I = -q\vec{E}(\vec{r}) \cdot \vec{x}, \quad (2.2)$$

where  $q$  and  $\vec{x}$  are the charge and the coordinate operator of an electron, respectively. The electric field  $\vec{E}(\vec{r})$  can be further quantized as

$$\vec{E}(\vec{r}) = i\sqrt{\frac{\hbar\omega}{2\varepsilon}}(a^+ - a)u(\vec{r})\vec{e}, \quad (2.3)$$

where  $\omega$  is the angular frequency of the laser light and  $\varepsilon$  is the permittivity.  $a^+$  and  $a$  are the creation and the annihilation operators, respectively.  $u(\vec{r})$  represents the normalized optical mode and  $\vec{e}$  is the unit vector.

The transitions of electrons from the conduction band to the valence band result in the emission of photons. With time-dependent perturbation theory, the emission rate can be calculated as

$$\begin{aligned} W &= \frac{\pi q^2 \omega}{\varepsilon} |\langle V | \vec{e} \cdot \vec{x} | C \rangle|^2 (N_p + 1) g(\omega) |u(\vec{r})|^2 \\ &= \frac{\pi q^2 \omega}{\varepsilon} |\langle V | \vec{e} \cdot \vec{x} | C \rangle|^2 N_p g(\omega) |u(\vec{r})|^2 + \frac{\pi q^2 \omega}{\varepsilon} |\langle V | \vec{e} \cdot \vec{x} | C \rangle|^2 g(\omega) |u(\vec{r})|^2 \\ &= W_{st} + W_{sp}, \end{aligned} \quad (2.4)$$

where  $|C\rangle$  and  $|V\rangle$  represent the quantum states of the conduction band and the valence band, respectively.  $N_p$  is the total photon number and  $g(\omega)$ , the lineshape function, is a direct result of Fermi's golden rule.

The transition rate can be divided it into two terms, namely  $W_{st}$  and  $W_{sp}$ . The former term, proportional to  $N_p$ , corresponds to stimulated emission, a process in which new photons are generated coherently. It provides gain for semiconductor lasers. The latter term is referred to as spontaneous emission. It is independent on the photon number, suggesting that incoherent photons are generated in such a process. Interestingly and importantly, the spontaneous emission rate is always the same as the stimulated emission rate induced by a single photon. Such a relation sets the ratio between the magnitudes of the coherent and incoherent optical fields to be  $N_p : 1$ .

Now, we are going to switch to a classical picture to better describe the laser field, which is composed of the coherent and incoherent optical fields, as shown schematically in Fig. 2.1.

The incoherent optical field has a fixed magnitude but a random phase relative to the coherent optical field. The red circle in Fig. 2.1 represents its ensemble. The magnitude and the phase of the laser field fluctuate with the normal and tangential parts of the incoherent optical field, which are essentially the noise sources. Evidently, the non-monochromaticity of the laser field is originated from spontaneous emission.

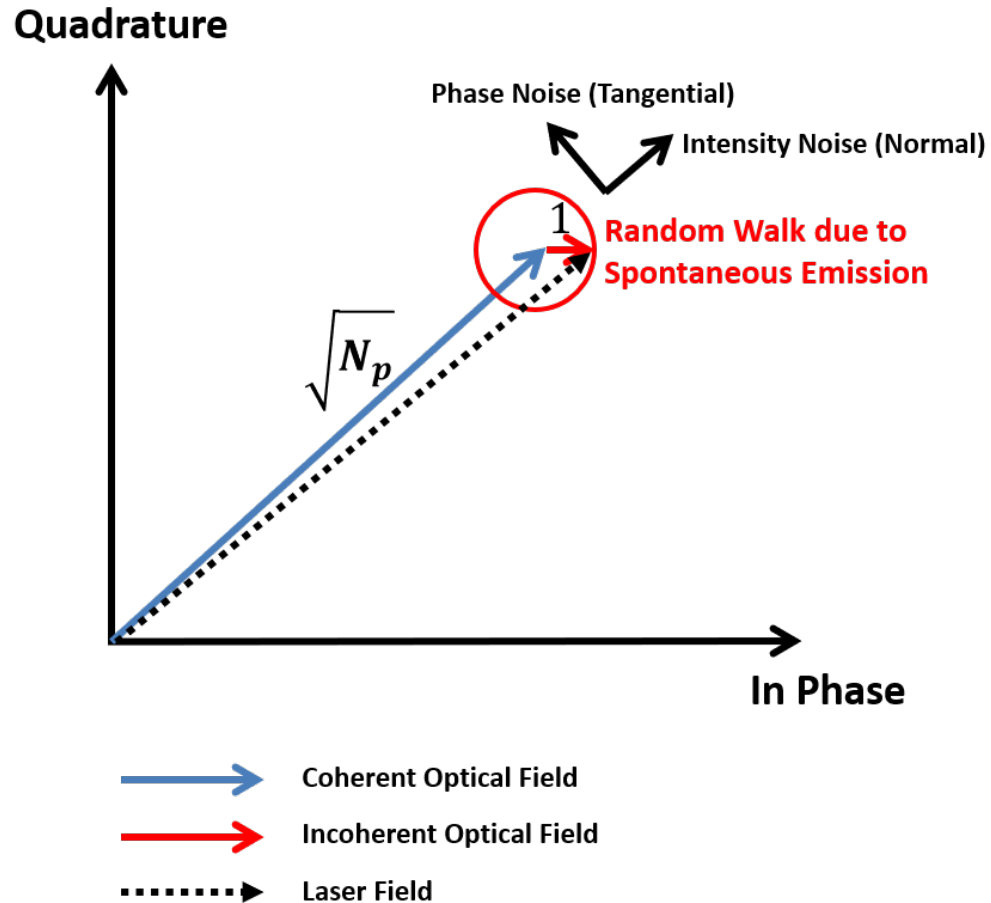


Figure 2.1 Phasor model of spontaneous emission

As discussed before, it is the phase noise of lasers that mostly broadens the power spectrum, namely the lineshape, of the laser field, of which the full width half maximum (FWHM), i.e. the laser linewidth, was first derived by Schawlow and Townes [22], and is now well known as the S-T linewidth:

$$\Delta\nu_{ST} = \frac{W_{sp}}{4\pi N_p}. \quad (2.5)$$

### 2.1.2 Coupling between intensity noise and frequency noise

The real linewidth of semiconductor lasers is typically larger than the S-T linewidth because in semiconductor lasers, the intensity noise is coupled to the phase noise, causing additional broadening of the lasers' power spectrum, of which the mechanism is shown schematically in Fig. 2.2. The laser intensity noise perturbs the stimulated emission rate and induces fluctuations of the inverted electron number. Therefore, the gain, proportional to the inverted electron number, also gets perturbed, causing the fluctuations of the refractive index of the lasing mode because of their interconnection described by Kramers-Kronig relations. The drift of the mode index leads to the drift of the lasing frequency, i.e. additional phase noise and a more broadened optical spectrum.

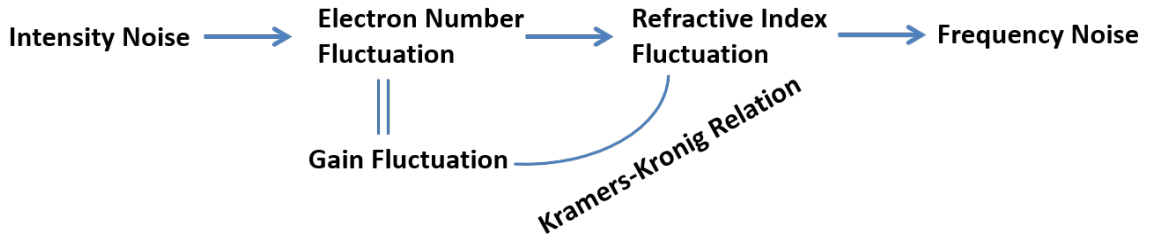


Figure 2.2 Coupling between laser intensity noise and frequency noise

This coupling mechanism is known as linewidth enhancement, whose effect on the laser linewidth can be expressed as

$$\Delta\nu_H = \frac{W_{sp}}{4\pi N_p} (1 + \alpha^2), \quad (2.6)$$

where  $\alpha$  is the linewidth enhancement factor and was first introduced by Charles Henry [23]. Its value can be calculated using

$$\alpha = \frac{\partial\chi_r/\partial N_e}{\partial\chi_i/\partial N_e}, \quad (2.7)$$

where  $\chi_r$  and  $\chi_i$  are the real and imaginary parts of the optical susceptibility, respectively and  $N_e$  represents the electron number. The linewidth enhancement factor describes the magnitude of the coupling between laser intensity noise and phase noise, whose value is typically between two and ten in semiconductor lasers.

### 2.1.3 Direct current modulation of semiconductor lasers

In addition to laser linewidth, laser frequency noise PSD is also a widely used measure for laser coherence. Before officially introducing it, in this section, we are going to talk about direct current modulation of semiconductor lasers, which is closely related to laser frequency noise PSD.

The direct current modulation process can be described with the following equations:

$$\begin{aligned}\frac{dN}{dt} &= \frac{I}{eV} - \frac{N}{\tau} - A(N - N_{tr})P \\ \frac{dP}{dt} &= A(N - N_{tr})P\Gamma_a - \frac{P}{\tau_p},\end{aligned}\tag{2.8}$$

where  $N$  and  $P$  represent the electron and photon number density, respectively.  $e$  is the electron charge and  $V$  is the total volume of the laser.  $\tau$  and  $\tau_p$  represent the electron and photon lifetime.  $A$  is the coefficient for stimulated emission and  $\Gamma_a$  is the mode confinement factor in the active region.  $I$  is the injected current.

We consider small signal modulation here, i.e. small perturbations around a steady state, and plug the attempted solution

$$\begin{aligned}I &= I_0 + i_1 e^{i\omega t} \\ N &= N_0 + n_1 e^{i\omega t} \\ P &= P_0 + p_1 e^{i\omega t}\end{aligned}\tag{2.9}$$

into (2.8), where  $I_0$ ,  $N_0$  and  $P_0$  are the current, the electron and photon number density of the steady state while  $i_1$ ,  $n_1$  and  $p_1$  represent the modulated parts.  $\omega$  is the modulation frequency. After some algebra, we obtain the modulation response

$$P_1 = -\frac{i_1 AP_0 \Gamma_a / eV}{\omega^2 - i\omega/\tau - i\omega AP_0 - AP_0/\tau_p}. \quad (2.10)$$

This is a typical second order filter. Depending on the relation between the electron and photon lifetime, the modulation response functions can be dramatically different, as shown in Fig. 2.3. If the photon lifetime is much shorter than the electron lifetime, which is the case for conventional III-V DFB lasers, the corresponding modulation response is peaked at the so-called relaxation resonance frequency, which is defined below. On the contrary, if the photon lifetime becomes comparable to the electron lifetime, the modulation response is damped and straightly rolls off beyond the relaxation resonance frequency. Such difference affects the semiconductor lasers' coherence significantly, which will be explained later.

The relaxation resonance frequency is defined as

$$\omega_R = \sqrt{\frac{AP_0}{\tau_p} - \frac{1}{2}\left(\frac{1}{\tau} + AP_0\right)^2}, \quad (2.11)$$

indicating how fast the laser can be modulated directly. It is worth pointing out that we did not take the parasitic capacitance of the materials into account. Hence, with regard to the practical modulation bandwidth of semiconductor lasers, the relaxation resonance frequency is the upper bound.

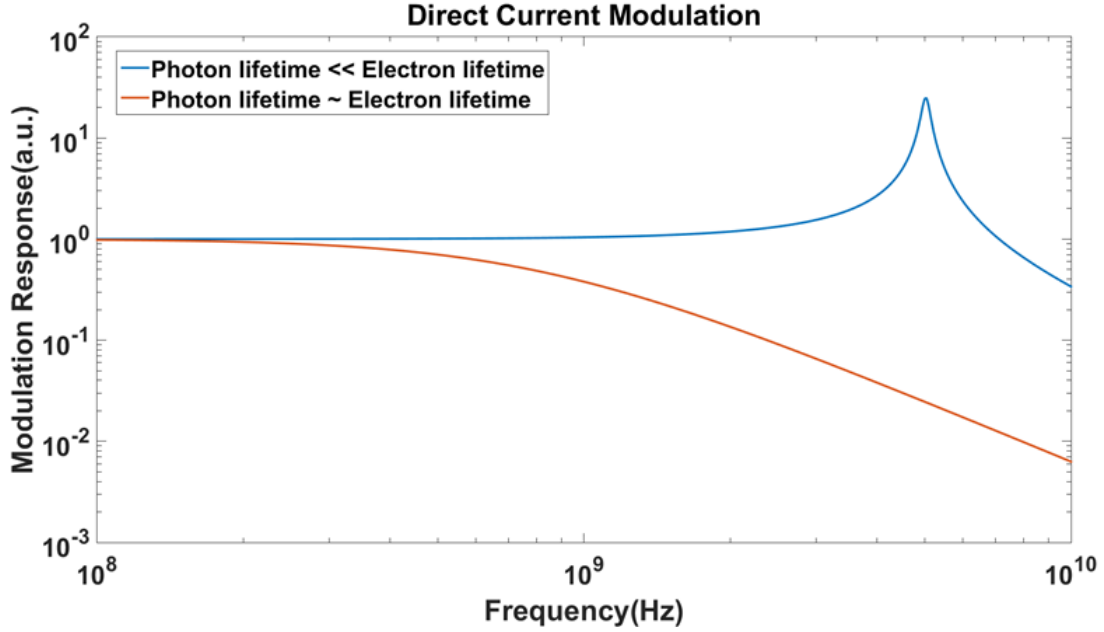


Figure 2.3 Normalized direct current modulation response of semiconductor lasers

#### 2.1.4 Laser frequency noise PSD

Single-sided laser frequency noise PSD is defined as

$$S_{\Delta\nu}(f) = 2 \int_{-\infty}^{+\infty} \langle \dot{\phi}(t)\dot{\phi}(t+\tau) \rangle e^{-i2\pi f\tau} d\tau, \quad (2.12)$$

where  $\langle \rangle$  denotes the time or ensemble average and  $\dot{\phi}(t)$  is the frequency noise.  $\tau$  and  $f$  represents the time delay and the frequency, respectively. Unlike laser lineshape, laser frequency noise PSD does not contain any explicit information on the optical field.

The frequency noise PSD of semiconductor lasers can be expressed as

$$\begin{aligned} S_{\Delta\nu}(f) &= \frac{\Delta\nu_{ST}}{\pi} \{1 + \alpha^2 H(f)\} \\ &= \frac{\Delta\nu_{ST}}{\pi} + \frac{\Delta\nu_{ST}}{\pi} \alpha^2 H(f), \end{aligned} \quad (2.13)$$

where  $H(f)$  represents the normalized direct current modulation response. The frequency noise PSD can be decomposed into two terms. The first term, which is a constant,

corresponds to the frequency noise generated by spontaneous emission while the second term, as a function of the linewidth enhancement factor, is a direct consequence of the coupling between laser intensity and frequency noise, which involves the process of modulating the electron number as manifested by the direct current modulation response. Far below and above the relaxation resonance frequency, the frequency noise PSD is white at the levels of  $\Delta\nu_H/\pi$  and  $\Delta\nu_{ST}/\pi$ , respectively. Around the relaxation resonance frequency, the frequency noise PSD can be either peaked or damped, depending on the relation between the electron and photon lifetime, as shown in Fig. 2.4.

So far, we have introduced two measures for laser coherence. Here comes a natural question: which one shall we use for our applications? Eventually, we would like to predict the lasers' performance in the coherent optical communication systems based on their phase coherence. Therefore, it is more straightforward and meaningful to use laser frequency noise PSD as the measure, to which the phase noise in the coherent communication systems is related in a simple way

$$\sigma_\varphi^2 = 4 \int_0^{+\infty} S_{\Delta\nu}(f) \frac{\sin^2(\pi f \tau_0)}{f^2} df, \quad (2.14)$$

where  $\tau_0$  is the symbol duration time and  $\sigma_\varphi^2$  represents the variance of the phase noise in the communication system. You may also ask 'is it possible that we can relate the lineshape to the frequency noise PSD so that the phase noise can be expressed as a function of the linewidth'. The answer to that question is, unfortunately, generally no. There is one special case in which those two measures can be used interchangeably and that is the laser frequency noise PSD being white [24]. Practically, due to the technical noise from current, environment, temperature controller and so on, the frequency noise PSD of semiconductor lasers is never white.

However, as both measures can be utilized reasonably to characterize laser coherence, they must be related to each other in some way. Such a subject will be discussed in detail in

Chapter 5, where a general relation between laser frequency noise PSD and lineshape is derived.

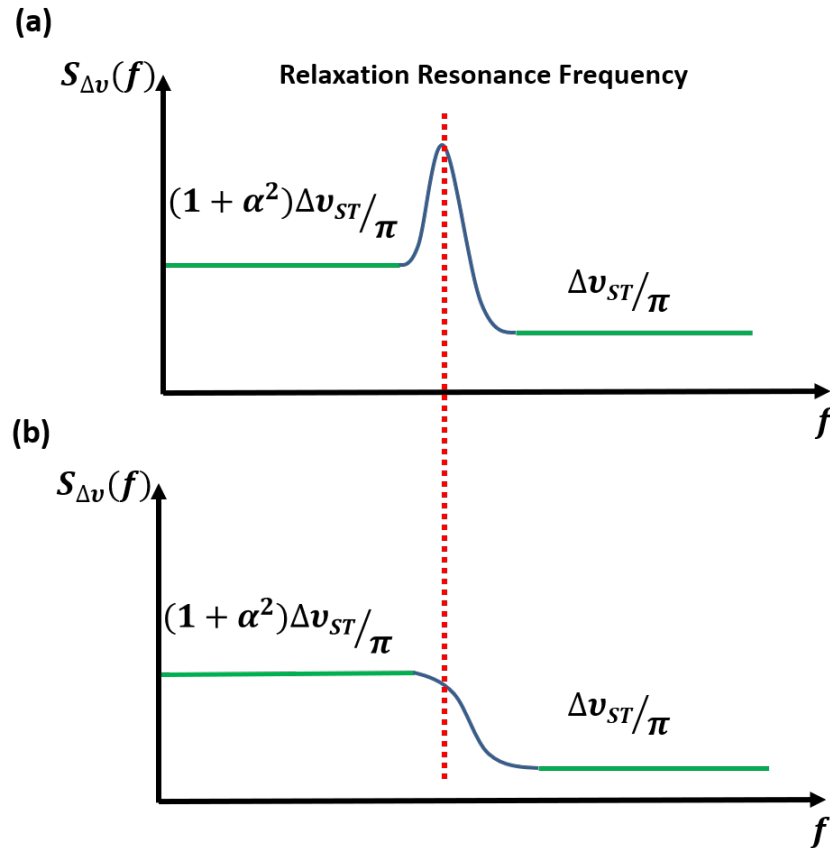


Figure 2.4 Frequency noise PSD of semiconductor lasers when (a) photon lifetime  $\ll$  electron lifetime and (b) photon lifetime  $\sim$  electron lifetime

## 2.2 High-coherence Si/III-V lasers

In the remainder, we will apply the theories to designing the high-coherence Si/III-V lasers. After that, we will present the fabrication process and the properties of the Si/III-V lasers.

### 2.2.1 Reduce quantum noise with mode engineering

To enhance the coherence of semiconductor lasers, we shall suppress the spontaneous emission rate

$$W_{sp} = \frac{\pi q^2 \omega}{\varepsilon} |\langle V | \vec{e} \cdot \vec{x} | C \rangle|^2 g(\omega) |u(\vec{r})|^2. \quad (2.15)$$

It can be accomplished by engineering the laser structure to reduce the mode confinement  $|u(\vec{r})|^2$  inside quantum wells. However, it inevitably leads to the reduction of the stimulated emission rate, the gain of semiconductor lasers

$$W_{st} = \frac{\pi q^2 \omega}{\varepsilon} |\langle V | \vec{e} \cdot \vec{x} | C \rangle|^2 N_p g(\omega) |u(\vec{r})|^2. \quad (2.16)$$

If the gain gets reduced significantly while the loss maintains, the threshold of the lasers would surge. To overcome such a problem, the loss of the lasers must be decreased by the same amount. It can be achieved by storing the optical energy pulled out of the gain materials, which are lossy due to heavy doping, in other materials with ultra-low loss. This mode engineering approach is not new. As a matter of fact, it is exactly why ECLs are very coherent. In that case, the optical energy is moved out of the lossy III-V materials and stored in the low-loss external cavities made of air or silica. The disadvantages of the external cavities have been discussed in chapter 1. What we intend to achieve here is effectively to replace the external cavities with low-loss silicon resonators, which can be heterogeneously integrated with III-V materials.

Besides, a large amount of photons can be stored in the low-loss silicon resonators. Thus, the S-T linewidth, which is proportional to the ratio between the spontaneous emission rate and the stored photon number, can be substantially reduced.

### 2.2.2 Hybrid Si/III-V lasers

The very first hybrid Si/III-V Fabry-Perot (FP) laser was demonstrated by John Bower's group at university of California, Santa Barbara (UCSB) [25]. The newly developed wafer bonding technology enables the heterogeneous integration, which allows us to fabricate the Si/III-V lasers with CMOS-compatible wafer-scale processing.

The structure of the high-coherence Si/III-V laser is shown in Fig. 2.5, with the III-V die on top of the silicon-on-insulator (SOI) substrate. The detailed layer structure of the III-V dies can be found elsewhere [26]. N-contact layers (n-doped InP) are bonded to the silicon substrate while P-contact layers (p-doped InP) are etched to form the mesa structure, defining the current path. A layer of silicon dioxide is deposited on top of the P-contact layers, preventing current leakage, on which a small window is opened for the electrical contact. The current is injected through the center piece of the mesa, to which the optical mode is evanescently coupled.

The lasing mode is mostly confined in the silicon rather than the III-V materials, of which the intensity profile is shown in Fig. 2.5. A thin layer of silicon dioxide, i.e. the spacer, is placed between the III-V materials and the silicon substrate, whose thickness can be adjusted during the fabrication process in order to tune the mode confinement factor in the quantum wells and therefore the phase coherence of the lasers. Theoretically, the Si/III-V lasers with thicker spacer are more coherent. However, the reckless increase of the spacer thickness may lead to a penalty on the threshold. As discussed in the previous section, in order to maintain the laser threshold, we need to make sure the gain and the loss get reduced by the same factor, which can only be achieved if the loss of the optical energy in the low-loss materials is negligible. However, as we move more and more optical energy into the silicon, to the point when the total loss in the silicon becomes comparable to the total loss in the III-V materials, the decrease of the gain would exceed the decrease of the loss, resulting in the increase of the laser threshold. In our experiments, the spacer thickness is kept below 100 nm.

The detailed fabrication process of the Si/III-V lasers can be found elsewhere [26-29]. Here, we simply show the flow chart in Fig. 2.6 (a) and briefly talk about each step, giving you some sense of how hybrid Si/III-V lasers are fabricated. The same fabrication techniques can be applied to other hybrid platforms.

First, the silicon resonators are fabricated with e-beam lithography followed by two-step plasma etching. A thin layer of chrome is used as the hard mask for the second etching to

avoid the aspect ratio effect. An SEM image of a typical silicon resonator is shown in Fig. 2.6 (b).

Second, the III-V dies are wafer-bonded onto the silicon substrates with their original substrates removed afterwards using chemicals. The surface of the silicon resonators and the III-V dies must stay extremely clean for the success of wafer-bonding. At this point, we have achieved the heterogenous integration, of which an optical image is shown in Fig. 2.6 (c).

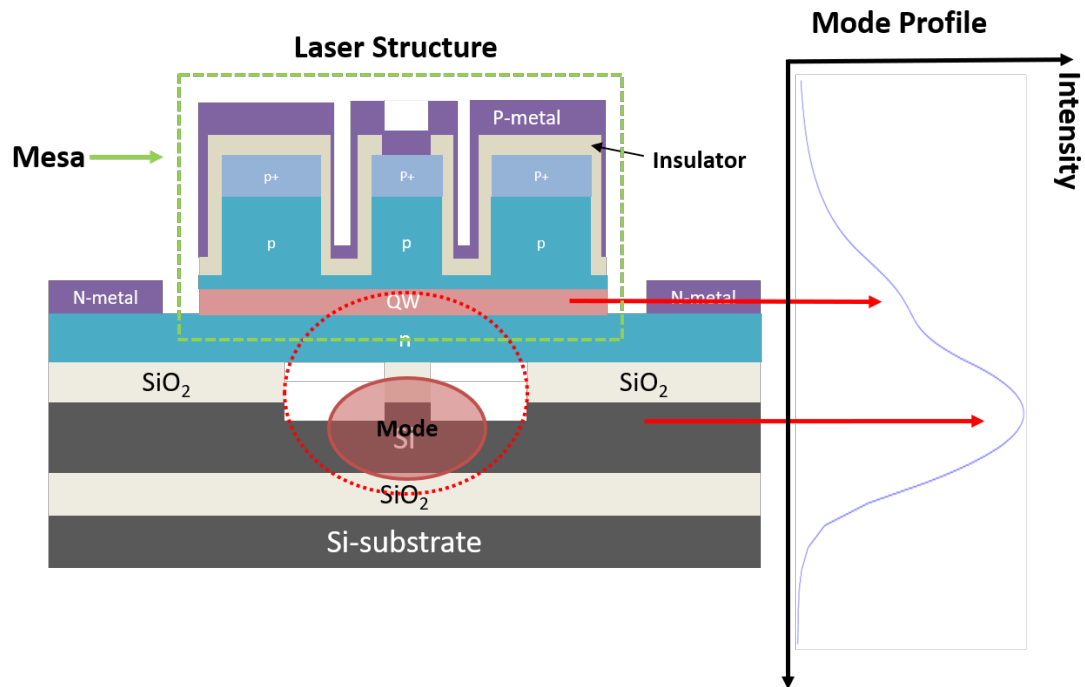
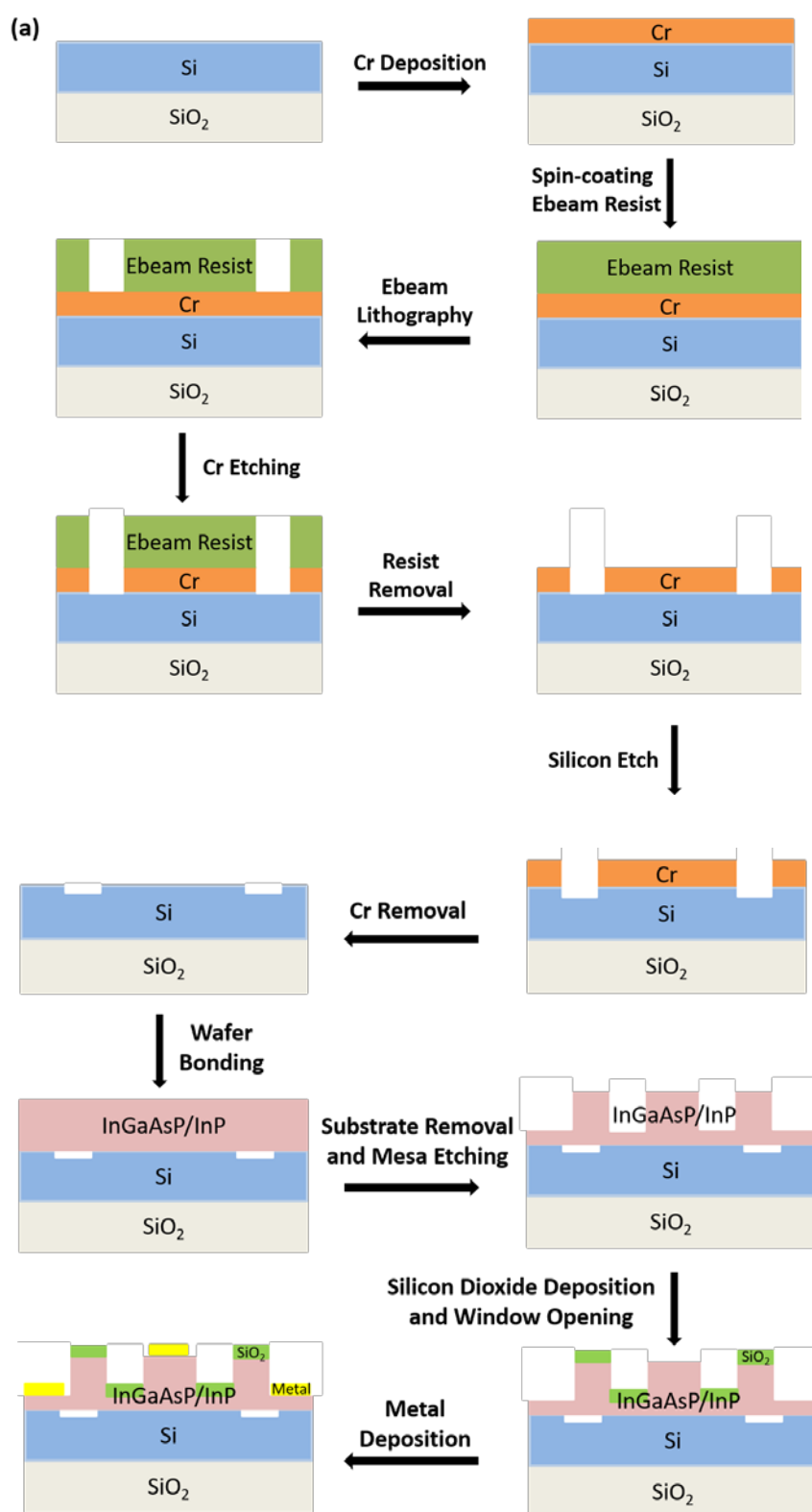


Figure 2.5 Structure and mode profile of Si/III-V lasers. The red dash line indicates that the lasing mode is evanescently coupled to the quantum wells

Third, the mesa structure is defined on the remaining III-V materials with multi-step photolithography and wet etching. Afterwards, a layer of silicon dioxide is deposited using chemical vapor deposition (CVD). A window is then opened on the silicon dioxide layer for metal contacts.

At last, metal contacts are deposited onto the mesa. Rapid thermal annealing (RTA) is often applied to the chips for good ohmic contacts. The final laser chips are shown in Fig. 2.6 (d). There are hundreds of laser devices on a single chip. After lapping and cleaving, we can measure the properties of individual devices, which will be presented in the following sections.



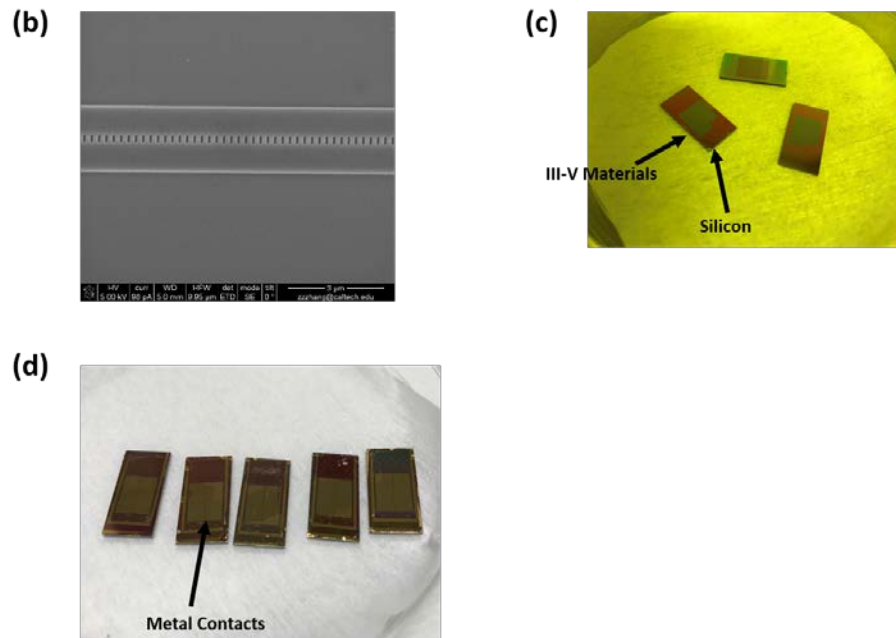


Figure 2.6 (a) Flow chart of laser fabrication, (b) SEM image of the silicon resonator, (c) Optical image of the laser chip after wafer-bonding and (d) Optical image of the final laser chip

### 2.2.3 Laser characterization: power and spectrum

The power-current curves under various temperature and the optical spectrum of the hybrid Si/III-V laser are shown in Fig. 2.7 (a) and (b), respectively. The laser has a threshold of roughly 60 mA, more than 3 mW output power under room temperature and a side mode suppression ratio (SMSR) over 50 dB. The maximum current that can be pumped into the laser is about 160 mA, beyond which the laser output power drops because of thermal effects. Compared to commercial III-V DFB lasers, the efficiency of the Si/III-V laser is low. This is probably because the quality of the quantum wells gets degraded during the wafer bonding process.

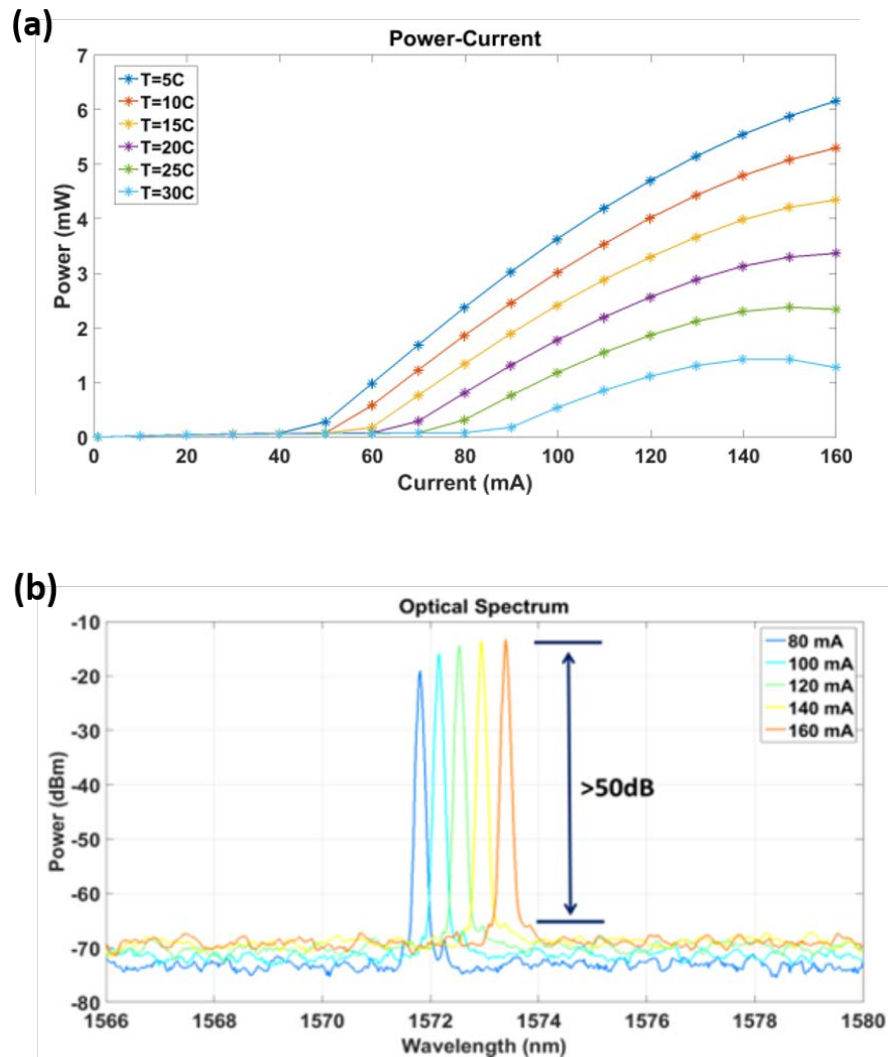


Figure 2.7 (a) LIV curves under various temperature and (b) optical spectra of Si/III-V lasers

#### 2.2.4 Laser characterization: relaxation resonance frequency and alpha parameter

We have introduced the concepts of the alpha parameter and the relaxation resonance frequency in section 2.1.2 and 2.1.3, respectively, and discussed what roles they play in laser frequency noise PSD in section 2.1.4. Those two critical parameters of the Si/III-V lasers can be obtained by measuring the lasers' direct current modulation responses including both the intensity and frequency modulation responses. The relaxation resonance frequency is the modulation bandwidth and the alpha parameter, representing the coupling strength between

laser intensity and frequency noises, can be obtained by taking the ratio between the frequency and intensity modulation depths [30].

The measurement setup is shown in Fig. 2.8. The laser's intensity and frequency modulation responses are measured with the first and second optoelectronic loops, respectively. The network analyzer produces small electrical modulation signals and measures the response. In the frequency modulation response measurement, a Mach-Zehnder interferometer (MZI) is utilized as the frequency discriminator, with the laser locked to its quadrature point using an electrical feedback circuit.

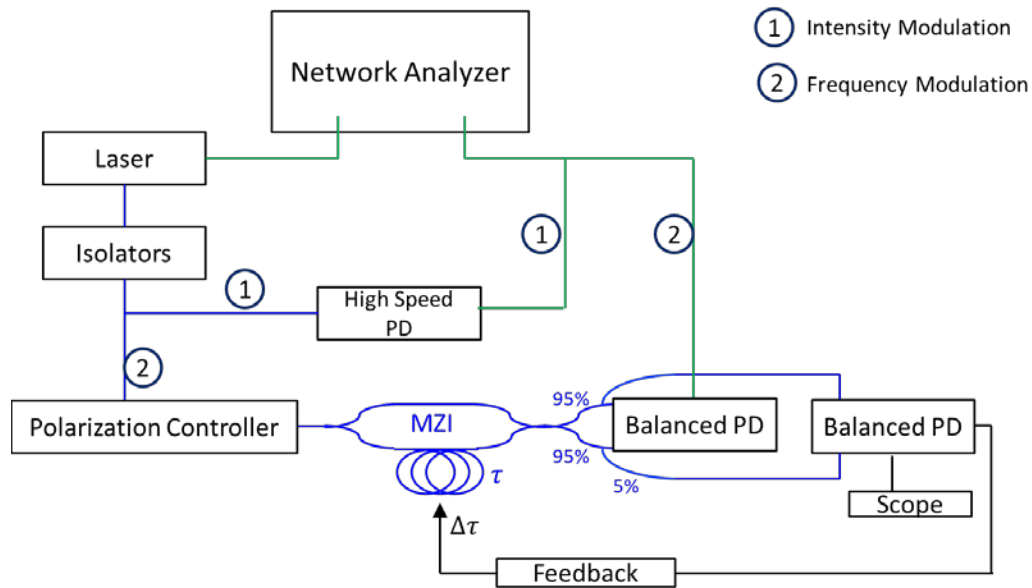


Figure 2.8 Measurement setups for laser modulation response

The Si/III-V laser's modulation responses are displayed in Fig. 2.9. Both the intensity and frequency modulation responses start to roll off at the relaxation resonance frequency, which is around 1 GHz. The ratio between the frequency and intensity modulation depths, indicating the coupling between laser intensity and frequency noise, is shown in the inset in Fig. 2.9. At relatively low frequencies, thermal effects are dominant as the thermo-optic coefficient of silicon is quite large. At high frequencies, thermal effects, due to their slow dynamics, become negligible and the coupling is purely due to carrier effects, i.e. linewidth

enhancement. The ratio curve in the inset approaches to a constant at high frequencies, which is the alpha parameter with a value of 2.57 in this case.

In addition to laser frequency noise PSD, the coupling between laser intensity and frequency noise plays an important role in lasers' feedback sensitivity. We will come back to the ratio curve in Chapter 4, where the feedback sensitivity of the Si/III-V laser is investigated.

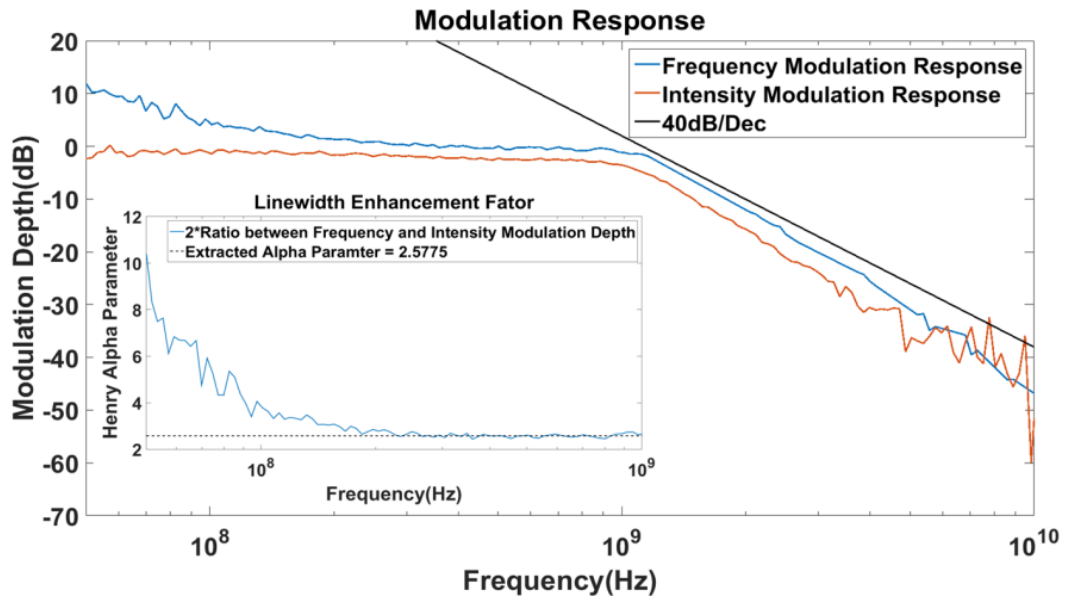


Figure 2.9 Modulation responses and alpha parameters of Si/III-V lasers

### 2.2.5 Laser characterization: frequency noise PSD

Finally, it comes to examining the coherence of the Si/III-V lasers. The setup for measuring laser frequency noise PSD is shown in Fig. 2.10. An MZI with a free spectral range (FSR) of roughly 1.5 GHz is used as the frequency discriminator. The laser is locked to its quadrature point with the same electrical feedback circuit used for frequency modulation response measurement. Balanced photodetectors are used to minimize the effects of the intensity noise on the measurement. The laser frequency noise PSD can be derived based on the PSD of the output of the balanced photodetectors [26, 31-33].

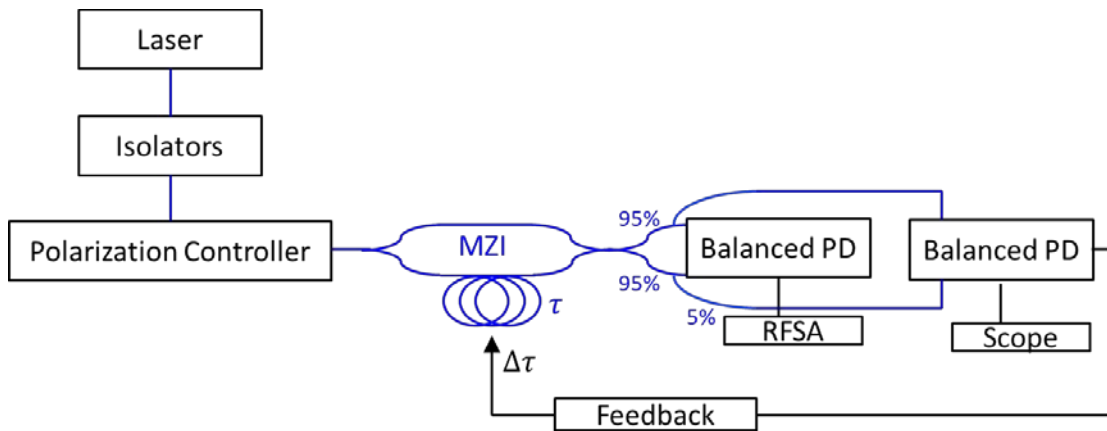


Figure 2.10 Measure setup for laser frequency noise PSD. RFSA: radio frequency spectrum analyzer

The results are shown in Fig. 2.11. Due to the response bandwidth of the MZI, we can only measure the frequency noise PSD below the relaxation resonance frequency. The measured frequency noise PSD corresponds to a  $\Delta\nu_H$  of 5.4 KHz. Using the alpha parameter obtained in the previous section, the S-T linewidth  $\Delta\nu_{ST}$  is calculated to be about 0.7 KHz.

For comparison, the frequency noise PSD of a typical commercial III-V DFB laser is displayed in Fig. 2.12. The  $\Delta\nu_H$  of the III-V DFB laser is on the order of MHz and the relaxation resonance frequency is around 10 GHz. Using equation (2.13) and assuming a modulation frequency of 20 GHz, the Si/III-V lasers generate at least an order of magnitude less phase noise than the commercial III-V DFB lasers in the coherent optical communications.

It is important to point out that the frequency noise around the relaxation resonance frequency of the III-V DFB laser contributes significantly to the phase noise due to its large magnitude and high bandwidth. Hence, the high coherence of the Si/III-V laser truly means low quantum noise, a small relaxation resonance frequency and a damped current modulation response, all of which are direct consequences of a large photon lifetime.

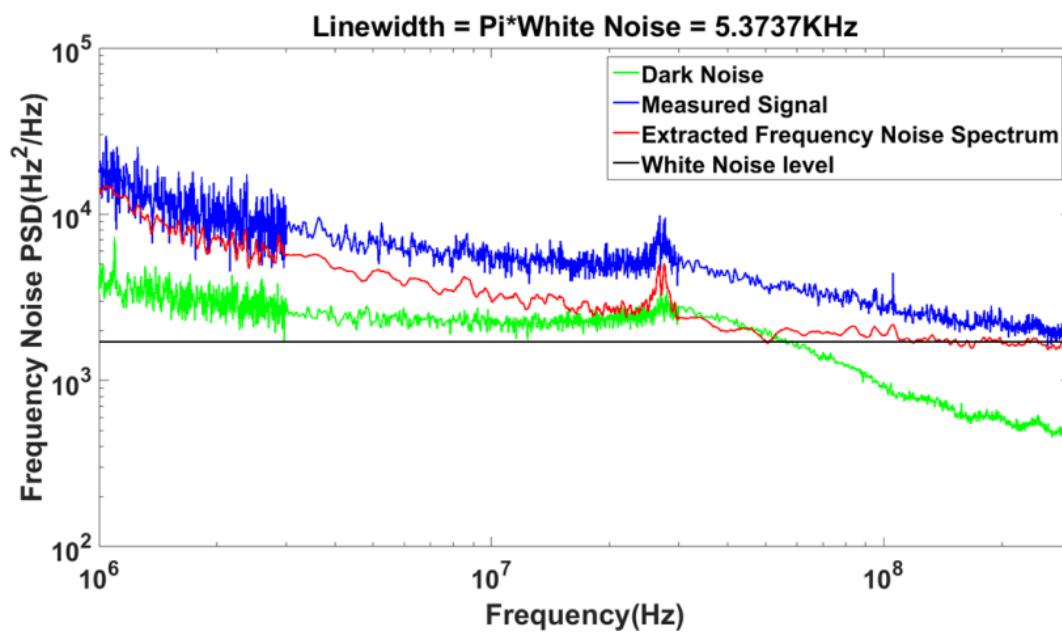


Figure 2.11 Frequency noise PSD of the Si/III-V laser

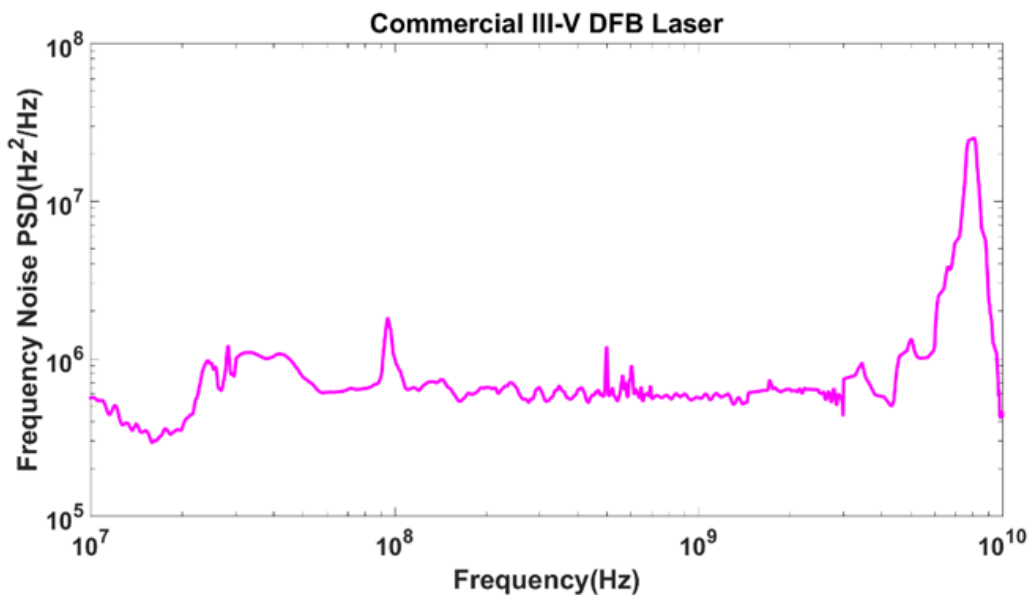


Figure 2.12 Frequency noise PSD of a commercial III-V DFB laser

### **2.3 Conclusions**

In this chapter, we have discussed how to design and fabricate high-coherence Si/III-V lasers and characterized their properties. With the merits of possessing both monolithic structure and high phase coherence, the hybrid Si/III-V lasers have great potential to be the light sources in the upcoming coherent optical communication systems.

## COHERENT OPTICAL COMMUNICATION

Coherent optical communication, as discussed in chapter 1, is considered as the indispensable solution to the ever-increasing demands for the data rate. Unlike traditional incoherent optical communications, they employ more complex modulation formats, leading to the fact that most electronic and photonic components in the coherent optical communication networks, such as modulators, demodulators and signal processing modules, are much different from their conventional counterparts. Here, we will give an overview of how information is encoded, decoded and processed in the coherent optical communications. Afterwards, the performance of the high-coherence Si/III-V lasers in the coherent optical communication system will be presented in comparison to the performance of a conventional III-V DFB laser and a commercial ECL.

### **3.1 Fundamentals of coherent optical communications**

A coherent optical communication link is shown schematically in Fig. 3.1, where a transmitter and a receiver are connected to each other with an optical fiber.

The transmitter consists of a laser as the light source and a dual-polarization IQ modulator for polarization division multiplexing (PDM). To fully use the capacity of optical fibers, different information can be encoded in the polarization as well as laser intensity and phase, by splitting the laser light into two beams, modulating them separately, rotating the polarization of one laser light by 90 degrees and eventually combining them together. Those are exactly the functions of IQ modulators.

In the receiver, lights with orthogonal polarizations are separated and then demodulated in a dual-polarization IQ demodulator, where the electro-optical conversion takes place. The obtained electrical signals must be processed digitally for the encoded information to be correctly retrieved, where multiple algorithms are applied for signal processing.

The details on how the IQ modulators and demodulators are physically constructed will be revealed in the following sections, which can help us understand how information is encoded and decoded in the coherent optical communications.

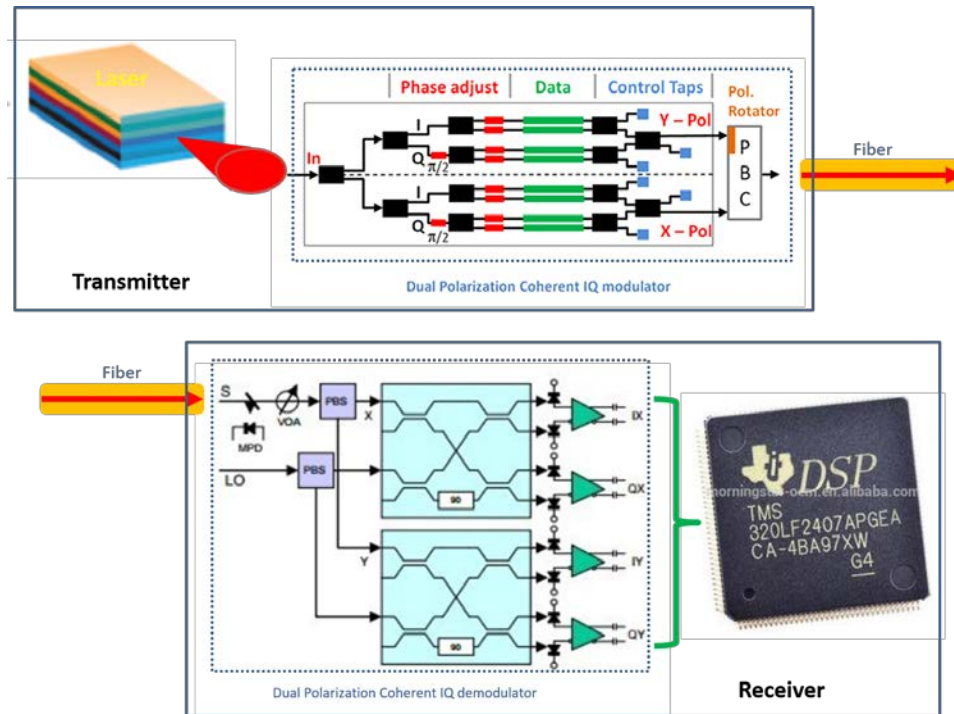


Figure 3.1 A coherent optical communication link

### 3.1.1 Quadrature amplitude modulation

The schematic structure of the IQ modulators is shown in Fig. 3.2 (a). Each lane in the figure represents a waveguide. The refractive index of a waveguide, which is flanked by two electrodes, can be tuned by applying different voltages, making such a structure a phase modulator. Two phase modulators connected by two 50/50 couplers and sharing the same ground constitute a Mach-Zehnder modulator (MZM), which is used for intensity modulation.

The IQ modulator works as follows. The laser field is equally split into two at the input. The two optical fields, known as in-phase and quadrature components, travel along two different

paths, where their intensity and phase are modulated independently, and eventually are combined at the output

$$\frac{E_{out}(t)}{E_{in}(t)} = \underbrace{\frac{1}{\sqrt{2}} \cos\left(\frac{u_I(t)}{2V_\pi} \pi\right)}_{\text{In Phase}} + i \underbrace{\frac{1}{\sqrt{2}} \cos\left(\frac{u_Q(t)}{2V_\pi} \pi\right)}_{\text{Quadrature}}, \quad (3.1)$$

where  $E_{in}(t)$  and  $E_{out}(t)$  represent the input and output optical fields.  $u_I(t)$  and  $u_Q(t)$  are the digitalized voltage signals applied to the MZMs, modulating the intensity of the in-phase and quadrature components, respectively.  $V_\pi$ , a key parameter of the MZM, denotes the voltage at which the phase difference between the two phase modulators is  $\pi$ .

This type of modulation is known as QAM, where both the amplitude and the phase of the light are modulated. To better illustrate that, an optical waveform of QAM is shown in Fig. 3.2 (b) as an example. The entire waveform consists of a sequence of optical pulses, each satisfying equation (3.1) and having independent amplitude and phase. The red and green arrows point to the places where the intensity and the phase of the pulses, due to modulation, are different. In the literature, we refer to each optical pulse as a symbol, i.e. the smallest unit carrying the information.

Conventionally, we use constellation diagrams, as shown in Fig. 3.2 (c), to represent the ensemble of the symbols, meaning that each symbol is mapped to a certain constellation in the diagram. We set the magnitudes of the in-phase and quadrature components as the two Cartesian coordinates. Hence, each symbol can be mapped to a certain point in that two-dimensional space, thus becoming a constellation. The amplitude and the phase of the symbol are now represented by the norm and the phase of its corresponding constellation. The set of all the constellations forms the constellation diagram. Each constellation diagram corresponds to a unique modulation format.

To encode the information, we map a sequence of bits to a certain constellation. If there are in total  $M = 2^N$  constellations, then each constellation represents a N-bit sequence. In other words, each symbol carries N bits of information. A quadrature-amplitude modulation

scheme with  $M$  constellations is referred to as M-QAM. In our experiments, both 16-QAM and 64-QAM are employed, whose constellation diagrams can be found in Fig. 3.2 (c).

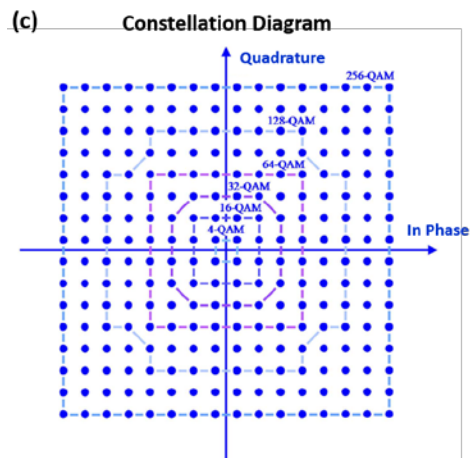
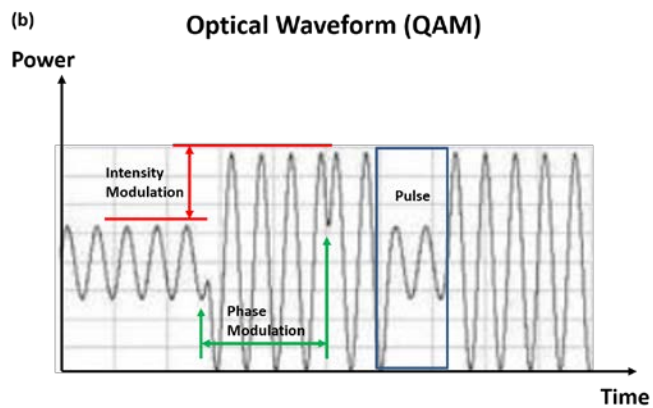
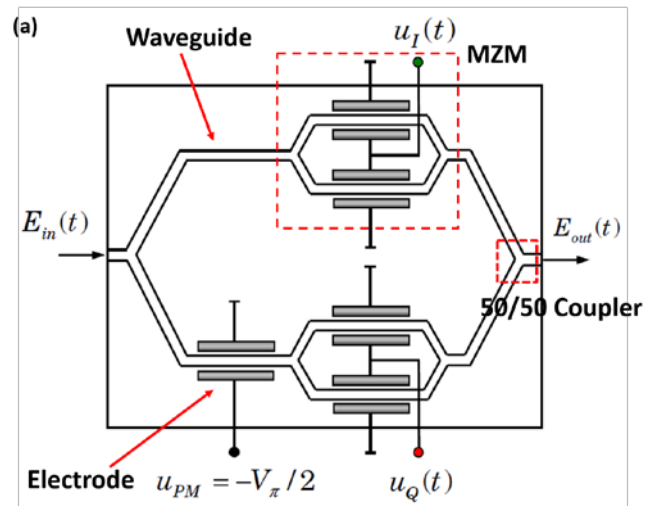


Figure 3.2 (a) An optical waveform of QAM, (b) Structure of an IQ modulator and (c) Constellation diagrams of QAM

### 3.1.2 Demodulation and detection

In the modulation process, mixing occurs between beams with orthogonal polarizations and between their in-phase and quadrature components. Demodulation is the reverse process of modulation, where different components get separated before the detection.

The structure of the IQ demodulators is shown schematically in Fig. 3.3 (a). A polarization beam splitter (PBS) is placed at the input to separate the optical fields with orthogonal polarizations. Each optical field and the light from a local oscillator (LO), a high-coherence tunable ECL in our case, are then hybridized in a 90 degree optical hybrid, which has two inputs and four outputs. Each output is composed of the two inputs with unique phase offsets, as shown in Fig. 3.3 (b). The phase offsets of two adjacent outputs differ by 90 degrees, which the name ‘90 degree optical hybrid’ implies.

In the detection process, two balanced photodetectors are used, each detecting two outputs of the four, whose phase offsets differ by 180 degrees, as shown in Fig. 3.3 (b). Assuming  $E_1(t)$  and  $E_2(t)$  are the LO and the signal, respectively, which can be expressed as

$$\begin{aligned} E_1(t) &= e^{i\omega_0 t} \\ E_2(t) &= a(t)e^{i\{\omega_0 t + b(t)\}}, \end{aligned} \quad (3.2)$$

where  $a(t)$  and  $b(t)$  represent the intensity and phase modulations, respectively, then the electrical signal from the upper balanced photodetector is

$$\text{Re}[a(t)e^{i\{b(t)+\varphi\}}] = a(t)\cos\{b(t) + \varphi\}, \quad (3.3)$$

where the ‘Re’ function takes the real part of a complex number and  $\varphi$  is a constant associated with the real structure of the 90 degree hybrid. It is equal to the in-phase component when  $\varphi$  vanishes. The signal from the lower balanced photodetector is

$$\text{Re}[ia(t)e^{i\{b(t)+\varphi\}}] = a(t)\sin\{b(t) + \varphi\}, \quad (3.4)$$

which is the quadrature component when  $\varphi$  vanishes. Hence, we have successfully separated the in-phase and quadrature components.

At this point, we have not retrieved the correct information yet as  $\varphi$  is still unknown. Besides, the previous analysis is valid only in ideal situations. Practically, different types of noise and the imperfection of the communication systems can distort the signals significantly. To extract the information correctly, the detected electrical signals need to be first digitalized by the analog to digital converter (ADC) and then processed digitally with multiple algorithms.

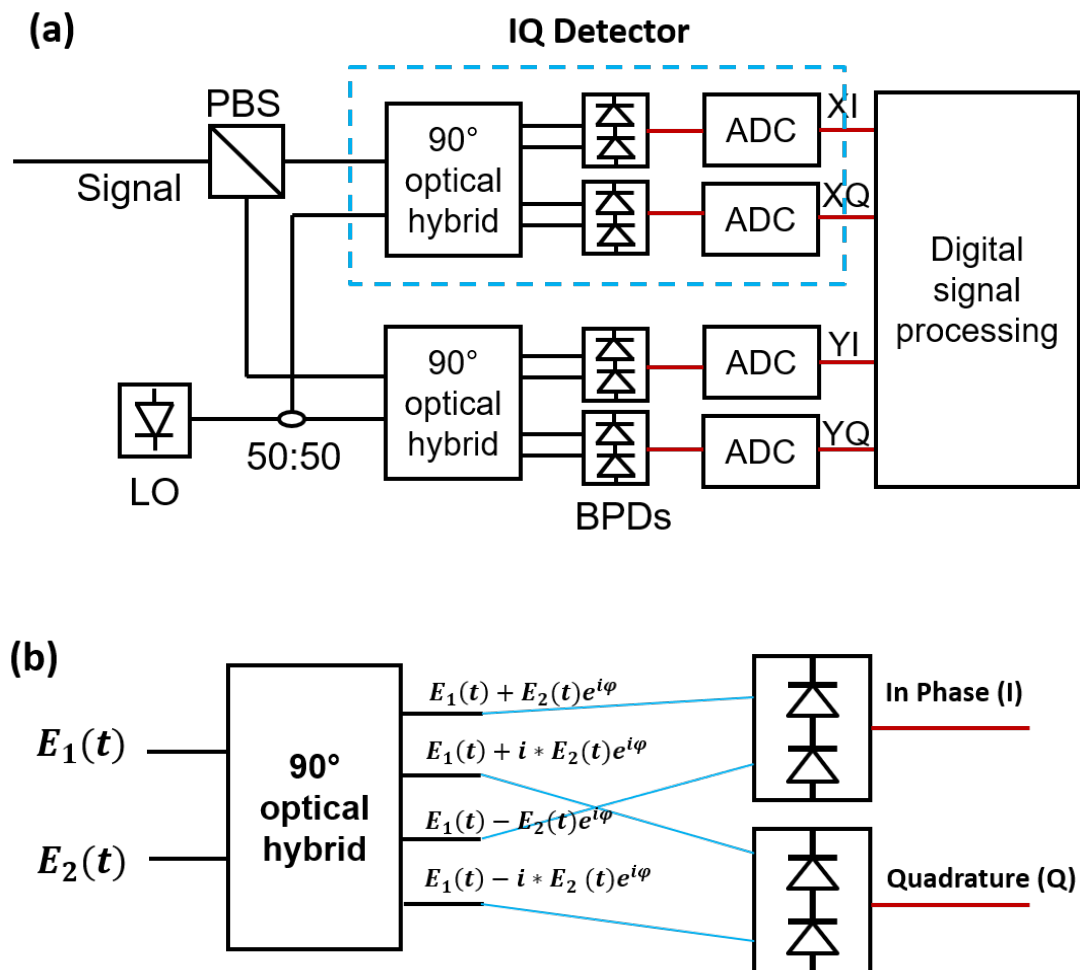


Figure 3.3 (a) Structure of coherent receivers (b) Demodulation

### 3.1.3 Digital signal processing (DSP)

The goal of DSP is to process the data in the electrical domain in order to mitigate impairments, both linear and nonlinear, deterministic and random. Generally speaking, there are two types of problems to be addressed in the DSP. The first one is the distortion of the detected signals, which usually arises from non-ideal communication channels and imperfect optoelectronic devices. For example, the polarization of the beams rotates while propagating in the single-mode optical fibers, causing crosstalk between signals encoded in the beams with orthogonal polarizations; the beating between the optical fields and the LOs is not strictly homodyne, leaving unwanted radio-frequency (RF) waves as the phase noise; the frequency response function of the electronics, such as amplifiers, is not flat within the modulation bandwidth, distorting the electrical pulses. Those problems should be resolved to get a decent signal to noise ratio.

The second type of problems is about the unknown initial phase of the signals. There is a variety of sources contributing to that initial phase, for example,  $\varphi$  in the previous analysis, which comes from the 90 degree hybrid. In addition, both the laser carrying the information and the LO have unknown initial phases, which are inherited by the electrical signals through the beating process. The arbitrary initial phase must be unwrapped or no phase information would be decoded correctly.

Our DSP module comprises seven functional blocks, as shown in Fig. 3.4. Each functional block represents an algorithm performing a certain task. The first functional block resamples the data, preparing the signals for the following processing. The next four functional blocks deal with the first type of problems. Polarization recovery deals with the polarization rotation of light in optical fibers, eliminating the crosstalk between the two channels with orthogonal polarizations. Dispersion compensation, just as the name implies, mitigates the effects of fiber dispersion. Frequency offset recovery finds out the beating frequency between the signal and the LO and compensates for its effects in the phase. Equalization deals with the non-flat frequency responses of the electronics.

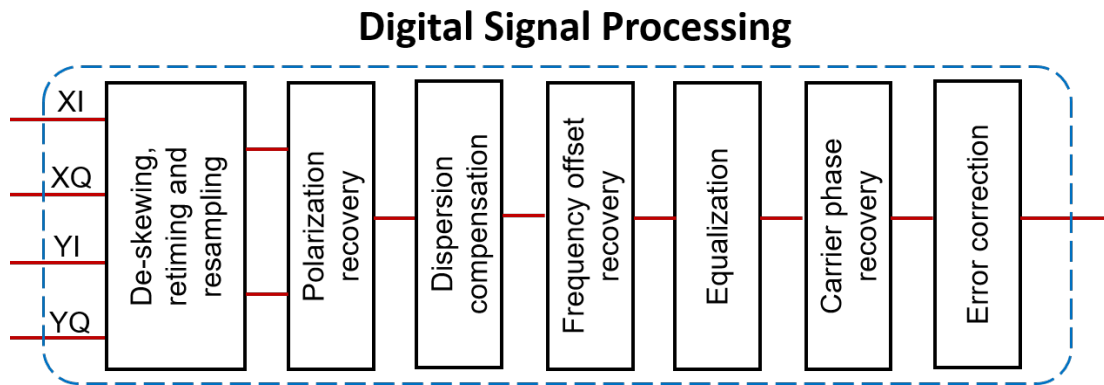


Figure 3.4 Digital signal processing module

Among those effects mentioned above, polarization rotation, dispersion and non-flat electronic response are naturally linear responses of the communication system, meaning that they can be mitigated by finding out the linear response function and applying its inverse function to the signals, which is exactly what these algorithms do. The frequency offset arises from the beating between the signal and the LO, a nonlinear process. The beating frequency can be figured out using Fourier transform. Its effect on the phase information would be subtracted digitally.

The sixth functional block, carrier phase recovery, is implemented to recover the unknown initial phase. As a matter of fact, it does more than that. If we treat the phase noise as a part of the unknown phase, the algorithm can be programmed adaptively not only to capture the initial phase, which is a constant, but also to predict the dynamic behaviors of the phase noise. Hence, after applying such an algorithm, the ultimate phase noise in the signals could be smaller than, but still related to, the value in equation (2.13). Plenty of phase recovery algorithms have been developed such as the one based on the Kalman filter, Viterbi-Viterbi (VV) algorithm and blind phase search (BPS) [34-36]. The latter two will be used in our experiments.

The goal of all the signal processing discussed so far is not eliminating all the errors but bringing the bit error rate (BER) down below a certain threshold so that the remaining errors can be corrected systematically. Usually, redundant bits, which are constructed following

certain rules, are encoded along with the information. Those rules impose strict relations between the information and the redundancy so that any error violating the rules can be detected and then corrected. After error correction, which is the last functional block in the DSP, the retrieved signal will be truly error-free and the information can be successfully decoded.

### **3.1.4 System performance**

Typically, we characterize lasers' system performance by measuring the BER as a function of optical signal to noise ratio (OSNR), which is defined to be the ratio between the laser output power and the power of optical white noise in a given bandwidth, typically 12.5 GHz.

When the OSNR is small, the dominant noise in the system is the intensity noise and therefore the BER becomes slightly dependent on the phase noise or the laser coherence. On the contrary, when the OSNR is large and the effects of the intensity noise can be neglected, the level of the phase noise solely determines the BER. In other words, the BER reaches its lower limit and stays constant at very high OSNR. Such a limit can only be lowered by decreasing the phase noise in the communication system, for example, using lasers with higher phase coherence.

The BER-OSNR curves under various levels of phase noise are depicted schematically in Fig. 3.5. Under the condition where there is no phase noise, the BER decreases rapidly as the OSNR increases, leading to a 'waterfall' curve (blue curve in Fig. 3.5). As the phase noise increases, the BER-OSNR curves become increasingly flat in the high OSNR region, where the BER reaches its lower limit.

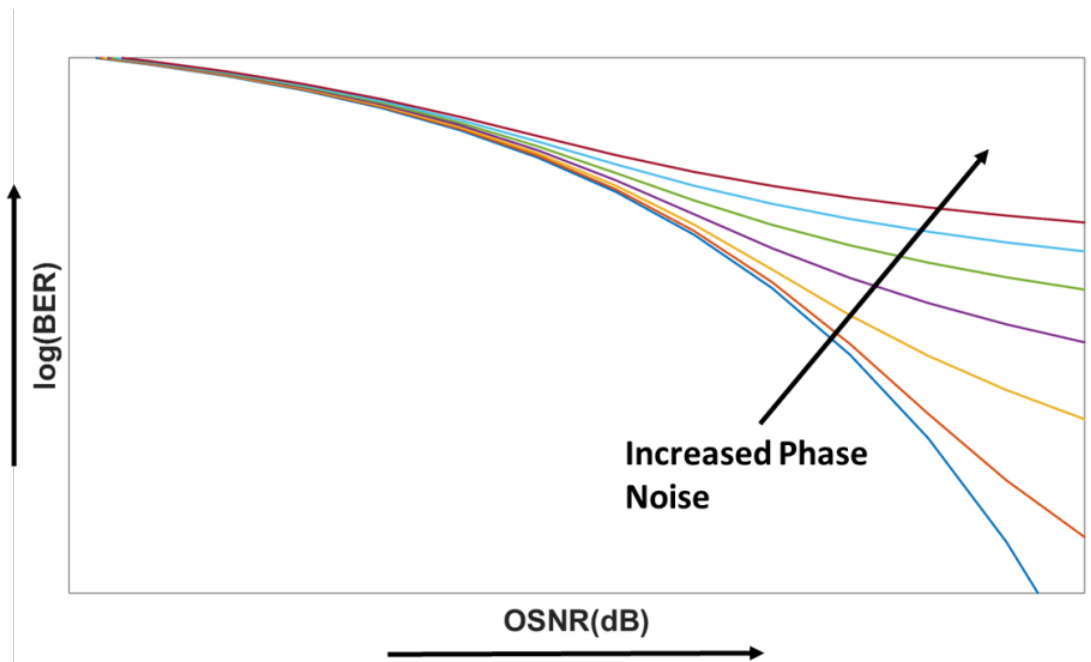


Figure 3.5 BER as a function of OSNR and phase noise. Black arrows indicate the direction in which the phase noise increases

### 3.2 Si/III-V lasers as the light sources

In this section, we will describe the use of the hybrid Si/III-V lasers as the light sources to conduct coherent optical communications. An ECL and a conventional III-V DFB laser, both of which are commercially available, are also tested for comparison.

#### 3.2.1 Back-to-Back coherent communications

We start with Back-to-Back (BTB) coherent optical communications. Back-to-Back means the output of the transmitter is connected to the input of the receiver with a very short optical fiber. In other words, the effects of communication channels such as dispersion and polarization rotation are negligible in this case.

The whole measurement setup is shown schematically in Fig. 3.6. The laser lights are loaded with 20 GBaud 16-QAM or 20 GBaud 64-QAM data signals, which are generated using an arbitrary waveform generator (AWG) operating at 92 GSa/s. The polarization of the light is adjusted with a polarization controller to minimize the insertion loss at the input of the IQ

modulator. An optical white noise source serves as the source of the intensity noise and a variable optical attenuator (VOA) is inserted into the communication link to tune the OSNR. The optical signals are coherently received with a tunable ECL as the LO. The decoded information is processed offline and the BER, as a function of the OSNR, is measured by error counting. As we want to measure the raw BER, there is no error correction in the DSP.

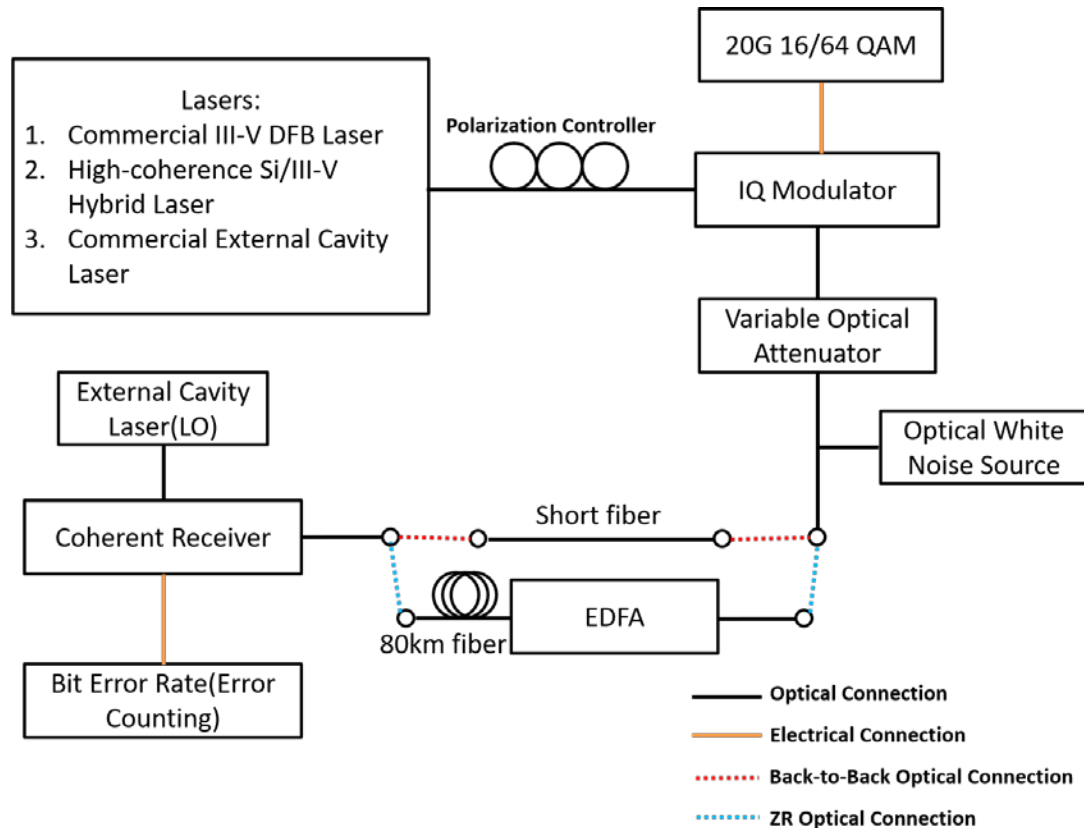


Figure 3.6 Measurement setup for coherent optical communications

### 3.2.2 Si/III-V laser vs III-V DFB laser vs external cavity laser

The frequency noise PSD of all three lasers used in the experiment is shown in Fig. 3.7. The conventional III-V DFB laser is much noisier than our Si/III-V laser and the ECL. The difference between the Si/III-V laser and the ECL is, however, marginal, with the ECL being slightly more coherent.

We have mentioned before in section 3.1.3 that phase recovery algorithms can reduce the phase noise in the communication systems and therefore modify the lasers' system performance to some extent, which will be demonstrated later. In our experiments, two types of phase recovery algorithms are used, namely VV and BPS. Comparing these two, BPS is more powerful and able to reduce the phase noise further than VV but requires more computing resources.

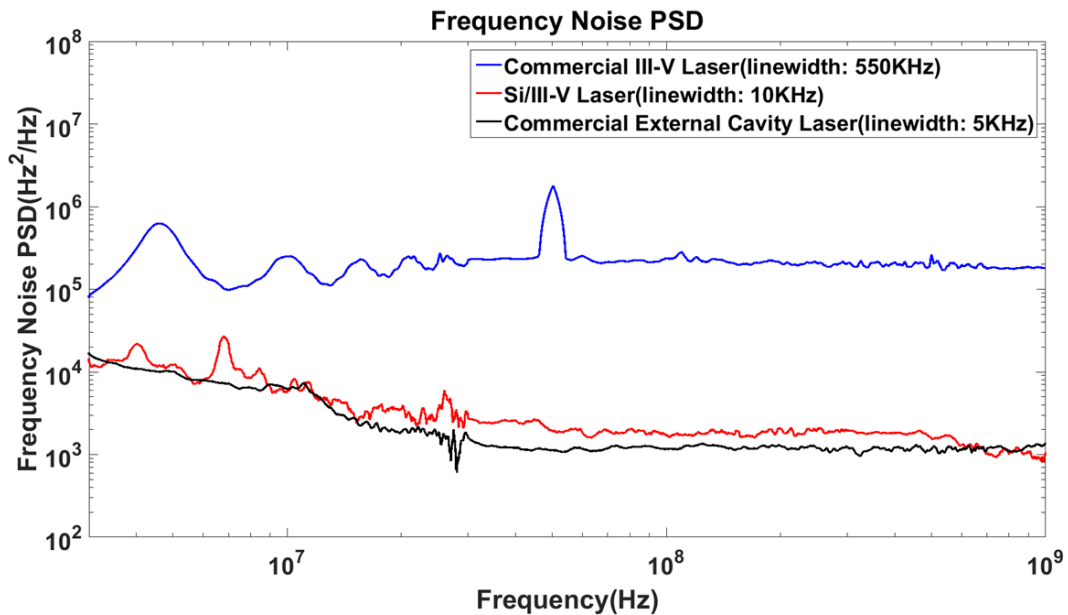


Figure 3.7 Frequency noise PSD of lasers used in the experiments

The 16-QAM results are shown in Fig. 3.8 (a). There is no significant difference between the Si/III-V laser and the ECL. The BER of those two lasers decreases sharply as the OSNR increases with no sign of reaching the lower bound, meaning that the level of the phase noise in the communication systems is quite low. Besides, different phase recovery algorithms do not lead to different system performance in those two cases.

In contrast, the BER of the III-V DFB laser with VV approaches to a constant at high OSNR, where the system performance is limited by the phase noise. With BPS, the BER does decrease monotonically as the OSNR increases as BPS helps to further reduce the phase

noise in the system but the III-V DFB laser's performance is still a little bit worse than the other two lasers at high OSNR, indicating slightly larger phase noise in the system.

The constellation diagrams in Fig. 3.8 (b) confirm our descriptions. The phase noise is negligible in all cases except one, the conventional III-V DFB laser with VV, where the shear deformation of the constellations indicates the existence of non-negligible phase noise.

The magenta dash line in Fig. 3.8 (a) represents the threshold of implementing hard-decision forward error correction (FEC), meaning that if the BER drops below the threshold, all the errors can be corrected using standard error correction methods with 7% overhead [37]. Such a condition can be met in all cases of 16-QAM. However, with VV, additional OSNR penalty of roughly 4 dB must be paid for the III-V DFB laser. With BPS, the III-V DFB laser performs as 'good' as the other two. But there are still downsides, which will be discussed later.

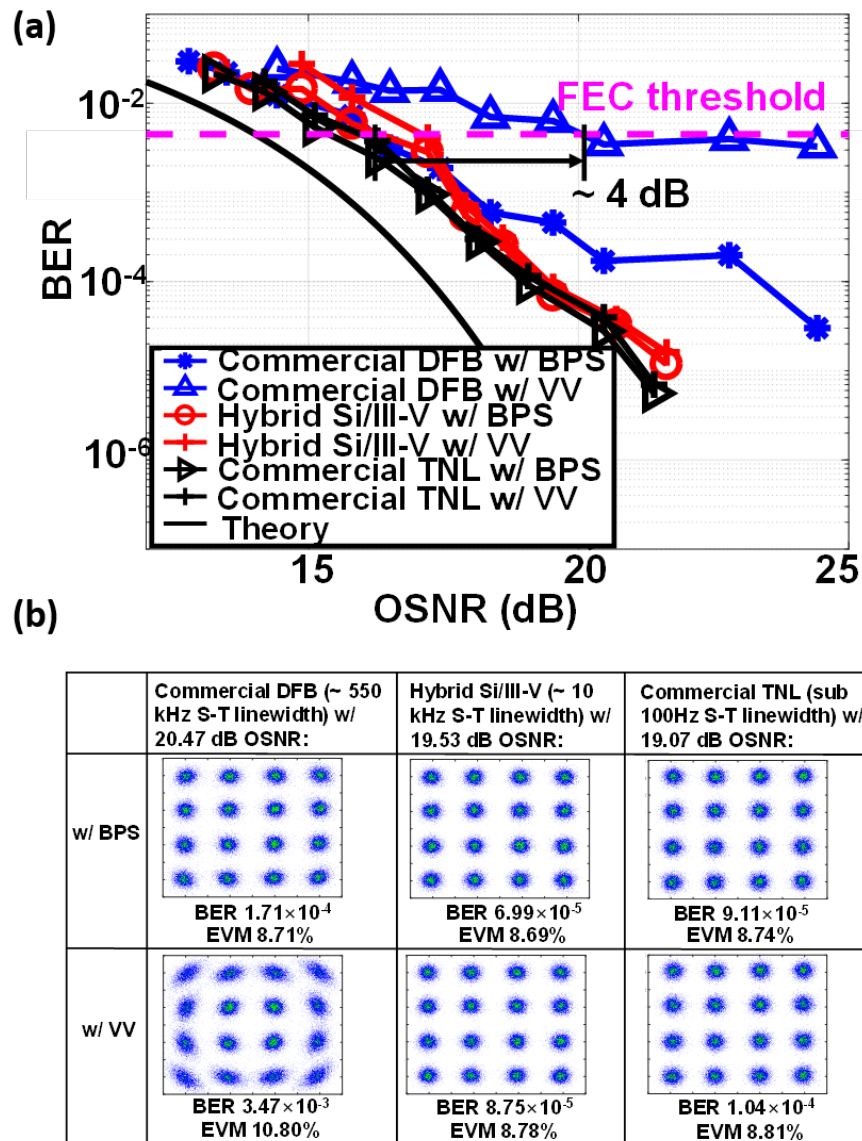


Figure 3.8 20 GBaud 16-QAM (a) system performance and (b) Constellation diagrams

Why those two phase recovery algorithms have significantly different impacts on the conventional III-V DFB laser but not on the Si/III-V laser or the ECL can be understood in the following way. Because of the high phase coherence of the Si/III-V laser and the ECL, the corresponding phase noise in the system is so small that as long as the phase recovery algorithm can successfully recover the constant initial phase, the performance would be good. Hence, using VV or BPS does not lead to much different system performance. For the

conventional III-V DFB laser, its much lower coherence results in much larger phase noise in the system. Therefore, with VV, which does not track the phase noise very closely, large phase noise still remains in the system while more powerful algorithms like BPS can help to suppress the phase noise a lot, leading to a dramatical improvement. That is exactly why we see the conventional III-V DFB laser performs so differently with those two algorithms.

At this point, one may wonder since phase recovery algorithms like BPS are so powerful, why do we need algorithms like VV or even high-coherence lasers for coherent optical communications? The answer to the question is twofold. First, the capability of phase recovery algorithms is limited. For example, the 64-QAM results are shown in Fig. 3.9, where BPS is used with all three lasers. Unlike 16-QAM, the performance of the III-V DFB laser cannot meet the condition of implementing hard-decision FEC in this case because BPS cannot reduce the phase noise to the level that 64-QAM can tolerate. Apparently, the effectiveness of phase recovery algorithms depends on both the laser coherence and the modulation format.

Second, as mentioned before, powerful algorithms like BPS require a great deal of computing resources, which inevitably increases the power consumption and the latency [38, 39], both of which are unfavorable in practical coherent communication networks. Hence, economically, monolithic high-coherence semiconductor lasers and simple phase recovery algorithms are the best combination for coherent optical communications, for example, the hybrid Si/III-V laser and VV for BTB 20GBaud 16-QAM.

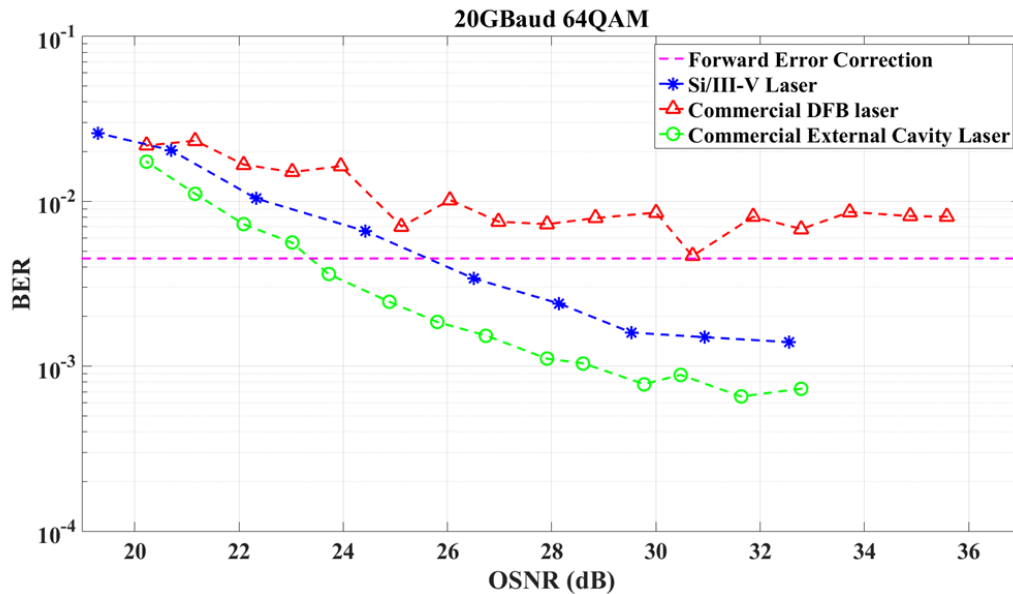


Figure 3.9 20 GBaud 64-QAM system performance

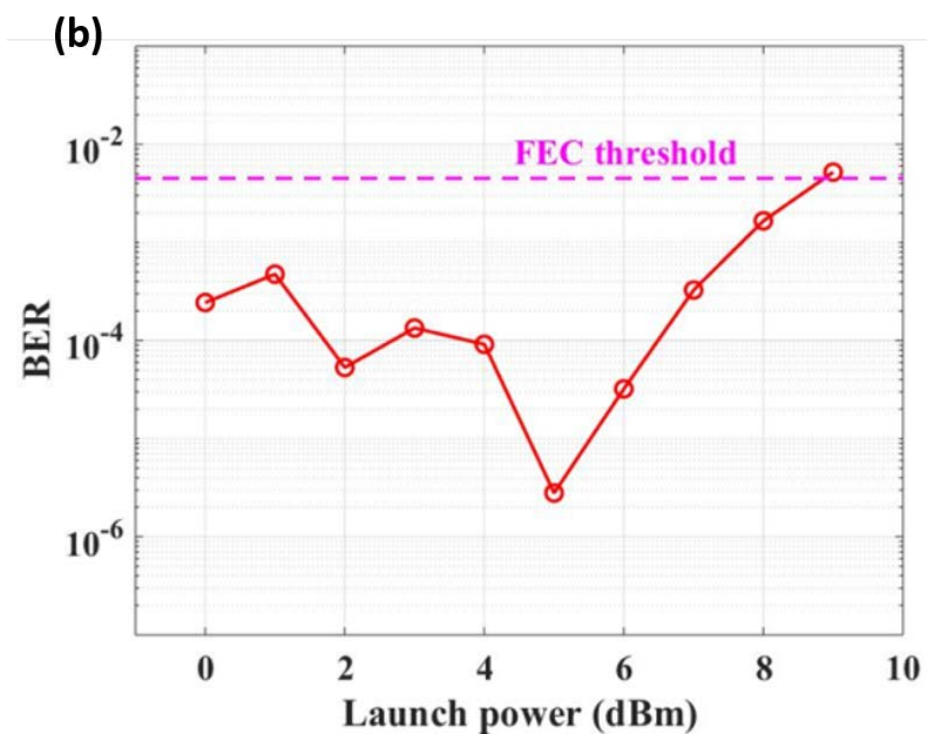
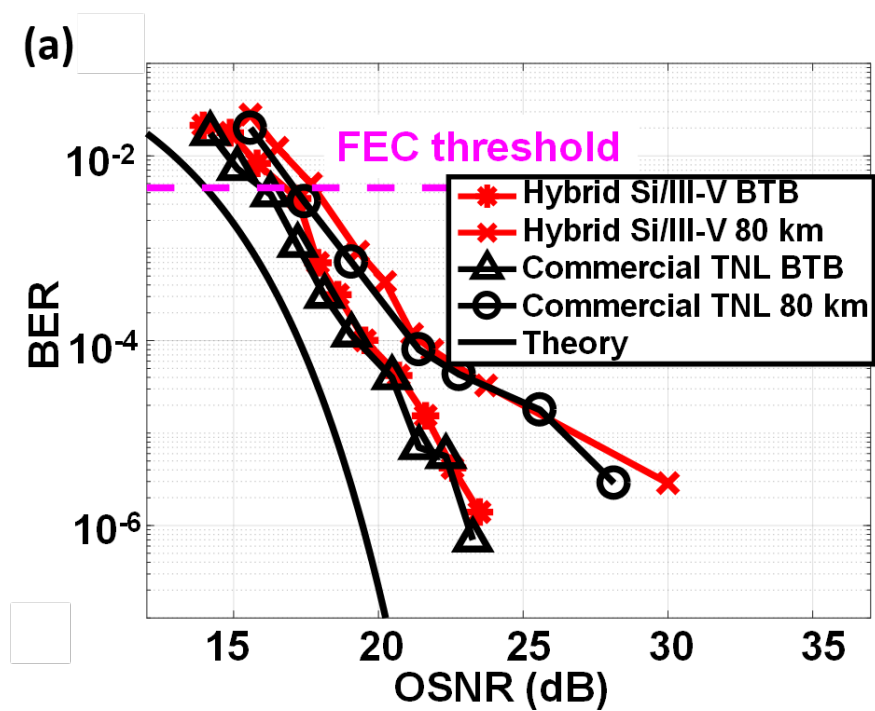
### 3.2.3 ZR coherent communications

In real-world applications, we conduct fiber optical communications within certain distances, where effects like dispersion, polarization rotation and fiber nonlinearity all come into play. Here, we investigate the lasers' performance in ZR coherent communications. ZR is a terminology for 80 km, which is approximately the range of metropolitan communications. The experimental setup is also shown in Fig. 3.6, where a short fiber connecting the transmitter to the receiver is replaced by an 80-km-long optical fiber and an erbium-doped optical amplifier (EDFA), which is used to compensate for the propagation loss.

The linear responses of the communication channel, including dispersion and polarization rotation, can be easily compensated by DSP, as discussed earlier. However, compensation for fiber nonlinearity remains challenging. Among all the types of fiber nonlinearity, we are mainly concerned about the Kerr nonlinearity. It induces intensity-dependent refractive index, which means intensity modulation and pulse broadening due to dispersion can result in unwanted phase modulation and thus a new source of phase noise, which is irrelevant to the laser coherence but dependent on the power. The BER in ZR coherent communications becomes dependent not only on the OSNR but also on the launch power at the input of the

fibers [40, 41]. Therefore, to achieve the best system performance, i.e. the lowest BER, the launch power into the fiber should be optimized.

The Si/III-V laser and the ECL are tested in ZR coherent optical communications, whose performance of 16-QAM and 64-QAM is shown in Fig. 3.10 (a) and (c), respectively. The two lasers still possess similar performance. The dependence of the BER on the launch power is shown in Fig. 3.10 (b) and (d), where the optimized launch power used for communication experiments corresponds to the lowest BER. Throughout the experiments, BPS is used for phase recovery because of nonlinearity-induced phase noise. Compared to BTB communications, there is degradation of the system performance, which can be mostly attributed to fiber nonlinearity. However, both lasers can still work with hard-decision FEC in both 16-QAM and 64-QAM.



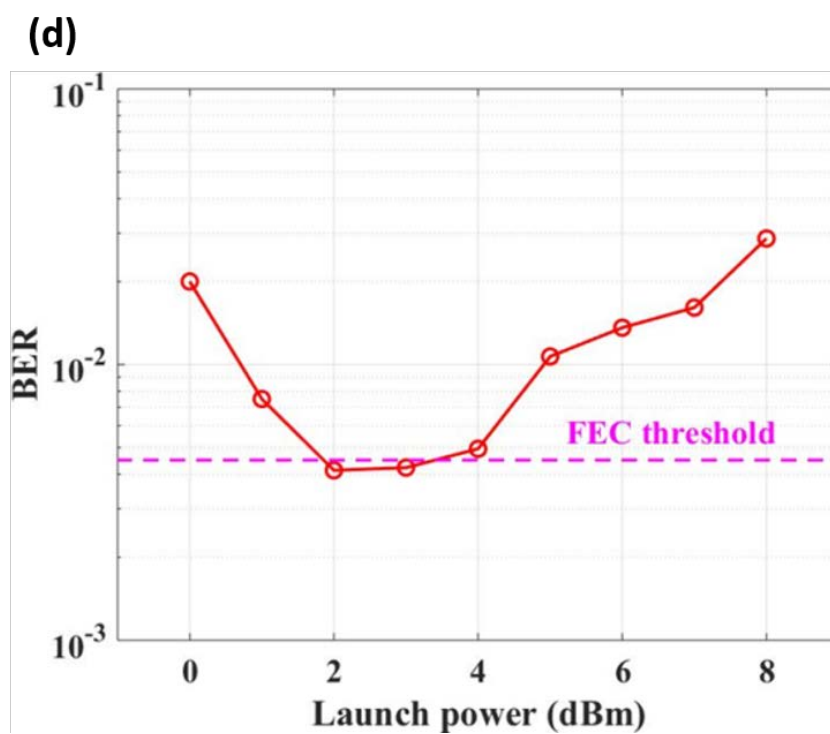
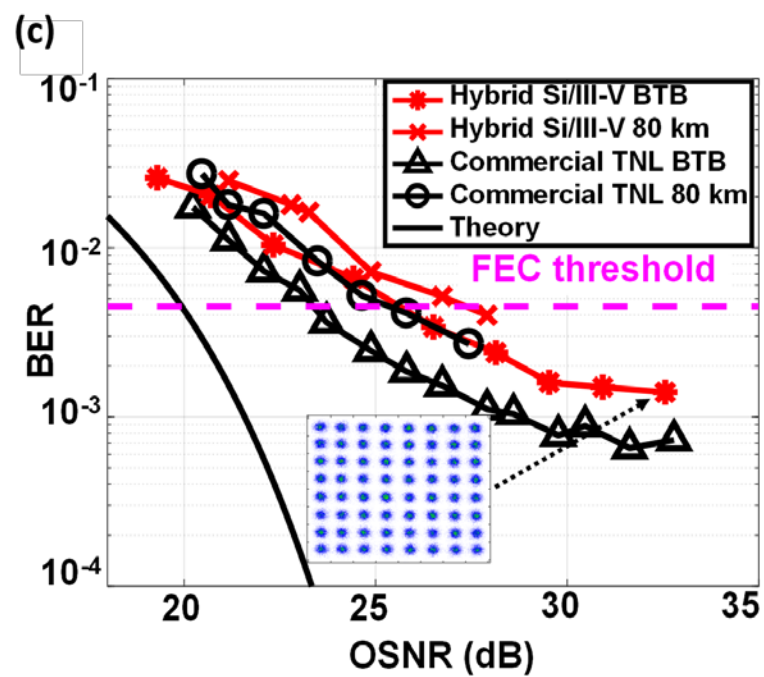


Figure 3.10 ZR communication system performance (a) 16-QAM (b) power optimization for 16-QAM (c) 64-QAM (d) power optimization for 64-QAM

### **3.3 Conclusions**

In this chapter, we have investigated the system performance of three different lasers, namely the ECL, the conventional III-V DFB laser and our high-coherence Si/III-V laser. As a result, the Si/III-V laser's performance is comparable to the ECL's and much better than the conventional III-V DFB laser's. Hence, the hybrid Si/III-V lasers, with their monolithic structure and high phase coherence, are very promising light sources for future coherent optical communication networks.

## FEEDBACK SENSITIVITY OF SEMICONDUCTOR LASERS

The historical studies on optical feedback's effects on semiconductor lasers can be dated back to 1980s. The properties of semiconductor lasers can be improved with very little optical feedback [42-44] while a slightly higher level of optical feedback can degrade semiconductor lasers, rendering them useless. In practical situations, the level of optical feedback varies from one scenario to another and cannot be precisely controlled. Conventionally, optical isolators are packaged with every semiconductor laser to mitigate optical feedback. However, as the field is moving rapidly towards photonic integration, optical isolators, which used to be the solution, now become the obstacle since they cannot be fabricated on chip, thwarting the integration between semiconductor lasers and other photonic devices. Consequently, we shall resolve the issue of optical feedback with a novel solution, which facilitates photonic integration. An appealing solution that we come up with is to develop monolithic semiconductor lasers with intrinsic insensitivity to optical feedback, which requires the lasers to be equipped with high-Q resonators to block a significant amount of optical feedback from entering. The hybrid Si/III-V lasers, with their high-Q resonators originally designed for high coherence, are expected to be very robust against optical feedback. Hence, the same lasers that we develop for coherent optical communication are now strong contenders to be the integrated light sources.

This chapter is organized as follows. In the first half of this chapter, we are going to establish the theories on how coherent and incoherent optical feedback affects laser frequency noise PSD, respectively. In the second half of this chapter, the feedback sensitivity of the Si/III-V laser is examined experimentally in comparison to a conventional III-V DFB laser without optical isolators. The results illustrate that the Si/III-V laser is capable of preserving its phase coherence under much larger optical feedback than the III-V DFB laser and functioning properly in the isolator-free coherent optical communications under conditions where the

performance of the III-V DFB laser degrades dramatically. In addition, we will verify the theories based on the experimental results.

#### 4.1 Coherent optical feedback and incoherent optical feedback

Optical feedback can be classified into two categories, namely coherent and incoherent optical feedback, as shown in Fig. 4.1. Coherent optical feedback, such as reflection from an external mirror, is explicitly correlated with the laser output while incoherent optical feedback, like amplified spontaneous emission (ASE), originates in a different and independent light source, such as an optical amplifier, and thus is uncorrelated with the laser output.

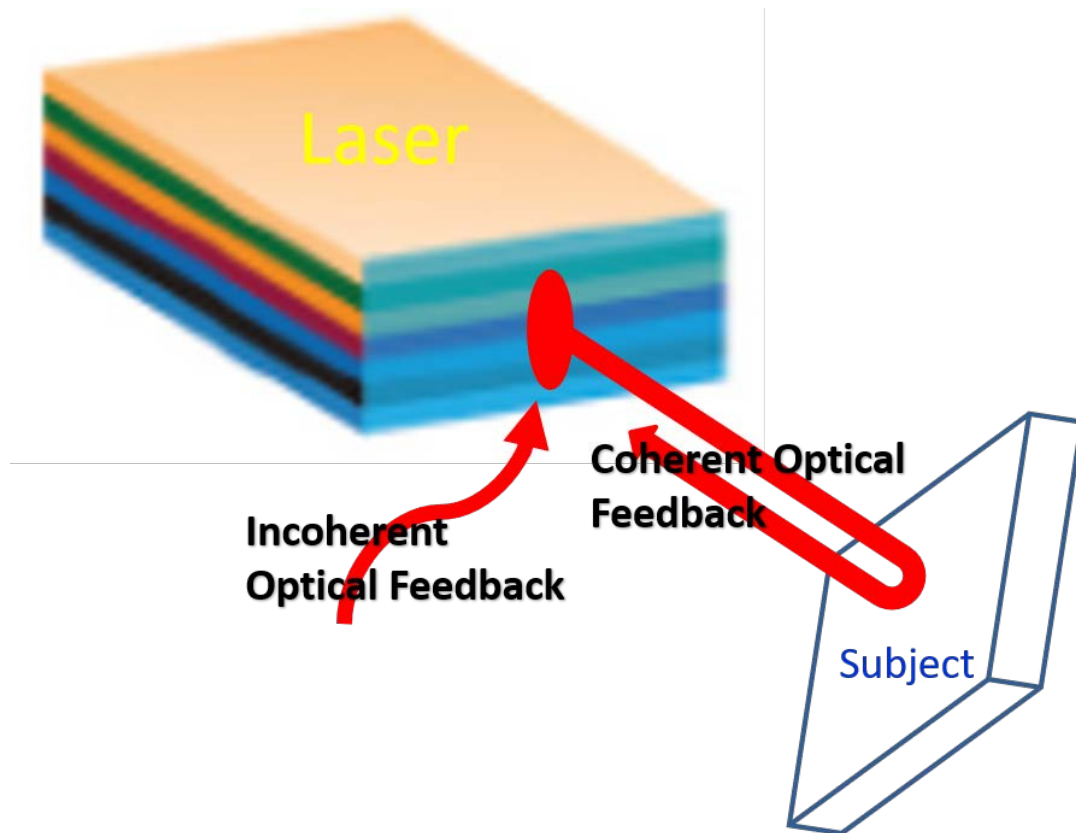


Figure 4.1 Optical feedback

In semiconductor lasers, spontaneous emission is the single noise source, which the intensity and phase noises arise from. The intensity noise is then coupled to the phase noise through

the mechanism of linewidth enhancement. The noise source and the coupling mechanism together determine the frequency noise PSD of semiconductor lasers, which has been discussed in chapter 2. By introducing optical feedback into the laser system, either the noise source or the coupling between laser intensity and phase noises changes, resulting in the modification of the laser frequency noise PSD and eventually affecting the lasers' performance in coherent optical communications.

#### 4.2 Coherent optical feedback effects on laser coherence

In this section, we analyze how coherent optical feedback modifies laser coherence, of which a simple model is shown schematically in Fig. 4.2. The noise source in this case is still spontaneous emission in the laser active region as external mirrors or equivalent are passive devices. However, due to the correlation between the coherent optical feedback and the laser internal field, additional coupling channels between the laser intensity and phase noises are created. The dynamic equations of laser noises under coherent optical feedback can be written as [45]

$$\dot{I}(t) = \{G(t) - \gamma_p\}I(t) + F_I(t) + \kappa r_{ext} \cos(\varphi)I(t - \tau) - A_0 \kappa r_{ext} \sin(\varphi)\{\Phi(t - \tau) - \Phi(t)\} \quad (4.1)$$

and

$$\dot{\Phi}(t) = \alpha\{G(t) - \gamma_p\} + F_\Phi(t) + \kappa r_{ext} \cos(\varphi)\{\Phi(t - \tau) - \Phi(t)\} + \kappa r_{ext} \sin(\varphi)\{I(t - \tau) - I(t)\}/A_0, \quad (4.2)$$

where  $I(t)$  and  $\Phi(t)$  represent laser intensity noise and phase noise, respectively.  $\tau$  is the round-trip delay time of the optical feedback.  $r_{ext}$  is the mirror refractivity and  $\varphi$  is the additional phase shift from the external mirror.  $A_0$  is the amplitude of the laser field in the cavity and  $\kappa$  is the coupling rate of the optical feedback back into the laser resonator.  $F_I(t)$  and  $F_\Phi(t)$  are Langevin noise terms corresponding to spontaneous emission.  $G(t)$  represents the intensity-dependent gain (gain-saturation) and  $\alpha$  is the linewidth enhancement factor.



Figure 4.2 Schematic diagram of coherent optical feedback

Notice that we do not take the dynamics of the electron number, which is directly related to the gain, into account. As a matter of fact, we treat its response to be instantaneous in order to simplify the gain saturation process. Such a trick is valid for the dynamics below the relaxation resonance frequency.

Equation (4.1) and (4.2) are written in two colors, where the black part is the intrinsic dynamics of the laser noises while the red part represents the additional couplings created by coherent optical feedback. The coupling mechanisms without and with coherent optical feedback are shown schematically in Fig. 4.3 (a) and (b), respectively. Under coherent optical feedback, the intensity and phase noises are coupled to each other, which will fundamentally change the laser frequency noise PSD.

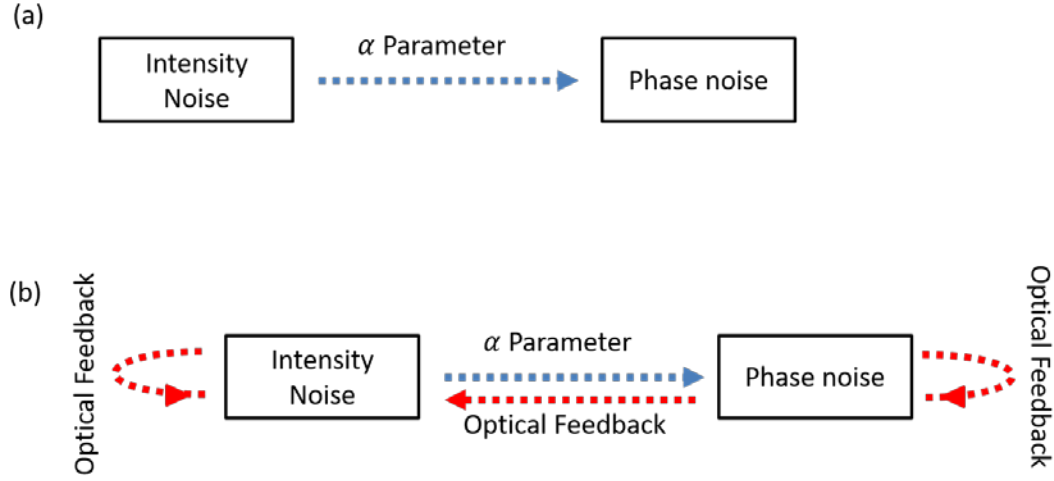


Figure 4.3 Noise coupling (a) w/o coherent optical feedback and (b) w/ coherent optical feedback

We perform Fourier transformation of these two equations in the frequency domain and, after some algebra, obtain

$$S_{\Delta\nu-\text{feedback}}(\Omega) = \frac{S_{\Delta\nu}(\Omega)}{|1 + \kappa r_{\text{ext}} \tau \sqrt{1 + \alpha^2} \frac{e^{i\Omega\tau} - 1}{i\Omega\tau}|^2}, \quad (4.3)$$

where  $S_{\Delta\nu-\text{feedback}}(\Omega)$  and  $S_{\Delta\nu}(\Omega)$  are the laser frequency noise PSD with and without coherent optical feedback and  $\Omega$  is the angular frequency. Mathematically, the effect of coherent optical feedback on the laser frequency noise PSD appears in the denominator of equation (4.3), whose magnitude can be quantified by the following parameter:

$$C = \kappa r_{\text{ext}} \tau \sqrt{1 + \alpha^2}. \quad (4.4)$$

Our definition matches Petermann's [46, 47], where a special case of an FP laser was dealt with. The denominator also possesses a very interesting feature, i.e. a periodic term, which means the denominator approaches the local minimums periodically in the frequency domain. If the C-parameter is much larger than unity, the denominator at the local minimums can be much smaller than unity, leading to spikes in the laser frequency noise PSD.

Those spikes can be viewed equivalently as side modes, the rising of which eventually drives single-mode lasers into multi-mode region. If we keep increasing the level of coherent optical feedback, at some point, the side modes will be strong enough to compete with the original lasing mode, causing the lasers to be unstable. This phenomenon is referred to as coherence collapse, where the lasers' behavior is totally chaotic and coherence is dramatically degraded [48-52].

Based on the previous definition of the C-parameter, it is impossible to characterize lasers' sensitivity to coherent optical feedback in any absolute sense because the effects depend on not only the feedback level but also the distance between the laser and the external reflection point, which varies from one scenario to another. However, in any given situation, the difference between any two lasers' feedback sensitivity is the same as the ratio between the corresponding C-parameters is only dependent on the intrinsic parameters of the lasers.

### **4.3 Incoherent optical feedback effects on laser coherence**

Incoherent optical feedback, originated from an independent light source, naturally serves as a new noise source. Because it is uncorrelated to the laser output, it does not create new coupling channels and the additional noise induced in the laser resonators is pure intensity noise. Hence, the power of the incoherent optical feedback solely determines the degree of the modification of the laser coherence and we can characterize the lasers' sensitivity to incoherent optical feedback in an absolute sense.

Here, we would like to study in particular how the ASE noise from semiconductor optical amplifiers (SOAs) modifies laser coherence, as shown schematically in Fig. 4.4, because, in practical applications, SOAs can be integrated with semiconductor lasers and other photonic devices in order to boost the output power and compensate for large insertion loss from the passive devices [53, 54]. The difference from coherent optical feedback is that the ASE noise possesses a wide optical spectrum (roughly white optical noise in C-band) and therefore can interact with multiple modes rather than just the lasing mode.

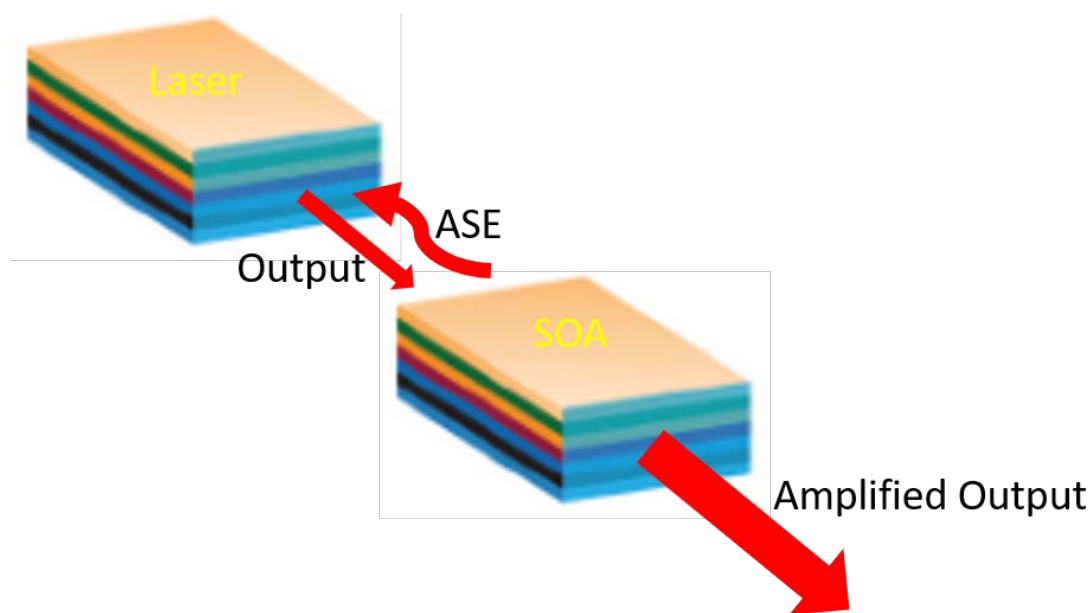


Figure 4.4 Schematic diagram of incoherent optical feedback

We should not be confused about the difference between the ASE noise as the incoherent optical feedback and the optical white noise added into the coherent optical communication system in chapter 3. The former one affects the laser's properties, for example phase coherence, so that the system performance gets altered. The latter one is directly related to OSNR, on which the system performance depends, but does not have any impacts on the laser itself. Those two noise sources, in fact, can coexist in a communication system, which will be shown in our measurement setup for lasers' sensitivity to incoherent optical feedback.

To study how the ASE noise affects the laser frequency noise PSD, we can still write down the dynamic equations of the laser noises and do the analysis in the same way as we deal with coherent optical feedback. Such analysis, however, is quite tedious and frankly unnecessary. We can simply treat the ASE noise as equivalent to spontaneous emission, generating intensity noise in the lasers, as shown in Fig. 4.5. The induced intensity noise is coupled to the laser frequency noise through the mechanism of linewidth enhancement as well, leading to the degradation of the laser coherence. Since the ASE-induced intensity noise is white noise whose PSD is proportional to the feedback power, the laser frequency noise

PSD under incoherent optical feedback should remain white and increases linearly with the ASE power fed back.

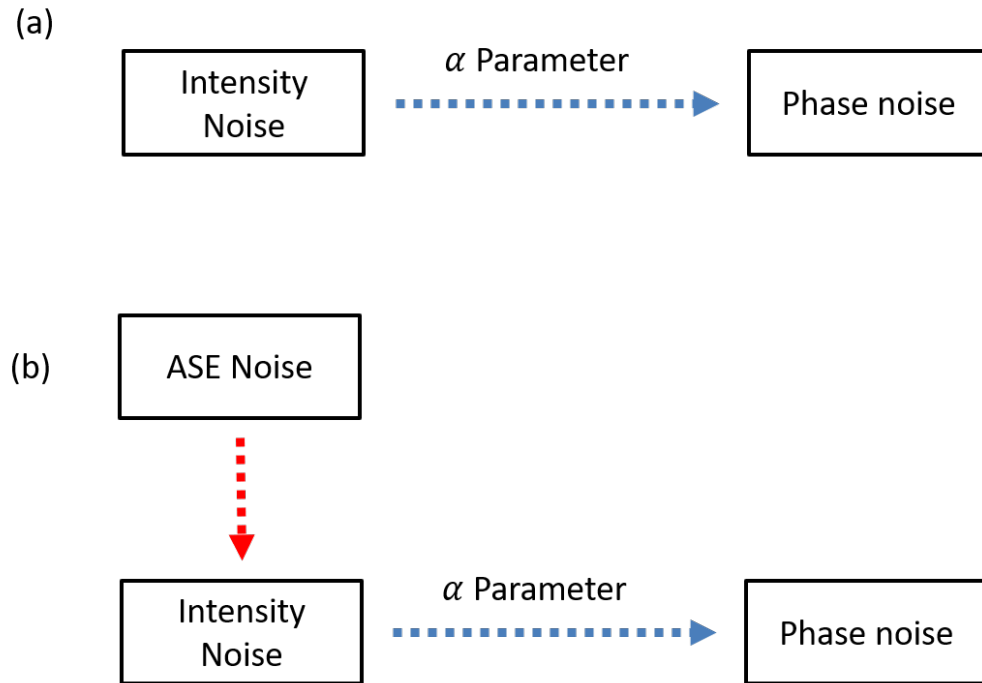


Figure 4.5 Noise coupling (a) w/o incoherent optical feedback and (b) w/ incoherent optical feedback

#### 4.4 Lasers' sensitivity to optical feedback

Conventional III-V DFB lasers, the main light sources in today's optical networks, are quite sensitive to optical feedback. Even a small amount of optical feedback can cause dramatic degradation of their performance, thwarting large-scale photonic integration. As fabricating optical isolators on chip remains extremely challenging despite some progress, replacing conventional III-V DFB lasers with monolithic semiconductor lasers with intrinsic insensitivity to optical feedback becomes a much more intriguing approach.

To enhance the lasers' robustness, preventing the optical feedback from entering the laser resonator is the key, which can be achieved by employing mirrors with the reflectivity approaching to unity. However, such an approach cannot be applied to conventional III-V

DFB lasers as it will reduce dramatically the output power, rendering the III-V DFB lasers useless. To resolve such a problem, it is necessary for semiconductor lasers to have resonators with very low internal loss so that much stronger optical field can be built inside to compensate for the reduction of the output coupling in order to get the same level of laser output power.

As discussed in Chapter 2, the Si/III-V lasers are designed in a way that most of the optical energy is stored in the low-loss silicon rather than high-loss III-V materials. The mode engineering approach increases the lasers' intrinsic quality factor by several orders of magnitude, which allows us to use high-Q resonators without sacrificing the output power. The high-Q resonators can block a significant amount of optical feedback and thus we expect the Si/III-V lasers to be much more insensitive to optical feedback than conventional III-V DFB lasers, which will be validated later.

#### **4.5 Laser frequency noise PSD under coherent optical feedback**

In this section, we are going to investigate experimentally the lasers' capability of preserving their phase coherence under coherent optical feedback. The measurement setup is shown in Fig. 4.6, where the red arrows represent the propagation of the coherent optical feedback. The coherent optical feedback loop is constructed by coupling part of the laser output back into the laser cavity via the optical circulator, emulating mirror reflection. A booster optical amplifier (BOA) and a VOA are inserted into the optical feedback loop in order to control the feedback level. The power fed back is calibrated using a high-precision photodetector, which is then converted into the effective reflectivity to be the feedback level. An optical isolator is placed in front of the frequency noise PSD measurement system to avoid any unwanted optical feedback. Finally, the frequency noise PSDs of the lasers are measured under various levels of optical feedback.

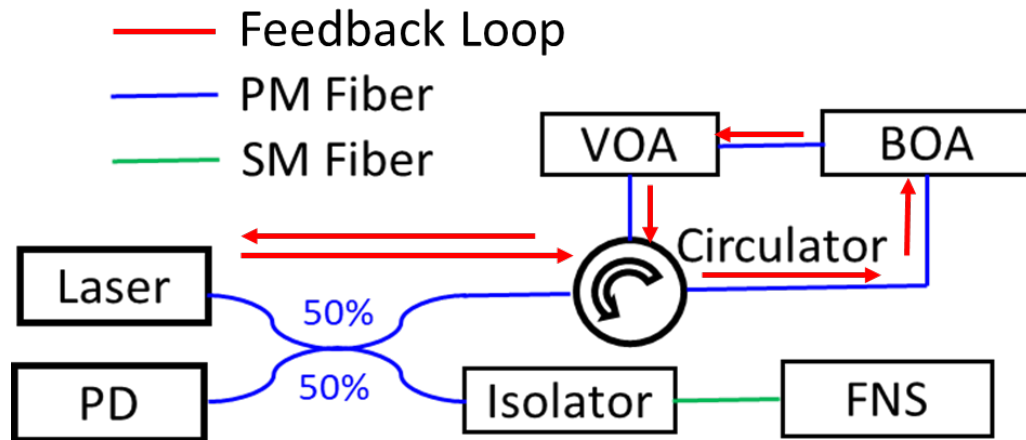


Figure 4.6 Measurement setup for laser frequency noise PSD under coherent optical feedback

The results are shown in Fig. 4.7 (a) and (b). The conventional III-V DFB laser is extremely sensitive to coherent optical feedback. As the feedback level of -50 dB, the RF oscillations, i.e. the side modes, start to emerge. With the increase of the feedback power, the side modes get stronger. On the contrary, the frequency noise PSD of the Si/III-V laser is barely changed up to a feedback level of -31 dB. Beyond that level, the frequency noise PSD at relatively low frequencies increases significantly, which deviates completely from the theory presented in the section 4.2 and will be explained later. The increase of the frequency noise PSD at relatively low frequency won't jeopardize the system performance severely because of its small bandwidth and therefore very limited contribution to the phase noise, as indicated by equation (2.9).

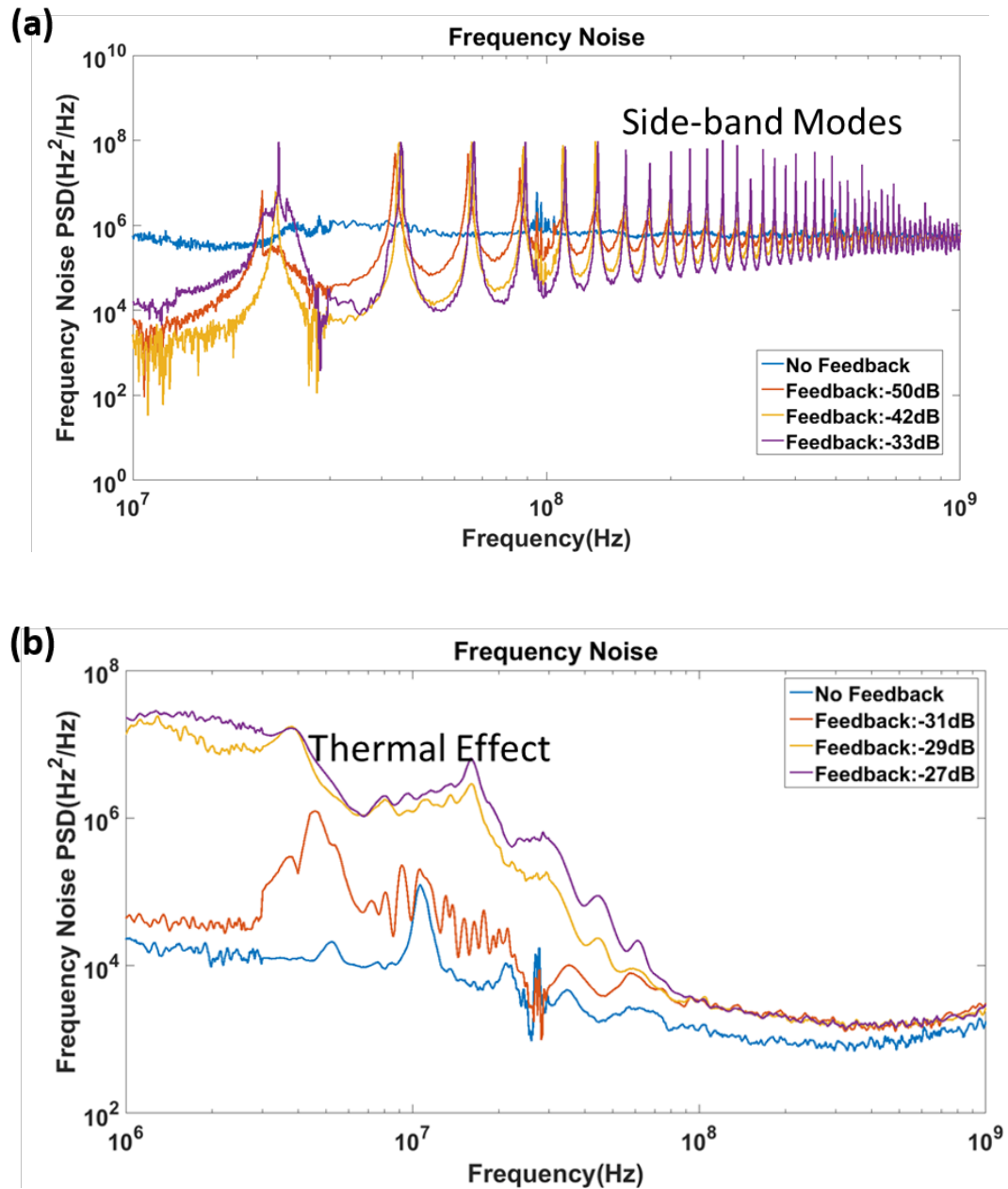


Figure 4.7 Frequency noise PSD of (a) the III-V laser and (b) the Si/III-V laser under various levels of coherent optical feedback

To determine why the frequency noise PSD of the Si/III-V laser under coherent optical feedback differs significantly from the theory, we shall revisit the dynamic equations in section 4.2. In the original theory, we treat linewidth enhancement as the only intrinsic

coupling mechanism between laser frequency noise and intensity noise while ignoring others such as thermal effects, which are severe in the Si/III-V lasers [33, 55- 56]. As a matter of fact, the alpha parameter in equation (4.2) should be replaced by a frequency-dependent response function, which takes all the coupling mechanisms into account, to make the original theory more rigorous. The exclusion of other coupling mechanisms could be the reason why the frequency noise PSD of the Si/III-V laser under coherent optical feedback deviates from the theory.

We have obtained the coupling curve between the intensity noise and the phase noise of the Si/III-V laser, which is initially presented in Fig. 2.8 and now reproduced in Fig. 4.8. The coupling strength is much larger at low frequencies due to thermal effects. If that is indeed responsible for the bizarre frequency noise PSD of the Si/III-V laser under coherent optical feedback, then the increase of the frequency noise PSD should take place only within the bandwidth of the thermal effects. By comparing Fig. 4.7 to 4.8, we confirm that indeed both the coupling strength and the frequency noise PSD increase rapidly as the frequency decreases in the identical frequency range, i.e. below 100 MHz, which validates the explanation that large thermal effects cause the rising of the laser frequency noise PSD at low frequencies.

This behavior is not observed in the III-V DFB laser is because the thermal impedance of the conventional III-V DFB laser, which is well packaged, is quite small and therefore the thermal effects are negligible. Hence, what we have observed from the III-V DFB laser is purely due to the carrier effect, i.e. linewidth enhancement, and agrees with the original theory.

Our Si/III-V laser tested in the experiments is unpackaged, leading to poor thermal management. We do expect its robustness to be improved with better packaging, for example, with flip-chip bonding [57]. Nevertheless, its frequency noise PSD at high frequencies staying unaffected indicates its superb insensitivity to coherent optical feedback. Our experimental results illustrate that the Si/III-V laser is more stable against coherent optical feedback than the conventional III-V DFB laser by at least 19 dB. As argued before,

lasers' system performance should not be degraded severely by the increase of the frequency noise PSD at low frequencies. Therefore, we do expect the difference between the two lasers' system performance would be larger than 19 dB, which will be demonstrated later in the chapter.

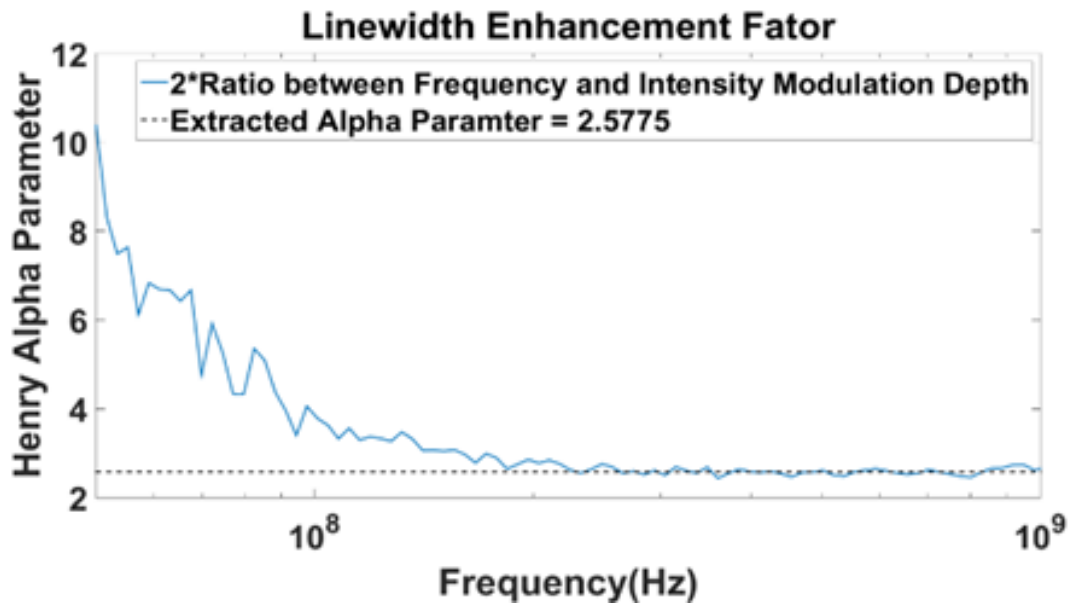


Figure 4.8 Coupling between intensity noise and phase noise

#### 4.6 Laser frequency noise PSD under incoherent optical feedback

Here, we study the impacts of incoherent optical feedback on laser coherence. Previously, we used a very simple model to predict the consequences, which will be validated here.

The measurement setup is shown in Fig. 4.9. The output of the BOA, serving as the ASE noise source, is injected directly into the laser cavity via the optical circulator. The laser frequency noise PSD is measured under various ASE power.

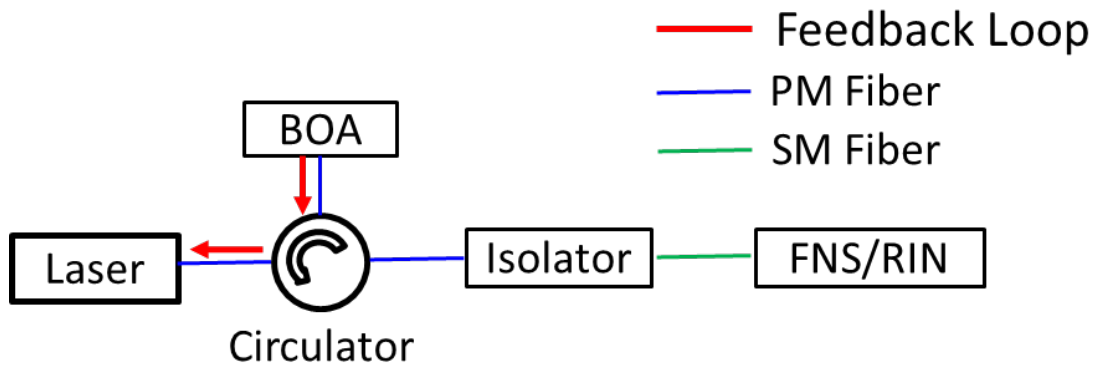


Figure 4.9 Measurement setup for laser frequency noise PSD under incoherent optical feedback

The ASE noise possesses a wide optical spectrum in C-band, as shown in Fig. 4.10 (a). It interacts with multiple optical modes and induces additional intensity noise in all those modes, which is clearly manifested by the increase of power in all the non-lasing modes in Fig. 4.10 (b) and (c).

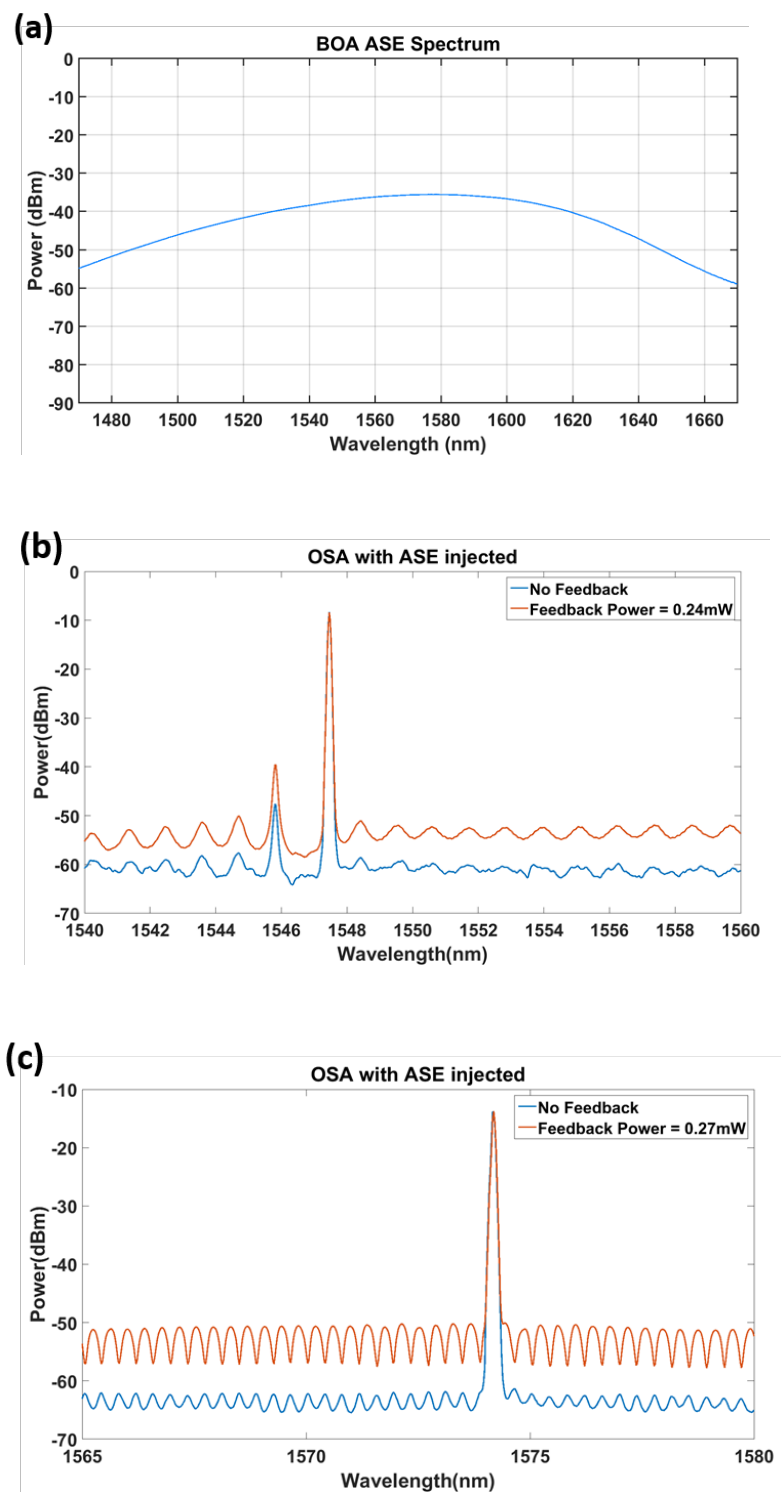


Figure 4.10 (a) ASE noise spectrum and optical spectra of (b) the hybrid Si/III-V laser and (c) the III-V DFB laser with ASE noise injected

The measurement results are shown in Fig. 4.11 (a) and (b). The frequency noise PSD of both lasers remains white under incoherent optical feedback, which agrees with our theory. The laser linewidth, interpreted by the white noise floor, is plotted as a function of the injected ASE power in Fig. 4.11 (c). The red lines are linear regression, which fit the data very well. Hence, the prediction that the laser frequency noise PSD increases linearly with the injected ASE power has been verified.

The major difference between the Si/III-V laser and the conventional III-V DFB laser lies at the slopes of those two red lines. The slope extracted for the III-V laser is 32 MHz/mW while only 0.2 MHz/mW for the Si/III-V laser, which is two orders of magnitude smaller. This result shows the Si/III-V laser is much more insensitive to incoherent optical feedback than the conventional III-V DFB laser by two orders of magnitude.

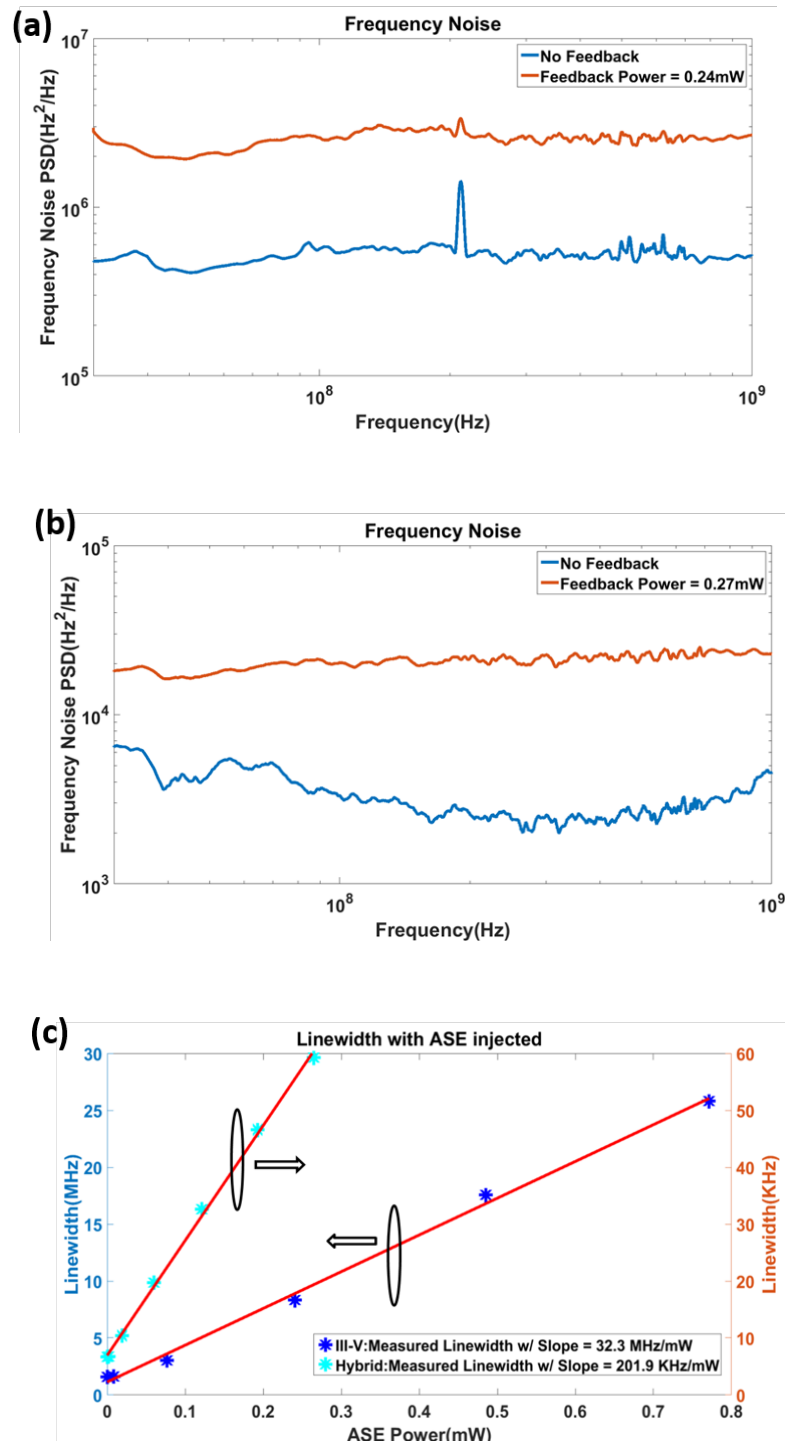


Figure 4.11 Frequency noise PSD of (a) the III-V laser and (b) Si/III-V laser w/ and w/o the existence of incoherent optical feedback and (c) the corresponding linewidth as a function of ASE power

So far, we only have indirect evidence to support our theory. To directly validate the theory, we measure the intensity noise PSD under incoherent optical feedback to see whether the increments of laser intensity and frequency noises match with each other. In this experiment, only the III-V DFB laser is used, of which the intensity noise around the relaxation resonance frequency can be accurately measured, as shown in Fig. 4.12 (a).

The results are shown in Fig. 4.12 (b). The level of the intensity or frequency noise PSD of the III-V DFB laser under no incoherent optical feedback is set as the reference point. The increment of the laser noise is characterized by the ratio between the level of noise under the optical feedback and the reference point. There exists a very good match between the increments of the intensity noise PSD and the frequency noise PSD, which confirms our explanation that the ASE-induced intensity noise is coupled to the laser frequency noise via linewidth enhancement, leading to the broadening of the laser lineshape. Our theory, in spite of being very simple, describes accurately the effects of incoherent optical feedback on laser coherence.

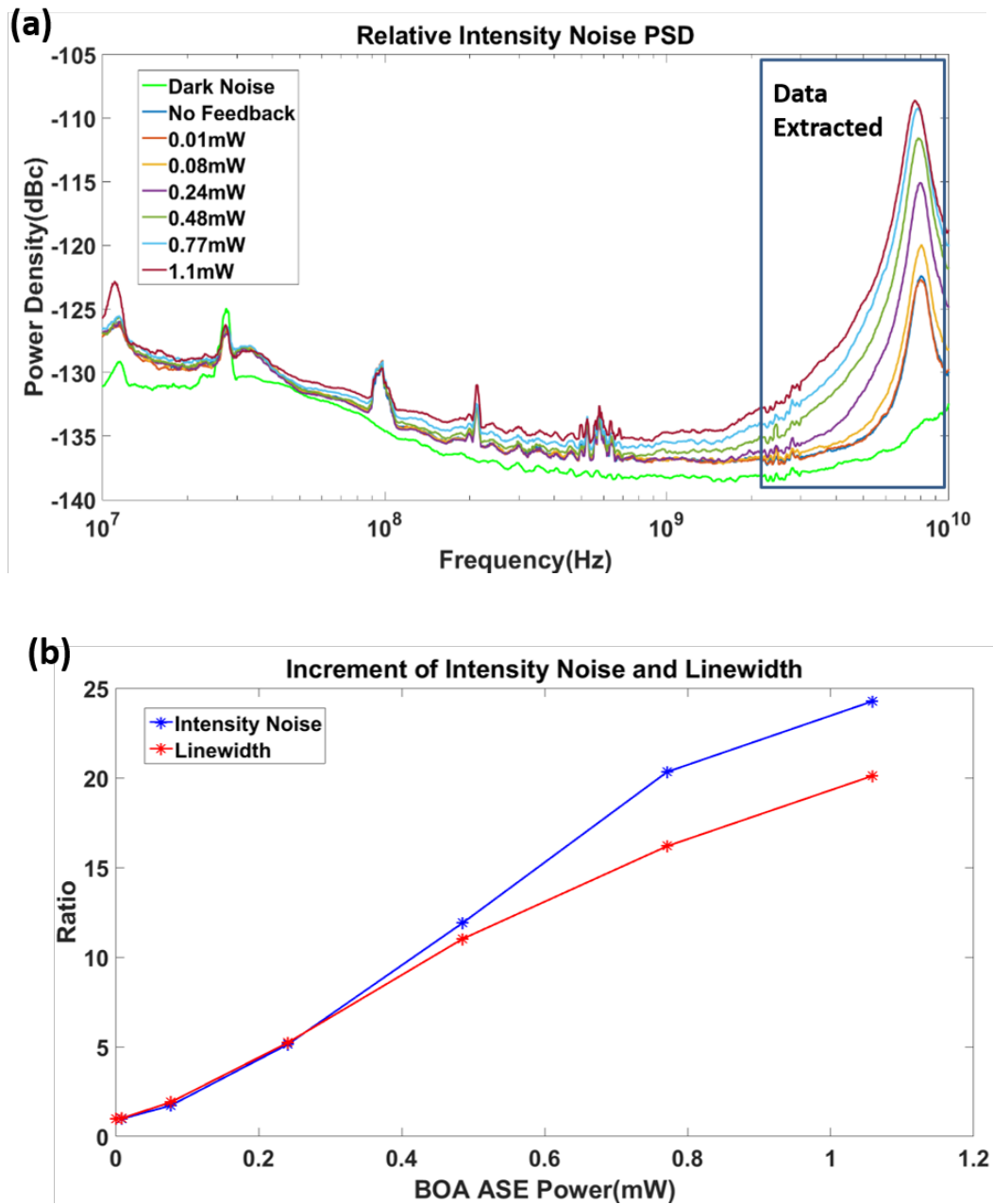


Figure 4.12 (a) Intensity noise PSD of the III-V DFB laser at various injected ASE power and (b) the increment of laser intensity noise and laser frequency noise, respectively

To summarize, our Si/III-V laser is much more robust against coherent and incoherent optical feedback than the III-V DFB laser. Particularly, the Si/III-V laser is capable of preserving its phase coherence under much larger optical feedback, which is critical for isolator-free

coherent optical communications. In the rest of this chapter, we are going to investigate the feedback sensitivity of the lasers in the coherent optical communication systems.

#### 4.7 System performance under coherent optical feedback

We begin with examining the lasers' system performance under coherent optical feedback. The measurement setup is shown schematically in Fig. 4.13. The coherent optical feedback loop is constructed in the same way as in Fig. 4.6. The semiconductor lasers, subject to a variable-controlled coherent optical feedback, are used as the light sources to carry data signals. We characterize the system performance by measuring the BER-OSNR curves at various levels of coherent optical feedback.

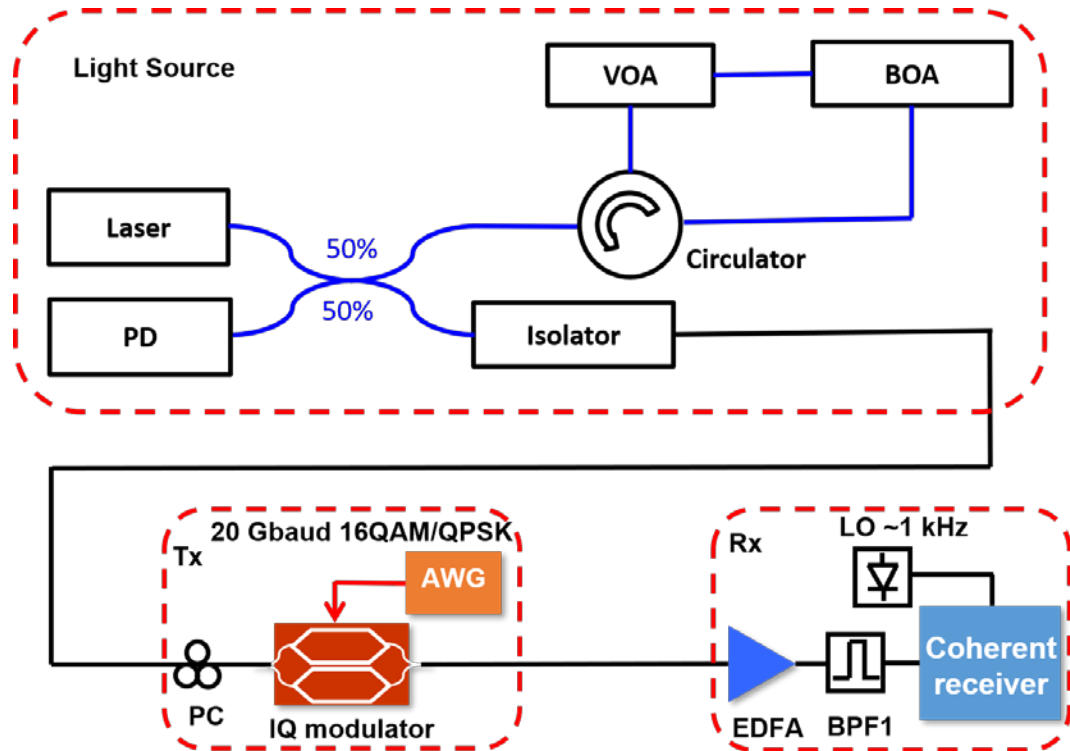


Figure 4.13 Measurement setup for coherent optical feedback

The modulation formats for the hybrid Si/III-V laser and the III-V DFB laser are chosen to be 20 GBaud 16-QAM and 20 GBaud quadrature phase shift keying (QPSK), respectively, given their intrinsic coherence. The results are shown in Fig. 4.14 (a) and (b). The III-V DFB

laser is very sensitive to coherent optical feedback. The BER-OSNR curves of the III-V DFB laser start to shift upwards at a feedback level of -45.5 dB, indicating a degradation of the system performance. Beyond -41.5 dB, the coherent communication system is driven into chaos, where the phase information is completely washed out, as revealed by the constellation diagrams in Fig. 4.15. Hence, at a feedback level of -41.5 dB or beyond, it is impossible to conduct coherent optical communications successfully with the conventional III-V DFB laser.

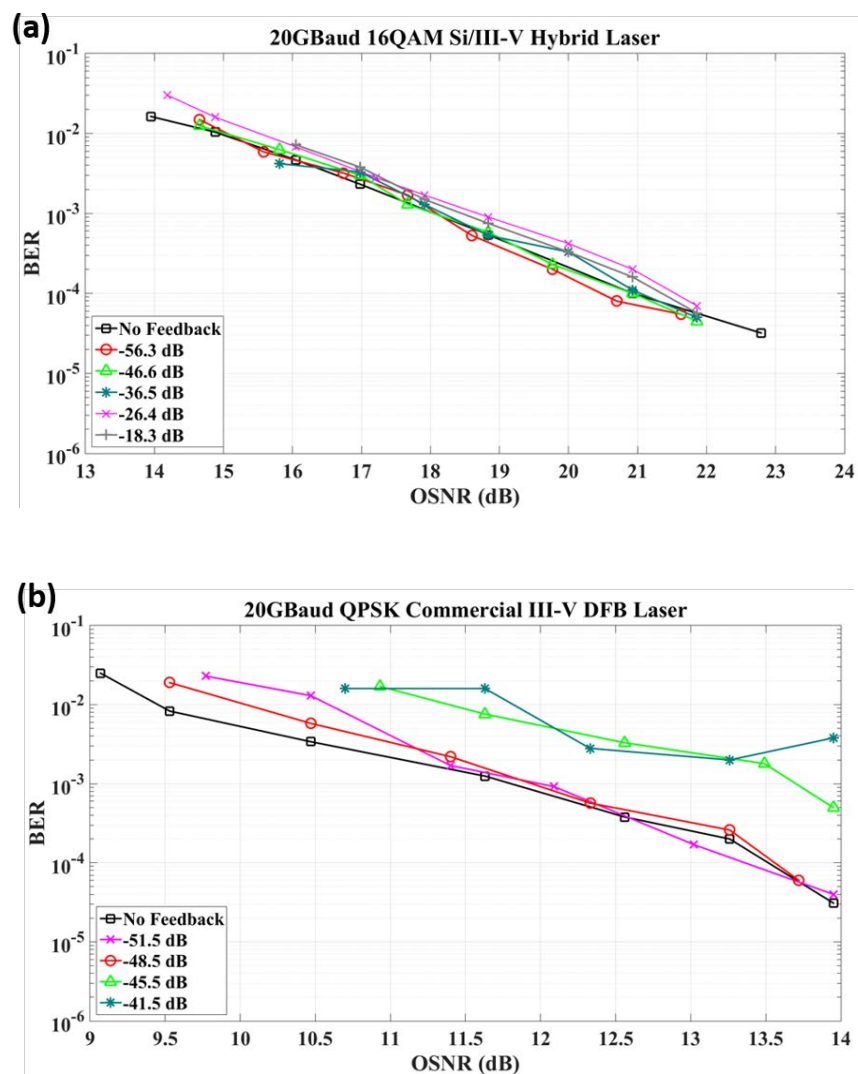


Figure 4.14 System performance of (a) the Si/III-V laser and (b) the III-V DFB laser under coherent optical feedback

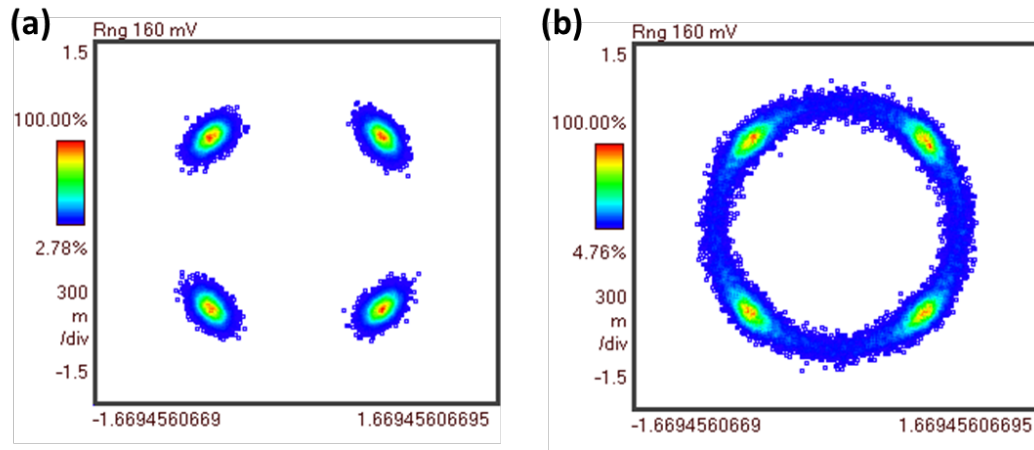


Figure 4.15 Constellation diagrams of the III-V DFB laser (a) w/o optical feedback and (b) with the feedback level beyond -41 dB

On the contrary, the BER-OSNR curves of the Si/III-V laser stay almost unchanged by coherent optical feedback. Even at the feedback level of -18.3 dB, the largest feedback level that can be achieved in the experiments, there is no obvious degradation of its system performance. Based on the data, the Si/III-V laser is more robust against coherent optical feedback than the conventional III-V DFB laser by at least 27.2 dB. For the record, commercial optical isolators typically provide optical isolation between 25 dB and 30 dB, which suggests that, in terms of sensitivity to coherent optical feedback, the Si/III-V laser is as stable as the commercial III-V DFB laser packaged with an optical isolator.

#### 4.8 System performance under incoherent optical feedback

In this section, we investigate how incoherent optical feedback affects semiconductor lasers' system performance. The incoherent optical feedback loop is constructed in the same way as in Fig. 4.9 and the whole measurement setup is shown in Fig. 4.16. In a manner similar to the previous method of data collection, we measure the BER-OSNR curves under various ASE power fed back.

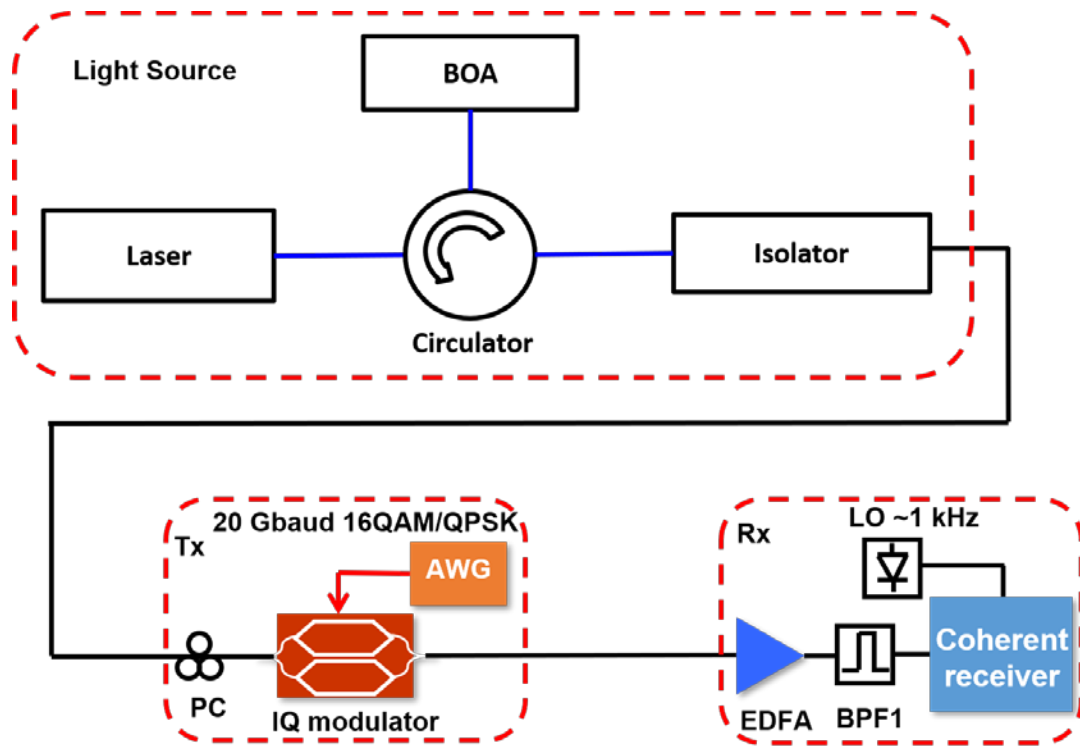


Figure 4.16 Measurement setup for incoherent optical feedback

The results are shown in Fig. 4.17 (a) and (b). The BER-OSNR curves of the Si/III-V laser are barely affected by incoherent optical feedback. However, those of the III-V DFB laser keep shifting upwards with the increase of the feedback power, demonstrating the degradation of its system performance. The constellation diagrams of the III-V DFB laser in Fig. 4.18 clearly illustrates the increase of the phase noise in the communication system. However, this kind of degradation, which gradually deepens as the feedback power increases, is quite different from what we have observed under coherent optical feedback. Previously, across a certain level of coherent optical feedback, -41 dB in our case, the communication system experiences a sharp transition from being functional to being dysfunctional.

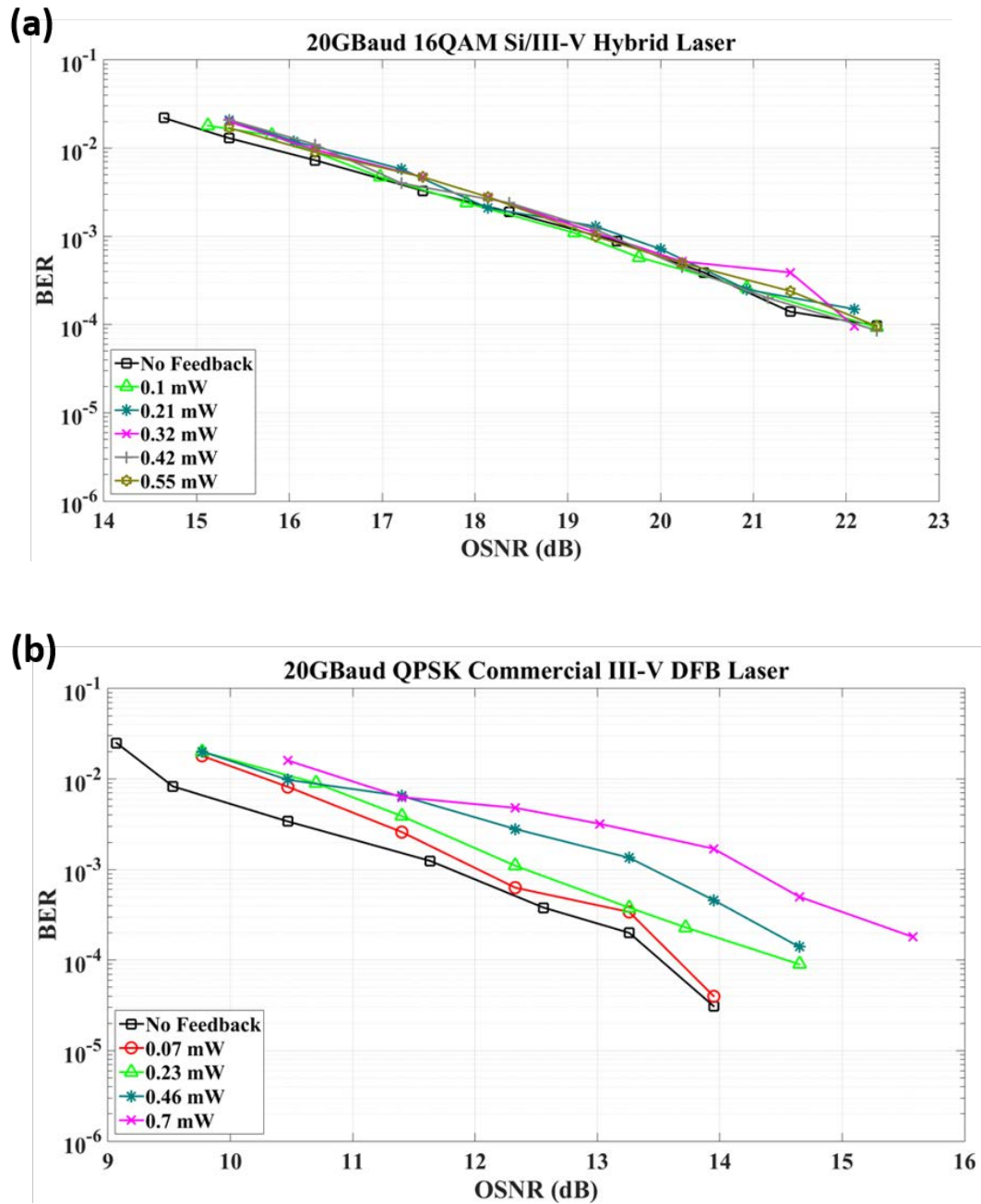


Figure 4.17 System performance of (a) the Si/III-V laser and (b) the III-V DFB laser under incoherent optical feedback

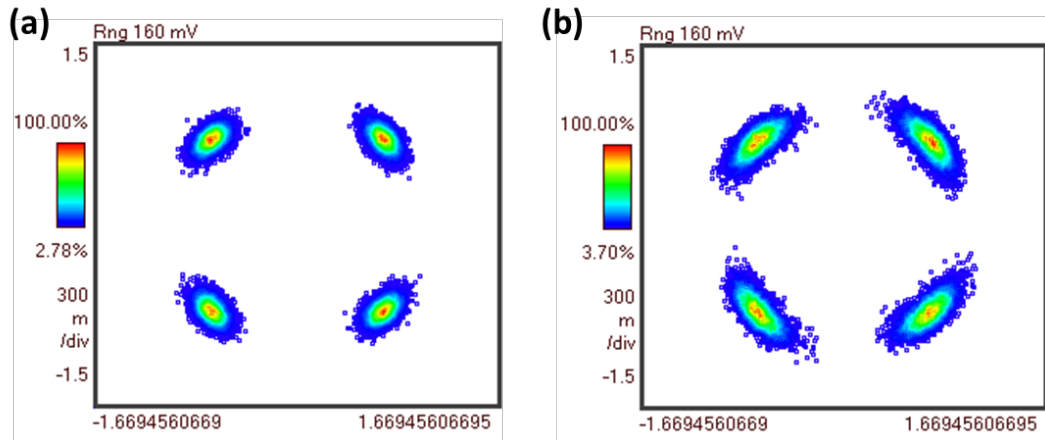


Figure 4.18 Constellation diagrams of the III-V DFB laser (a) w/o optical feedback and (b) with the ASE power of 0.7 mW

#### 4.9 OSNR penalty due to optical feedback

A more straightforward tool to use for comparing the system performance under different situations would be the OSNR penalty, which is defined as the increase of the OSNR relative to that of the reference, in this case the OSNR under the condition without optical feedback, at a fixed BER, in our case  $10^{-3}$ . The results are shown in Fig. 4.19 (a) and (b). As we can see, the OSNR penalty of the Si/III-V laser is quite small, namely less than 1 dB in all cases, indicating its robustness against optical feedback. While for the conventional III-V DFB laser, coherent optical feedback at -46.6 dB can cause an OSNR penalty of 2 dB. The OSNR penalty approaches infinity at the feedback level beyond -41.5 dB because of the chaotic system performance. Besides, incoherent optical feedback can cause a maximum OSNR penalty of 2.5 dB. From the OSNR penalty data, it is obvious that the degradation patterns of the conventional III-V DFB laser are different under coherent and incoherent optical feedback. The former one possesses a much sharper transition than the latter one.

Once again, the results show that the Si/III-V laser can indeed function without severe degradation in the isolator-free coherent optical communication system, a precondition to its usage in photonic integrated circuits.

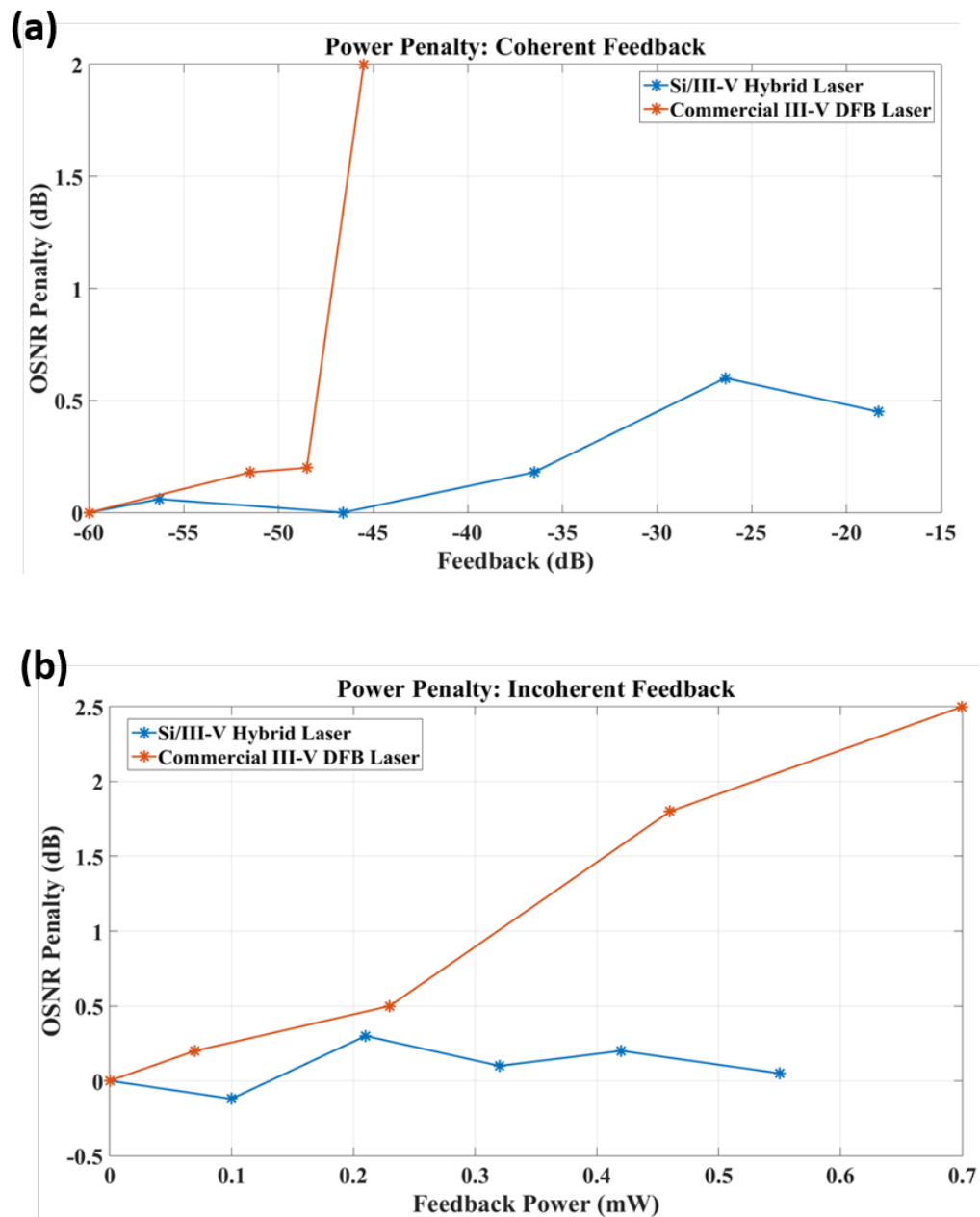


Figure 4.19 Power penalty due to (a) coherent and (b) incoherent optical feedback

#### 4.10 Conclusions

In this chapter, we have investigated the sensitivity of the Si/III-V laser and the conventional III-V DFB laser to both coherent and incoherent optical feedback, respectively. Unlike the conventional III-V DFB laser, the Si/III-V laser, due to its built-in high-Q resonator, can

preserve its phase coherence under much higher levels of optical feedback, leading to its more stable system performance in an isolator-free environment. The superiority of the Si/III-V laser to the conventional III-V DFB laser lies at not only the phase coherence but also the robustness against optical feedback, making them stunningly suitable to be the integrated light sources. Our work will have great impacts on how the semiconductor lasers of the next generation will be made.

## A GENERAL RELATION BETWEEN LASER FREQUENCY NOISE PSD AND LINESHAPE

There are two means of characterizing laser coherence. The first one is laser frequency noise PSD, which has been used by us in all the experiments. We prefer using it because of its close relation to the phase noise in coherent optical communications (see equation (2.13)). The second one is laser lineshape, the PSD of the laser field, of which the FWHM is known as the laser linewidth, for example, the S-T linewidth introduced in chapter 2.

In the current literature, the two measures are very often used interchangeably as a premise to characterize laser coherence. This will be shown to be wrong in what follows. In this chapter, we will show how those two are related to each other in general.

We are not the first group addressing the issue. Previous approaches are limited to numerical computation or analysis on special cases [58-62], which do not provide physical insights. Here, we derive a general relation, which we refer to as the Central Relation, between the frequency noise PSD and the lineshape of laser light, which turns out to be surprisingly simple. The Central Relation affords new insights into laser coherence, including how it can be engineered with optical filtering.

### 5.1 Derivation of the general relation

The electric field of laser light can be expressed as

$$E = E_0 e^{i\{\omega_0 t + \psi(t)\}}, \quad (5.1)$$

where  $\psi(t)$  represents the phase fluctuations due to random or deterministic modulation, whose average value vanishes.  $E_0$  is the amplitude and  $\omega_0$  is the angular frequency of the light. The lineshape function (single-sided spectrum) of the laser light is represented by the PSD of the laser field, which is the Fourier transform of the correlation function of the field

$$S_E(\omega) = 2 \int_{-\infty}^{+\infty} e^{-i\omega\tau} \langle E^*(t)E(t+\tau) \rangle d\tau, \quad (5.2)$$

where  $\langle \rangle$  represents the time average.

The correlation function can be calculated as [60, 63]

$$\begin{aligned} \langle E^*(t)E(t+\tau) \rangle &= E_0^2 e^{i\omega_0\tau} \langle e^{i\{\psi(t+\tau)-\psi(t)\}} \rangle \\ &= E_0^2 e^{i\omega_0\tau} e^{-\frac{1}{2}\langle \{\psi(t+\tau)-\psi(t)\}^2 \rangle} \\ &= E_0^2 e^{i\omega_0\tau} e^{-2 \int_0^{+\infty} S_{\Delta\nu}(f) \frac{\sin^2(\pi f\tau)}{f^2} df}. \end{aligned} \quad (5.3)$$

Since intensity fluctuations are strongly damped due to gain saturation,  $E_0^2$  is taken as a constant.

$$S_{\Delta\nu}(f) = 2 \int_{-\infty}^{+\infty} e^{-i2\pi f\tau} \langle \dot{\psi}(t)\dot{\psi}(t+\tau) \rangle d\tau \quad (5.4)$$

is the single-sided frequency noise PSD. The central frequency of lineshape is just  $\omega_0$ .

We define a new function  $\eta(\nu)$  by means of the relation

$$\frac{1}{2\pi} \int_{-2\pi\nu+\omega_0}^{2\pi\nu+\omega_0} S_E(\omega) d\omega = \{1 - \eta(\nu)\} E_0^2. \quad (5.5)$$

Notice that if we integrate over the whole laser lineshape function, we get the total power of the laser light, namely

$$\frac{1}{2\pi} \int_{-\infty+\omega_0}^{+\infty+\omega_0} S_E(\omega) d\omega = E_0^2, \quad (5.6)$$

so that the function  $\eta(\nu)$  is equal to the total power contained outside the integrated frequency range of width  $4\pi\nu$  straddling the central laser frequency  $\omega_0$ . The function  $\eta(\nu)$  can be expressed as

$$\eta(\nu) = \frac{1}{E_0^2} \left\{ \frac{1}{2\pi} \int_{-\infty+\omega_0}^{-2\pi\nu+\omega_0} S_E(\omega) d\omega + \frac{1}{2\pi} \int_{2\pi\nu+\omega_0}^{+\infty+\omega_0} S_E(\omega) d\omega \right\} \quad (5.7)$$

and it vanishes as  $\nu$  approaches infinity.

The use of (5.2) and (5.3) in (5.5) leads to

$$\frac{1}{2\pi} \int_{-2\pi\nu+\omega_0}^{2\pi\nu+\omega_0} d\omega \int_{-\infty}^{+\infty} e^{i(\omega_0-\omega)\tau} e^{-2 \int_0^{+\infty} S_{\Delta\nu}(f) \frac{\sin^2(\pi f \tau)}{f^2} df} d\tau = 1 - \eta(\nu). \quad (5.8)$$

Integrating over the angular frequency  $\omega$  leads to

$$2\nu \int_{-\infty}^{+\infty} \text{sinc}(2\pi\nu\tau) e^{-2 \int_0^{+\infty} S_{\Delta\nu}(f) \frac{\sin^2(\pi f \tau)}{f^2} df} d\tau = 1 - \eta(\nu). \quad (5.9)$$

We use the following mathematical relations to deal with sinc functions:

$$\begin{aligned} \text{sinc}(2\pi\nu\tau) &= W(2\pi\nu\tau) \quad \text{as } \nu \rightarrow \infty \\ \text{sinc}\left(\frac{2\pi f}{4\nu}\right) &= W\left(\frac{2\pi f}{4\nu}\right) \quad \text{as } \nu \rightarrow \infty, \end{aligned} \quad (5.10)$$

where  $W(x)$  is equal to 1 when  $|x| \leq \pi/2$  and vanishes otherwise. The upper equation is valid as both  $2\nu \text{sinc}(2\pi\nu\tau)$  and  $2\nu W(2\pi\nu\tau)$  are asymptotically identical to  $\delta(\tau)$  function. The lower equation is simply the Fourier transform of the upper one.

Using the definition of  $W(x)$  we can limit the range of integration in (5.9) to  $-\frac{1}{4\nu} \leq \tau \leq \frac{1}{4\nu}$ ,

which allows us to rewrite it as

$$2\nu \int_{\frac{1}{4\nu}}^{\frac{1}{4\nu}} e^{-2 \int_0^{+\infty} S_{\Delta\nu}(f) \frac{\sin^2(\pi f \tau)}{f^2} df} d\tau = 1 - \eta(\nu).$$

Since the integrand is an even function of  $\tau$

$$4\nu \int_0^{\frac{1}{4\nu}} e^{-2 \int_0^{+\infty} S_{\Delta\nu}(f) \frac{\sin^2(\pi f \tau)}{f^2} df} d\tau = 1 - \eta(\nu). \quad (5.11)$$

For sufficiently large  $\nu$ , the time variable  $\tau$  in (5.11) becomes small over the entire integral range so that we can Taylor-expand the exponential part and keep only the leading term

$$4\nu \int_0^{\frac{1}{4\nu}} \{1 - 2 \int_0^{+\infty} S_{\Delta\nu}(f) \frac{\sin^2(\pi f \tau)}{f^2} df\} d\tau = 1 - \eta(\nu). \quad (5.12)$$

Integrating over  $\tau$  first and get the following formula

$$\int_0^{+\infty} \frac{S_{\Delta\nu}(f)}{f^2} \{1 - \text{sinc}(\frac{\pi f}{2\nu})\} df = \eta(\nu). \quad (5.13)$$

The second term on the left side in equation (5.13) contains a sinc function and using the relation (5.10), we take the lower limit of integration at  $\frac{\pi f}{2\nu} = \frac{\pi}{2}$

$$\int_{\nu}^{+\infty} \frac{S_{\Delta\nu}(f)}{f^2} df = \eta(\nu). \quad (5.14)$$

The physical meaning of (5.14) is more apparent in a form, which results from a differentiation of both sides with respect to  $\nu$

$$\frac{S_{\Delta\nu}(\nu)}{\nu^2} = \frac{1}{E_0^2} \{S_E(\omega_0 + 2\pi\nu) + S_E(\omega_0 - 2\pi\nu)\}, \quad (5.15)$$

where the differential form of  $\eta(\nu)$  can be derived from equation (5.7).

Equation (5.15) constitutes a general relation between the frequency noise PSD  $S_{\Delta\nu}(\nu)$  and the lineshape function  $S_E(\omega)$  of the laser light. We will refer to it as the Central Relation. It shows that at high frequencies there is a one-to-one correspondence between the frequency noise and the lineshape function. Empirically, frequencies which are more than ten times the linewidth can be considered as sufficiently high for the Central Relation to apply; such a rule of thumb is confirmed by the experiments described in the following sections. Notice that we have made no assumptions regarding the physical origin of the frequency noise.

It is worth pointing out that the left side of equation (5.15) is essentially the phase noise PSD of the laser. The meaning of equation (5.15) can be interpreted as following. The frequency noise at high base band frequency affects the lineshape at the same frequency offset with respect to the optical central frequency. If the lineshape is symmetrical about the central frequency, which is true for laser lineshape, then any feature in the phase noise PSD at high frequency will appear identically in the lineshape and vice versa.

## 5.2 Validation of the Central Relation

To illustrate the validity of the Central Relation, both the frequency noise PSD and lineshape of a single laser have been measured. The measurement setups are shown in Fig. 5.1. The frequency noise PSD is measured as before. The laser's lineshape is obtained by beating the laser field with the field of a narrow-linewidth fiber laser and measuring the power spectrum of the beat signal.

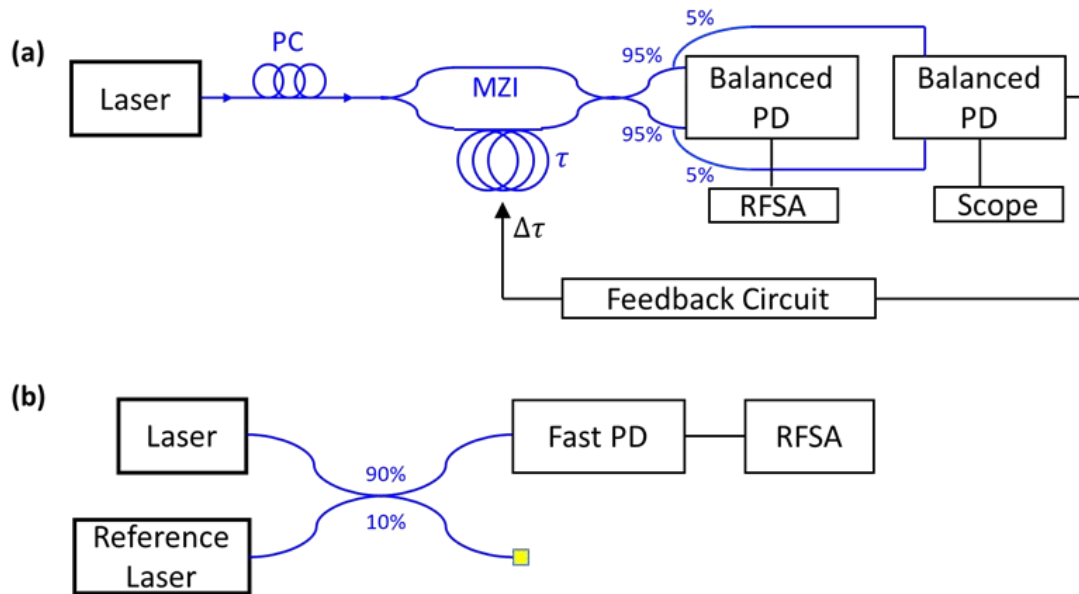


Figure 5.1 Measurement setups for (a) frequency noise power spectral density and (b) lineshape. PC: polarization controller; RFSA: radio frequency spectrum analyzer. A narrow-linewidth fiber laser is used as the reference laser

The laser's frequency noise is shown in Fig. 5.2(a). There exists some jitter at tens of megahertz in the spectrum, which comes from the controlling circuit of the laser. The lineshape of the laser is displayed in Fig. 5.2(b) and it contains two bumps, which are symmetrical about the central frequency. To show that the frequency noise PSD and the lineshape indeed obey the Central Relation (5.15), we first calculate the phase noise PSD, namely the left side of equation (5.15), based on the measured frequency noise PSD and then match it with the lineshape, as is shown in Fig. 5.2(b).

The jitter in the phase noise PSD is located at the same frequency as the bumps in the lineshape with respect to the central frequency. In addition, the bump reproduces the envelope of the jitter in the phase noise PSD. Because of the measurement resolution of the spectrum analyzer, we are unable to observe the individual lines in the lineshape. The general relation describes exactly the match between the frequency noise PSD and the optical lineshape and therefore we show experimentally the validity of the Central Relation.

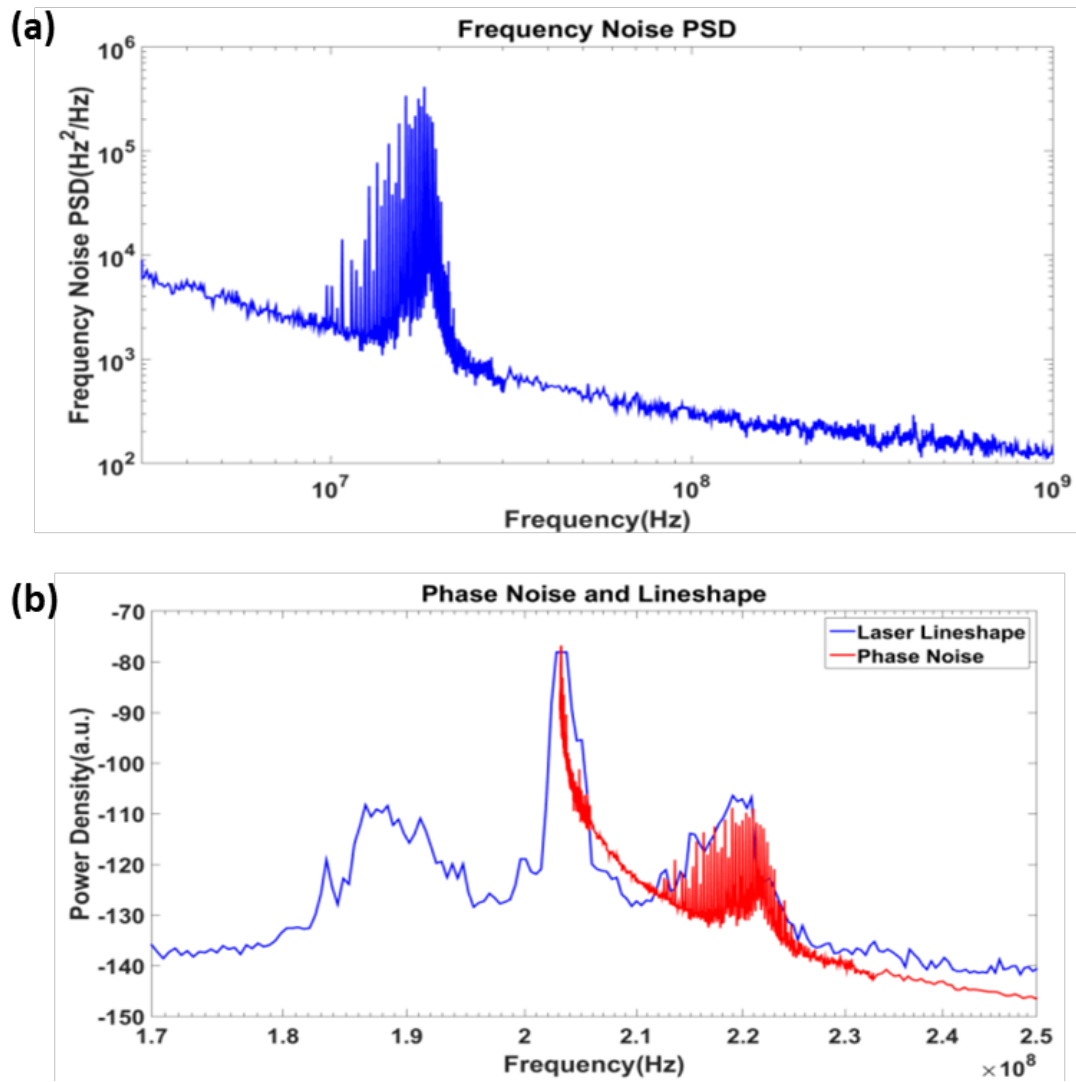


Figure 5.2 (a) Frequency noise PSD of the laser (b) Corresponding phase noise PSD and lineshape of the laser

### 5.3 Insights into the Central Relation

Equation (5.15), i.e. the Central Relation, illustrates the fundamental relation between laser frequency noise PSD and lineshape. What can we learn from such a relation? How do we apply such a relation? In this section, we are going to discuss some corollaries of the Central Relation along with the experimental proof.

### 5.3.1 Optical filtering of laser frequency noise PSD

The Central Relation (5.15) is valid for any laser light and can be used as a guide to custom-tailor the frequency noise PSD by optical filtering.

Consider the case where the laser light passes through a generalized filter, whose transmission is the function  $H(|\omega - \omega_0|)$ , which is centered at the same frequency as the laser. It is assumed to be symmetric about the central frequency. The filter possesses unity transmission near  $\omega_0$  and has negligible effects on the total power of the light. The output lineshape function is changed from  $S_E(\omega)$  to

$$S'_E(\omega) = S_E(\omega)H(|\omega - \omega_0|). \quad (5.16)$$

The Central Relation (6.15) also applies to the light exiting the filter, which leads to

$$\frac{S'_{\Delta\nu}(\nu)}{\nu^2} = \frac{1}{E_0^2} \{S'_E(\omega_0 + 2\pi\nu) + S'_E(\omega_0 - 2\pi\nu)\}, \quad (5.17)$$

where  $S'_{\Delta\nu}(\nu)$  represents the frequency noise PSD of the light modified by the filter. From equation (5.15), (5.16) and (5.17), it follows that

$$S'_{\Delta\nu}(\nu) = S_{\Delta\nu}(\nu)H(2\pi\nu), \quad (5.18)$$

where  $S_{\Delta\nu}(\nu)$  is the original frequency noise PSD of the laser. Equation (5.18) indicates that the frequency noise PSD at a base band frequency  $\nu$  is modified by the same transmission function of the filter at an optical frequency  $\omega_0 \pm 2\pi\nu$ . This equation indicates that the frequency noise at some high baseband frequency  $\nu$  can be controlled by optically filtering the tail of lineshape at the frequency offset  $\nu$  from the center. By correctly designing the transmission spectrum of the filter, the frequency noise can be tailored correspondingly.

Equation (5.18) appears alarmingly simple but consider the fact that demonstrates a tailoring of, for example, a microwaves spectrum near  $\nu$  by optical filtering at frequencies  $\omega_0 \pm 2\pi\nu$ , which are orders of magnitude larger. To demonstrate the significance of equation (5.18) and further illustrate the validity of (5.15), we pass the laser output field through an MZI with the FSR of 203 MHz, as shown in Fig. 5.3. The laser frequency is tuned to match one of the maximum-transmission frequencies of the MZI, which is schematically shown in Fig. 5.4. Notice that the Lorentzian linewidth of the laser is much smaller than the FSR, and therefore the laser power is preserved after transmission. However, equation (5.18) predicts that the frequency noise PSD should be modified by the transmission function of the MZI.

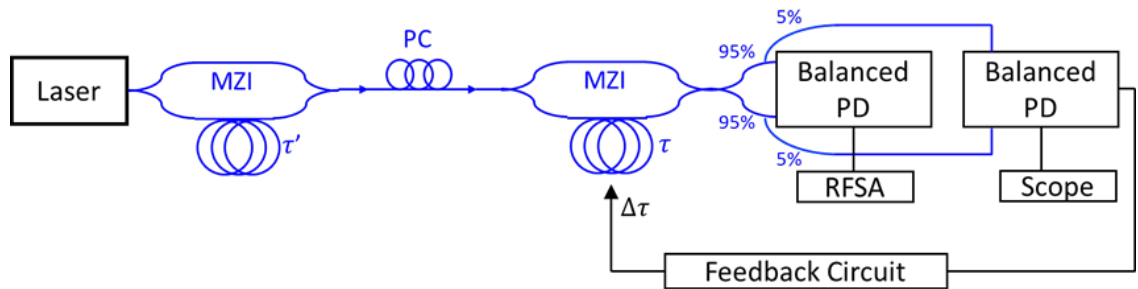


Figure 5.3 Measurement setup for the frequency noise PSD of laser output modified by the MZI with the free spectral range of 203 MHz

The measured frequency noise PSD, along with the intrinsic one, is shown in Fig. 5.5(a), which is modified dramatically by the MZI. To confirm the validity of equation (5.18), we take the ratio between those two frequency spectra, which is plotted in Fig. 5.5(b). The function is indeed the transmission spectrum of the MZI, which is sinusoid with an FSR of 203 MHz.

Being able to control laser frequency noise in any chosen frequency region is of great importance for technologies and applications which employ phase modulation of lasers and/or coherent detection. The corresponding phase noise of the system in general can be estimated with

$$\int_{\frac{1}{T}}^{\frac{1}{\tau}} S_{\Delta\nu}(f) df, \quad (5.19)$$

where  $T$  is the total acquisition time of the signal and  $1/T$  is usually very small;  $\tau$  represents the time interval between two successive samplings and therefore  $1/\tau$  is the sampling or modulation frequency.  $1/\tau$  is typically orders of magnitude larger than  $1/T$  and varies from one application to another. For example, in high-speed coherent optical communications, the modulation frequency can be as high as tens of GHz. However, for applications such as phase-sensitive LIDAR and imaging, a sampling frequency on the order of tens of MHz may be enough.  $S_{\Delta\nu}(f)$  represents the frequency noise PSD of laser light.

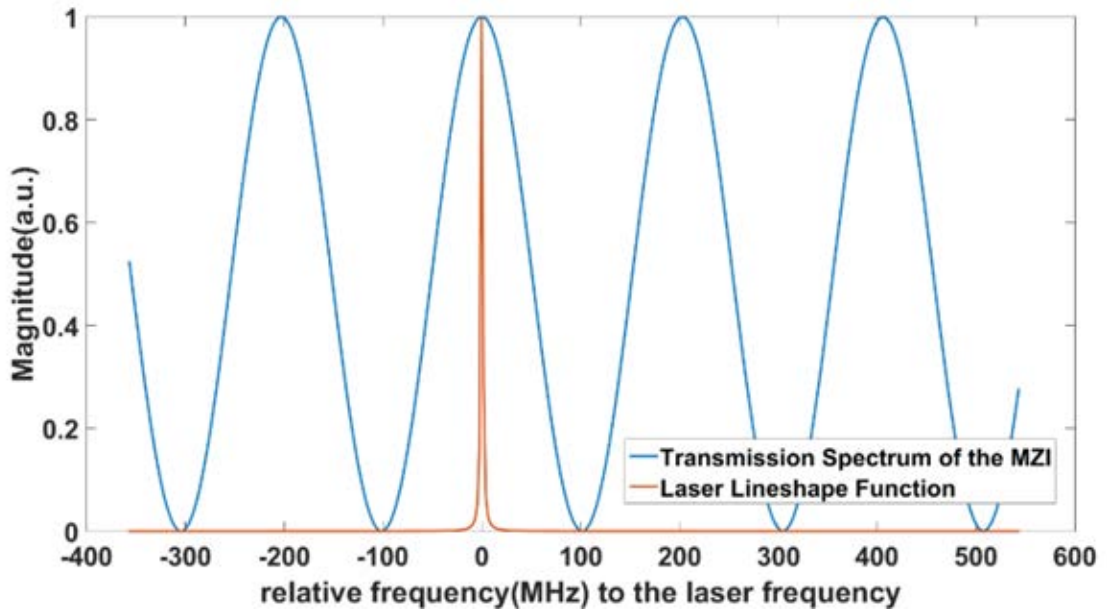


Figure 5.4 Schematic plot of the laser lineshape and transmission spectrum of the MZI; the laser frequency aligned to maximum transmission frequency of the MZI

In order to reduce the phase noise in the system, it is crucial to suppress the laser frequency noise PSD at frequencies close to the sampling or modulation frequency, namely

$$S_{\Delta\nu}(f)|_{f \sim \frac{1}{\tau}}, \quad (5.20)$$

because it occupies the largest bandwidth and thus contributes mostly to the phase noise. Therefore, optical filtering offers a brand-new way of engineering the laser frequency noise PSD in any desired bandwidth to reduce the phase noise in the systems.

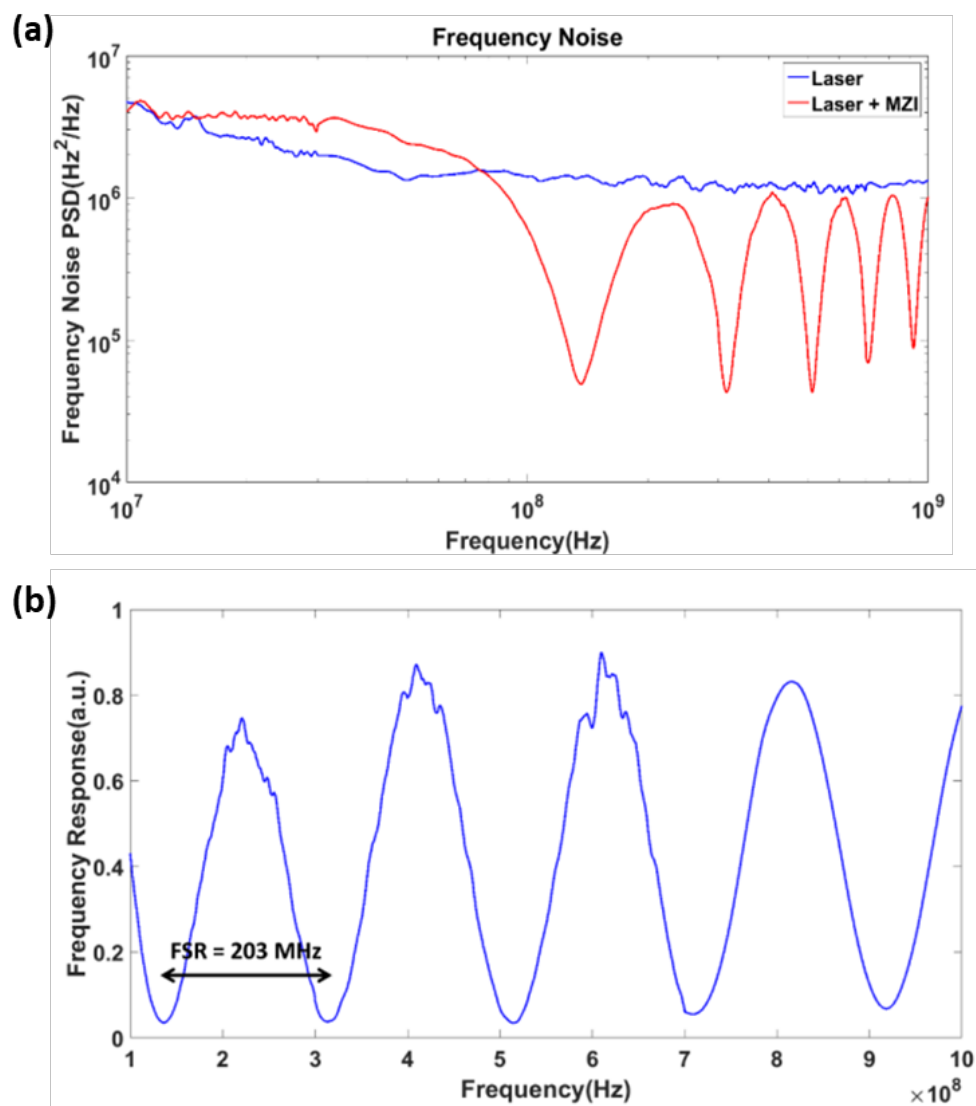


Figure 5.5 (a) Frequency noise PSD of the laser and laser passing through the MZI (b) Ratio between the two frequency noise PSDs

### 5.3.2 Is laser linewidth a good measure for laser coherence

In our previous experiments, it makes sense to use laser frequency noise PSD as the measure for laser coherence because of its straightforward relation to the phase noise in the coherent optical communications. However, we have never judged whether laser linewidth, the other common measure for laser coherence, is a good measure. In this section, we are going to answer that question.

The following is the logic. First, the phase noise in coherent optical communications is mostly relevant to the frequency noise PSD at high frequencies, indicated by equation (2.13). Second, the Central Relation reveals that the frequency noise PSD at high frequencies is only related to the tail of the optical lineshape. Hence, the laser linewidth, a characteristic of the body of the optical lineshape, is in general independent on the frequency noise PSD at high frequencies and therefore not a good measure for laser coherence in coherent optical communications.

To prove the conclusion, we examine three different lasers, two of which are the hybrid Si/III-V laser and the III-V DFB laser used before. The last one is the III-V DFB laser under very little coherent optical feedback, where the laser remains single-mode. The coherent optical feedback loop is constructed the same as before. We are going to measure their frequency noise PSD, optical lineshape and performance in the coherent optical communications.

The frequency noise PSDs of the lasers are shown in Fig. 5.6 and 5.7. The frequency noise PSD of the III-V DFB laser at low frequencies is significantly reduced by very little coherent optical feedback while at high frequencies, the RF oscillations are pretty weak. The optical lineshapes are shown in Fig. 5.8. Evidently, little coherent optical feedback can help to suppress the linewidth of the III-V DFB laser dramatically, making it as 'coherent' as the Si/III-V laser if laser linewidth is used as the measure for laser coherence [64-68]. The results validate our argument that laser linewidth is irrelevant to laser frequency noise PSD at high frequencies.

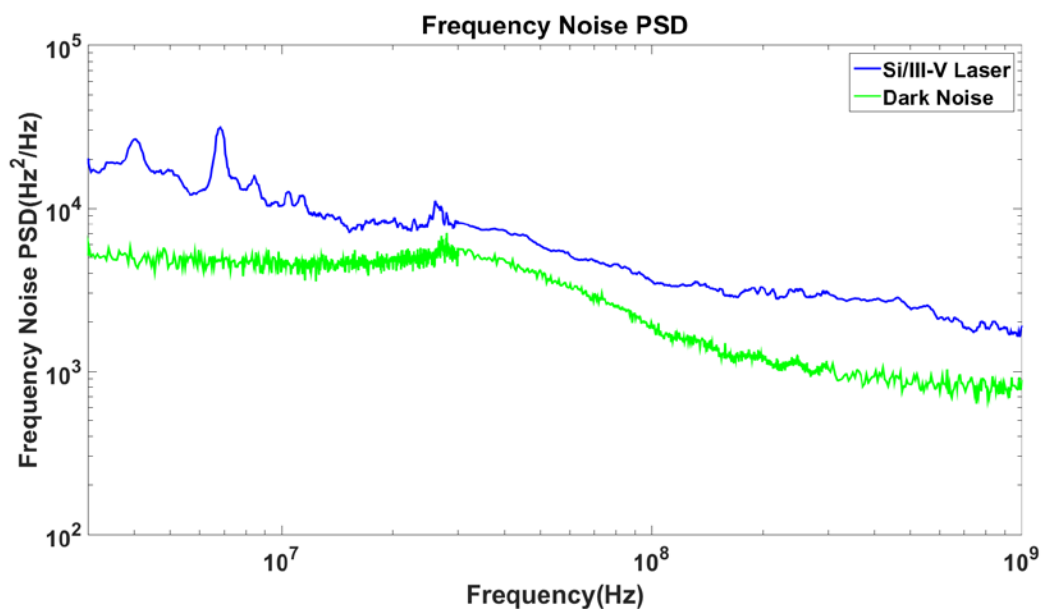


Figure 5.6 Frequency noise PSD of the Si/III-V laser

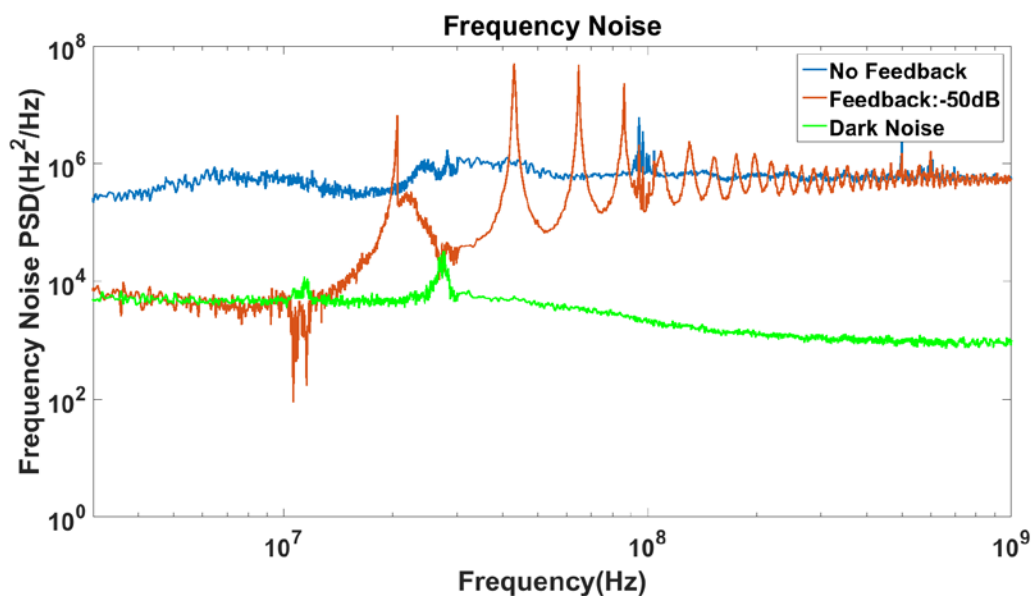


Figure 5.7 Frequency noise PSD of the III-V DFB laser w/o and w/ small coherent optical feedback

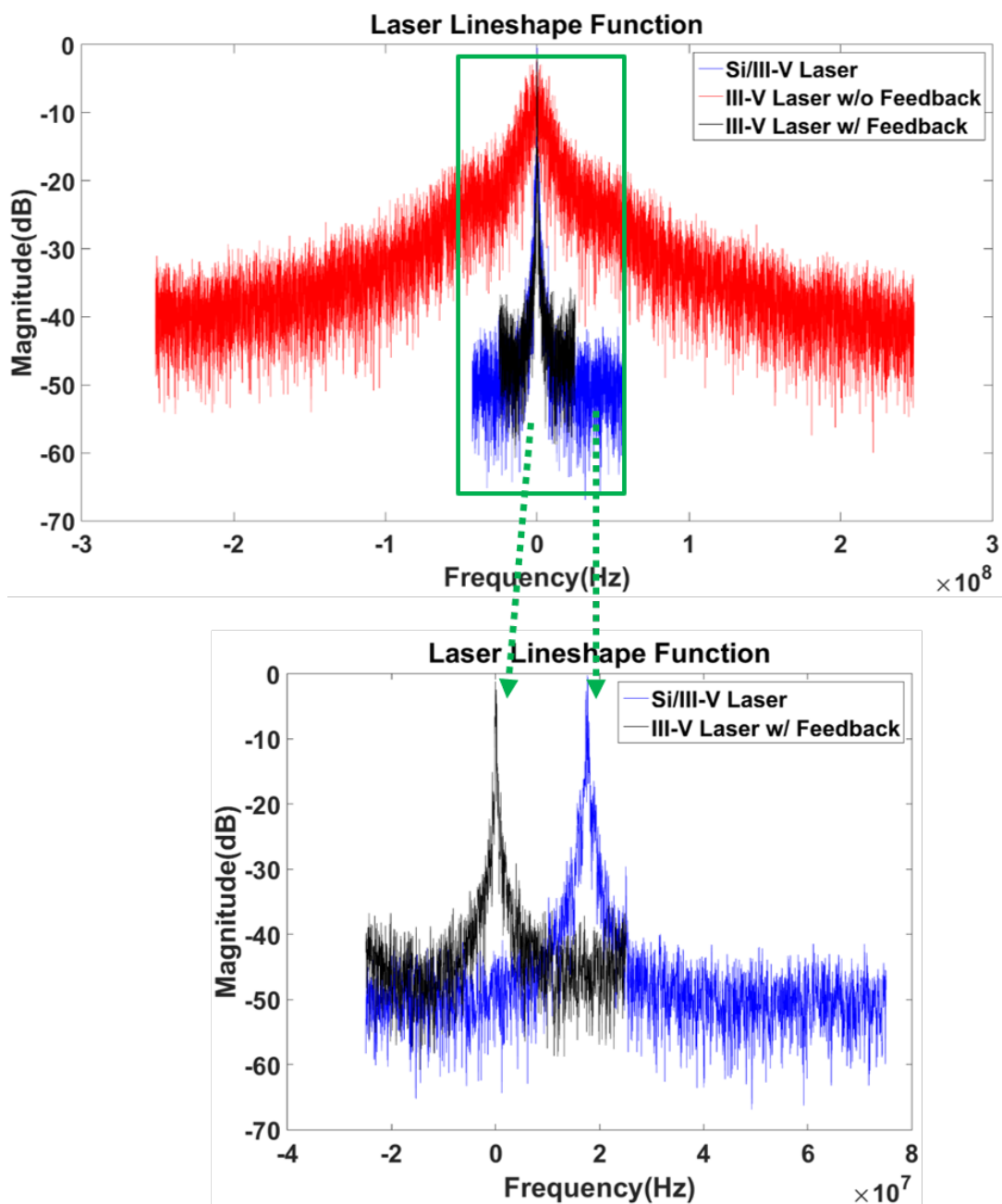


Figure 5.8 Optical lineshape of the three lasers

The three lasers are then tested in the coherent optical communication system. The results on 20 GBaud 16-QAM, shown in Fig. 5.9, indicate that the narrow linewidth of the III-V DFB laser under very little coherent optical feedback is useless as there is no obvious improvement of the laser's system performance. The Si/III-V laser is superior due to its ultra-low frequency

noise PSD at high frequencies. Such results confirm our conclusion that in general, laser linewidth is not a good measure for laser coherence when it comes to coherent optical communications.

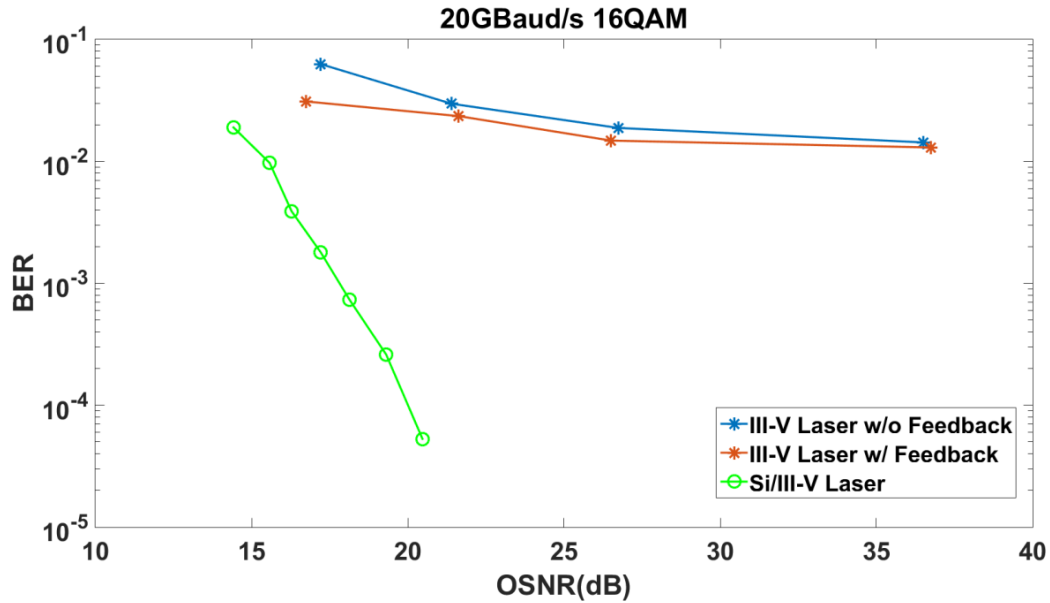


Figure 5.9 System performance of the three lasers

#### 5.4 Conclusions

In this chapter, we have derived a general relation, the Central Relation, between laser frequency noise PSD and lineshape. Predicted by the Central Relation and demonstrated experimentally, laser frequency noise PSD can be optically filtered, which offers us a new way of controlling laser phase coherence. Finally, we prove experimentally that laser linewidth is not a good measure for laser coherence in coherent optical communications, another prediction by the Central Relation.

## BIBLIOGRAPHY

- [1] J. R. Stern, J. W. Ballance, D. W. Faulkner, S. Hornung, D. B. Payne, and K. Oakley, "Passive optical local networks for telephony applications and beyond," *Electronics Letters* 23, 1255-1256 (1987).
- [2] C. F. Mélangé, X. Yin, B. Baekelandt, T. De Ridder, X.-Z. Qiu, J. Bauwelinck, J. Gillis, P. Demuytere, and J. Vandewege, "Fully DC-Coupled 10Gb/s Burst-Mode PON Prototypes and Upstream Experiments with 58ns Overhead," in *Optical Fiber Communication Conference, OSA Technical Digest (CD)* (Optical Society of America, 2010), OWX2.
- [3] G. Kramer, B. Mukherjee, and G. Pesavento, "IPACT a dynamic protocol for an Ethernet PON (EPON)," *IEEE Communications Magazine* 40, 74-80 (2002).
- [4] N. Cvijetic, "OFDM for Next-Generation Optical Access Networks," *Journal of Lightwave Technology* 30, 384-398 (2012).
- [5] S. Abbott, "Review of 20 years of undersea optical fiber transmission system development and deployment since TAT-8," in *2008 34th European Conference on Optical Communication, 2008*, 1-4.
- [6] Y. Miyamoto, K. Yonenaga, A. Hirano, N. Shimizu, M. Yoneyama, H. Takara, K. Noguchi, and K. Tsuzuki, "1.04-Tbit/s DWDM transmission experiment based on alternate-polarization 80-Gbit/s OTDM signals," in *24th European Conference on Optical Communication. ECOC '98 (IEEE Cat. No.98TH8398)*, 1998), 53-57 vol.53.
- [7] J. D. Reis, A. Shahpari, R. Ferreira, S. Ziaie, D. M. Neves, M. Lima, and A. L. Teixeira, "Terabit+ ( $192 \times 10$  Gb/s) Nyquist Shaped UDWDM Coherent PON With Upstream and Downstream Over a 12.8 nm Band," *Journal of Lightwave Technology* 32, 729-735 (2014).
- [8] S. Smolorz, E. Gottwald, H. Rohde, D. Smith, and A. Poustie, "Demonstration of a coherent UDWDM-PON with real-time processing," in *2011 Optical Fiber Communication Conference and Exposition and the National Fiber Optic Engineers Conference, 2011*, 1-3.
- [9] J. P. Elbers, N. Eiselt, A. Dochhan, D. Rafique, and H. Griebner, "PAM4 vs Coherent for DCI Applications," in *Advanced Photonics 2017 (IPR, NOMA,*

Sensors, Networks, SPPCom, PS), OSA Technical Digest (online) (Optical Society of America, 2017), SpTh2D.1.

- [10] D. Mahgerefteh, C. Liao, X. Zheng, Y. Matsui, B. Johnson, D. Walker, Z. F. Fan, K. McCallion, and P. Tayebati, "Error-free 250 km transmission in standard fibre using compact 10 Gbit/s chirp-managed directly modulated lasers (CML) at 1550 nm," *Electronics Letters* 41, 543-544 (2005).
- [11] J. Kreissl, V. Vercesi, U. Troppenz, T. Gaertner, W. Wenisch, and M. Schell, "Up to 40 Gb/s Directly Modulated Laser Operating at Low Driving Current: Buried-Heterostructure Passive Feedback Laser (BH-PFL)," *IEEE Photonics Technology Letters* 24, 362-364 (2012).
- [12] O. Ozolins, X. Pang, M. I. Olmedo, A. Kakkar, A. Udalcovs, S. Gaiarin, J. R. Navarro, K. M. Engenhardt, T. Asyngier, R. Schatz, J. Li, F. Nordwall, U. Westergren, D. Zibar, S. Popov, and G. Jacobsen, "100 GHz Externally Modulated Laser for Optical Interconnects," *Journal of Lightwave Technology* 35, 1174-1179 (2017).
- [13] F. Buchali, M. Chagnon, and K. Schuh, "Transmission Link Optimization for Coherent 4 Tb/s Extended Reach (ZR) Transmission," in *Optical Fiber Communication Conference (OFC) 2019, OSA Technical Digest (Optical Society of America, 2019)*, W2A.32.
- [14] E. Maniloff, S. Gareau, and M. Moyer, "400G and Beyond: Coherent Evolution to High-Capacity Inter Data Center Links," in *2019 Optical Fiber Communications Conference and Exhibition (OFC), 2019*, 1-3.
- [15] Y. Sasahata, K. Matsumoto, T. Nagira, H. Sakuma, K. Kishimoto, M. Suzuki, D. Suzuki, Y. Horiguchi, M. Takabayashi, K. Mochizuki, M. Gotoda, H. Aruga, and E. Ishimura, "Tunable 16 DFB laser array with unequally spaced passive waveguides for backside wavelength monitor," in *OFC 2014, 2014*, 1-3.
- [16] K. Mochizuki, Y. Ueno, K. Hasegawa, F. Hirose, S. Kajiya, M. Nogami, and H. Aruga, "Wavelength-tunable dual-output laser module with rear-side wavelength monitor for micro-ITLA," in *2015 European Conference on Optical Communication (ECOC), 2015*, 1-3.
- [17] R. Soref, "The Past, Present, and Future of Silicon Photonics," *IEEE Journal of Selected Topics in Quantum Electronics* 12, 1678-1687 (2006).
- [18] B. Jalali and S. Fathpour, "Silicon Photonics," *Journal of Lightwave Technology* 24, 4600-4615 (2006).

- [19] D. Thomson, A. Zilkie, J. E. Bowers, T. Komljenovic, G. T. Reed, L. Vivien, D. Marris-Morini, E. Cassan, L. Viot, J.-M. Fédéli, J.-M. Hartmann, J. H. Schmid, D.-X. Xu, F. Boeuf, P. O'Brien, G. Z. Mashanovich, and M. Nedeljkovic, "Roadmap on silicon photonics," *Journal of Optics* 18, 073003 (2016).
- [20] A. E. Lim, J. Song, Q. Fang, C. Li, X. Tu, N. Duan, K. K. Chen, R. P. Tern, and T. Liow, "Review of Silicon Photonics Foundry Efforts," *IEEE Journal of Selected Topics in Quantum Electronics* 20, 405-416 (2014).
- [21] W. A. Zortman, D. C. Trotter, and M. R. Watts, "Silicon photonics manufacturing," *Opt. Express* 18, 23598-23607 (2010).
- [22] A. L. Schawlow and C. H. Townes, "Infrared and Optical Masers," *Physical Review* 112, 1940-1949 (1958).
- [23] C. Henry, "Theory of the linewidth of semiconductor lasers," *IEEE Journal of Quantum Electronics* 18, 259-264 (1982).
- [24] A. Yariv and W. Caton, "Frequency, intensity, and field fluctuations in laser oscillators," *IEEE Journal of Quantum Electronics* 10, 509-515 (1974).
- [25] A. W. Fang, H. Park, O. Cohen, R. Jones, M. J. Paniccia, and J. E. Bowers, "Electrically pumped hybrid AlGaInAs-silicon evanescent laser," *Opt. Express* 14, 9203-9210 (2006).
- [26] C. T. Santis, "High-coherence hybrid Si/III-V semiconductor lasers," (California Institute of Technology, 2013).
- [27] S. T. Steger, "A fundamental approach to phase noise reduction in hybrid Si/III-V lasers," (California Institute of Technology, 2014).
- [28] Y. Vilenchik, "Narrow-linewidth Si/III-V lasers: A study of laser dynamics and nonlinear effects," (California Institute of Technology, 2015).
- [29] D. Kim, "Frequency Noise Control of Heterogeneous Si/III-V Lasers," (California Institute of Technology, 2018).
- [30] C. Harder, K. Vahala, and A. Yariv, "Measurement of the linewidth enhancement factor  $\alpha$  of semiconductor lasers," *Applied Physics Letters* 42, 328-330 (1983).
- [31] C. T. Santis, S. T. Steger, Y. Vilenchik, A. Vasilyev, and A. Yariv, "High-coherence semiconductor lasers based on integral high-Q resonators in hybrid

- Si/III-V platforms," *Proceedings of the National Academy of Sciences* 111, 2879 (2014).
- [32] H. Wang, D. Kim, M. Harfouche, C. T. Santis, N. Satyan, G. Rakuljic, and A. Yariv, "Narrow-Linewidth Oxide-Confined Heterogeneously Integrated Si/III-V Semiconductor Lasers," *IEEE Photonics Technology Letters* 29, 2199-2202 (2017).
- [33] M. Harfouche, "The coherence collapse regime of high-coherence Si/III-V lasers and the use of swept frequency semiconductor lasers for full field 3D imaging," (California Institute of Technology, 2018).
- [34] T. Inoue and S. Namiki, "Carrier recovery for M-QAM signals based on a block estimation process with Kalman filter," *Opt. Express* 22, 15376-15387 (2014).
- [35] A. Viterbi, "Nonlinear estimation of PSK-modulated carrier phase with application to burst digital transmission," *IEEE Transactions on Information Theory* 29, 543-551 (1983).
- [36] T. Pfau, S. Hoffmann, and R. Noé, "Hardware-Efficient Coherent Digital Receiver Concept With Feedforward Carrier Recovery for M-QAM Constellations," *Journal of Lightwave Technology* 27, 989-999 (2009).
- [37] M. Kauschke and C. Poppinga, "Method for iterative hard-decision forward error correction decoding," (Google Patents, 2007).
- [38] T. Kupfer, A. Bisplinghof, T. Duthel, C. Fludger, and S. Langenbach, "Optimizing Power Consumption of a Coherent DSP for Metro and Data Center Interconnects," in *Optical Fiber Communication Conference, OSA Technical Digest* (online) (Optical Society of America, 2017), Th3G.2.
- [39] X. Li, X. Chen, G. Goldfarb, E. Mateo, I. Kim, F. Yaman, and G. Li, "Electronic post-compensation of WDM transmission impairments using coherent detection and digital signal processing," *Opt. Express* 16, 880-888 (2008).
- [40] G. P. Agrawal, *Fiber-optic communication systems* (John Wiley & Sons, 2012), Vol. 222.
- [41] M. Seimetz, *High-order modulation for optical fiber transmission* (Springer, 2009), Vol. 143.

- [42] J. v. d. Ziel and R. Mikulyak, "Single-mode operation of 1.3  $\mu\text{m}$  InGaAsP/InP buried crescent lasers using a short external optical cavity," *IEEE Journal of Quantum Electronics* 20, 223-229 (1984).
- [43] L. Coldren and T. Koch, "External-cavity laser design," *Journal of Lightwave Technology* 2, 1045-1051 (1984).
- [44] L. Chinlon, C. Burrus, and L. Coldren, "Characteristics of single-longitudinal-mode selection in short-coupled-cavity (SCC) injection lasers," *Journal of Lightwave Technology* 2, 544-549 (1984).
- [45] N. Schunk and K. Petermann, "Minimum bit rate of DPSK transmission for semiconductor laser with a long external cavity and strong linewidth reduction," *Journal of Lightwave Technology*, vol. 5, pp. 1309-1314, 1987.
- [46] K. Petermann, *Laser diode modulation and noise* (Springer Science & Business Media, 2012), Vol. 3.
- [47] K. Petermann, "External optical feedback phenomena in semiconductor lasers," *IEEE Journal of Selected Topics in Quantum Electronics* 1, 480-489 (1995).
- [48] R. Tkach and A. Chraplyvy, "Regimes of feedback effects in 1.5- $\mu\text{m}$  distributed feedback lasers," *Journal of Lightwave Technology* 4, 1655-1661 (1986).
- [49] D. Lenstra, B. Verbeek, and A. D. Boef, "Coherence collapse in single-mode semiconductor lasers due to optical feedback," *IEEE Journal of Quantum Electronics* 21, 674-679 (1985).
- [50] G. C. Dente, P. S. Durkin, K. A. Wilson, and C. E. Moeller, "Chaos in the coherence collapse of semiconductor lasers," *IEEE Journal of Quantum Electronics* 24, 2441-2447 (1988).
- [51] H. Li, J. Ye, and J. G. McInerney, "Detailed analysis of coherence collapse in semiconductor lasers," *IEEE Journal of Quantum Electronics* 29, 2421-2432 (1993).
- [52] J. Wang and K. Petermann, "Noise analysis of semiconductor lasers within the coherence collapse regime," *IEEE Journal of Quantum Electronics* 27, 3-9 (1991).
- [53] K. In, K. Byung-Kwon, B. Yu-Dong, P. Byeonghoon, L. Sang-Moon, K. Young Hyun, and J. Dong-Hoon, "Design of amplifier- and modulator-

- integrated laser diode for 10-Gb/s 80-km transmission," *IEEE Journal of Selected Topics in Quantum Electronics* 11, 323-328 (2005).
- [54] I. Kim, B.-K. Kang, Y.-D. Bae, B. Park, S.-M. Lee, Y. H. Kim, and D.-H. Jang, "Transmission over 80 km at 10 Gb/s using the amplifier-and modulator-integrated laser diode," *IEICE transactions on electronics* 88, 984-989 (2005).
- [55] M. N. Sysak, D. Liang, R. Jones, G. Kurczveil, M. Piels, M. Fiorentino, R. G. Beausoleil, and J. E. Bowers, "Hybrid Silicon Laser Technology: A Thermal Perspective," *IEEE Journal of Selected Topics in Quantum Electronics* 17, 1490-1498 (2011).
- [56] M. N. Sysak, H. Park, A. W. Fang, J. E. Bowers, R. Jones, O. Cohen, O. Raday, and M. Paniccia, "Experimental and theoretical thermal analysis of a Hybrid Silicon Evanescent Laser," *Opt. Express* 15, 15041-15046 (2007).
- [57] S. Tanaka, S.-H. Jeong, S. Sekiguchi, T. Kurahashi, Y. Tanaka, and K. Morito, "High-output-power, single-wavelength silicon hybrid laser using precise flip-chip bonding technology," *Opt. Express* 20, 28057-28069 (2012).
- [58] K. Vahala and A. Yariv, "Semiclassical theory of noise in semiconductor lasers - Part I," *IEEE Journal of Quantum Electronics* 19, 1096-1101 (1983).
- [59] K. Vahala and A. Yariv, "Semiclassical theory of noise in semiconductor lasers - Part II," *IEEE Journal of Quantum Electronics* 19, 1102-1109 (1983).
- [60] G. Di Domenico, S. Schilt, and P. Thomann, "Simple approach to the relation between laser frequency noise and laser line shape," *Appl. Opt.* 49, 4801-4807 (2010).
- [61] B. Daino, P. Spano, M. Tamburrini, and S. Piazzolla, "Phase noise and spectral line shape in semiconductor lasers," *IEEE Journal of Quantum Electronics* 19, 266-270 (1983).
- [62] C. Henry, "Theory of the phase noise and power spectrum of a single mode injection laser," *IEEE Journal of Quantum Electronics* 19, 1391-1397 (1983).
- [63] A. Yariv and P. Yeh, *Photonics: optical electronics in modern communications* (Oxford Univ., 2006).
- [64] R. Wyatt, "Spectral linewidth of external cavity semiconductor lasers with strong, frequency-selective feedback," *Electronics Letters* 21, 658-659 (1985).

- [65] E. Patzak, A. Sugimura, S. Saito, T. Mukai, and H. Olesen, "Semiconductor laser linewidth in optical feedback configurations," *Electronics Letters* 19, 1026-1027 (1983).
- [66] K. B. MacAdam, A. Steinbach, and C. Wieman, "A narrow-band tunable diode laser system with grating feedback, and a saturated absorption spectrometer for Cs and Rb," *American Journal of Physics* 60, 1098-1111 (1992).
- [67] S. Bennetts, G. D. McDonald, K. S. Hardman, J. E. Debs, C. C. N. Kuhn, J. D. Close, and N. P. Robins, "External cavity diode lasers with 5kHz linewidth and 200nm tuning range at 1.55 $\mu$ m and methods for linewidth measurement," *Opt. Express* 22, 10642-10654 (2014).
- [68] T. Komljenovic, S. Srinivasan, E. Norberg, M. Davenport, G. Fish, and J. E. Bowers, "Widely Tunable Narrow-Linewidth Monolithically Integrated External-Cavity Semiconductor Lasers," *IEEE Journal of Selected Topics in Quantum Electronics* 21, 214-222 (2015).